Development and Mechanistic Analysis of *in vivo* Liposomal Nanoparticle Delivery of siRNA and mRNA

By

J. Robert Dorkin

B.A. Biological Chemistry
Swarthmore College, 2006

SUBMITTED TO THE DEPARTMENT OF BIOLOGY IN PARTIAL FULFILLMENT OF THE REQUIREMENTS FOR THE DEGREE OF

DOCTOR OF PHILOSOPHY

AT THE
MASSACHUSETTS INSTITUTE OF TECHNOLOGY

FEBRUARY 2016

Signature of Author: Signature redacted

J. Robert Dorkin
September 21st, 2015

Certified by: Signature redacted

Daniel G. Anderson
Associate Professor of Chemical Engineering
Thesis Advisor

Accepted by: Signature redacted

Michael Hemann
Associate Professor of Biology
Co-Chair, Biology Graduate Committee

Development and Mechanistic Analysis of *in vivo* Liposomal Nanoparticle Delivery of siRNA and mRNA

By

J. Robert Dorkin

Submitted to the Department of Biology on September 21st, 2015
in Partial Fulfillment of the Requirements for the Degree of Doctor of Philosophy

Abstract

A limited number of siRNA and mRNA based therapeutics have been developed largely due to the difficulties of efficaciously delivering RNA to cells *in vivo*. Liposomal nanoparticles (LNPs) have shown some success, but their design is limited by both a lack of information concerning the optimal lipid composition and insufficient data regarding the LNPs' interaction with their environment. Further elucidation of the physical properties of LNPs as well as their mechanisms of action will improve future development of RNA therapeutics.

Using a combinatorial lipid library, we identified four design criteria that are required for efficacious LNP delivery of siRNA: the presence of a tertiary amine, having lipid tails that are 13 carbons long, having three or more lipid tails, and having an LNP pKa of 5.4 or more. LNPs meeting all four of these conditions demonstrated 100% probability of efficaciously delivering siRNA to hepatocytes *in vivo*.

While numerous LNPs have been developed for siRNA delivery, few have been developed for mRNA delivery. Utilizing LNPs optimized for siRNA to deliver mRNA instead could rapidly reduce development time and cost for mRNA therapeutics. Here, we demonstrate that the relative efficacy of 48 different ionizable lipids were comparable for both siRNA and mRNA delivery, but that several formulation parameters must be modified for optimal mRNA delivery. These include a lower molar percent of the ionizable lipid, having a higher total lipid to RNA weight ratio, and containing conical phospholipids instead of cylindrical phospholipids.

Using LNPs to deliver RNA to cells other than hepatocytes has proven difficult. By incorporating a positive surface charge on the LNPs we redirected liver targeted liposomes to lung endothelial cells. Examination of the plasma proteins bound to the LNPs revealed apolipoprotein (Apo) B and ApoE attached to the hepatocellular targeted LNPs, with serum albumin and fibrinogen were bound to the lung targeted LNPs, and ApoA1 found on both types of LNPs. Subsequent *in vitro* experiments demonstrated that VLDL and HDL are important for hepatocellular and lung endothelial cell delivery, respectively. Plasma proteins function by improving the cellular uptake of the LNPs, as we demonstrated that ApoE is essential for hepatocellular uptake via macropinocytosis.

Thesis Supervisor: Daniel G. Anderson

Title: Associate Professor of Chemical Engineering

Acknowledgements

While I am unabashedly arrogant in my own scientific capabilities, even I must concede that my success is largely due to the multitude of brilliant, caring, and, er, unconventional people who have continually supported me both in my scientific career, and in the other aspects of my life. While thanking everyone individually would require another several chapters, there are some people who are directly responsible for my completing graduate school whom I would like to mention; the rest will have to settle for knowing they are in my heart.

To begin with, I want to thank Dr. Anderson for very generously letting me join his lab. His lab has been the perfect incubator for scientific discovery; I have had enough independence to explore whatever mad experiments entered my brain, while receiving enough guidance to make sure that my research remained feasible, relevant, and at least partially coherent. He has also afforded me with the opportunity to work with some amazing collaborators both in academia and in industry, exposing me to more exciting and innovative projects than a graduate student could ever hope for.

Another advantage of working in Dr. Anderson's lab has been the amazing post-docs from whom I have had the privilege of learning. Of the many intelligent and helpful researchers in his lab, three in particular really guided me in my research: Dr. Katie Whitehead, Dr. Yizhou Dong, and Dr. Arturo Vegas. All three were invaluable in teaching me new skill sets, sharing their projects with me, and helping me design my own projects. They have always been available and willing to help me, while still treating me with the respect of a peer. They all have found prestigious faculty positions, and their future graduate students will be very lucky to have them.

My work would have also been impossible without the help from Jung Yang, Faryal Mir, and Philip Chang. Without their technical skills I would still be in the animal facility, quietly cursing at the mice. More than just helping me with physical labor, they have offered suggestions and advice, helping me shift through the mountains of data to find the answers buried within.

I would like to thank the plethora of collaborators that I've had in the lab: Kevin Kauffman, Owen Fenton, Matthias Oberli, Siddharth Jhunjhunwala, Luke Ceo, Hao Yin, Piotr Kowalski, Ben Tang, Gaurav Sahay, Andreas Reichmuth, Lavanya Thapa, Karsten Olejnik, Omar Kahn, Amy Lin, Alan Chiu, and many more. I greatly appreciate them putting up with me, and indulging my insane ideas. Working with them, and the Anderson lab as a whole, has been a fun and insightful experience. I hope to continue collaborating with them in the future.

I greatly appreciate the guidance of my thesis committee members, Dr. Phillip Sharp and Dr. Michael Hemann, as well as my external examiner, Dr. Angela Koehler. My experiments benefited greatly from their suggestions and guidance. They helped to keep me on track, and made sure that I graduated in six years, and not sixteen.

I am deeply grateful and apologetic to Betsey Walsh, Tara Fawaz, Tiffany Greaves, and Connie Beal. I am constantly amazed by how organized you all are, and I can only image you are constantly amazed by how organized I'm not. Thank you for the numerous messages, reminders, and re-reminders. And thank you for not killing me when I still forgot.

Before even coming to MIT I was set on the RNA formulation path by two fantastic people: Dr. Vicki Sato, and Dr. Akin Akinc. Dr. Sato's guidance directed me to Alnylam after college, where I spent two and a half extremely productive and educational years as a research associate working with Dr. Akinc. I have no idea why he let me do half the things I did, but I will be forever grateful for the opportunities and independence he gave an overly-confident under-prepared recent graduate like myself. The two of them started me on my career path, and I am extremely lucky to know them both.

During my time at BB&N, Swarthmore, Alnylam, and MIT, I have been surrounded by incredible friends. Brilliant, humorous, and utterly deranged individuals, they have not kept me sane, but rather have joined me in my madness. I could not be more fortunate to have them all in my life; they are family, loyal and steadfast. They have seen me through hard times, and if it comes to it, they will see me through worse. Thank you.

And last, but certainly not least, I have to thank my family. Thank you Freya, for the wonderful support you've shown me this summer; whether it was in Newton or in Maine, you kept me sane while I was trying to work on my thesis. I know I sometimes try your patience, but thank you for putting up with me. Thank you Molly for being such a good sister to me; raising our parents isn't easy, and I don't think I could do it without you. You may have fled the country, but you are always in my thoughts, and a mere ocean won't save you from my nudging.

Thank you Mom and Dad. You are tremendously supportive and always have been. I can do no wrong in your eyes, and you have fought tooth and nail to defend me. In my darkest times, when I didn't like myself, your faith in me kept me going. Thank you Dad for the many scientific discussions. You have been an inspiration, and I hope, through my research, I can help people the way you have. Thank you Mom for encouraging my weirdness. You make me proud to be myself, and I appreciate that to no end.

And, because I am a narcissist, I'm going to thank myself. Good going Robert – you're pretty damn awesome.

Table of Contents

List of Figures and Tables

Abbreviations

Apo - Apolipoprotein
Cy5.5 – Cyanine 5.5
DODAP - 1,2-dioleoyl-3-dimethylammonium-propane
DOPC - 1,2-dioleoyl-sn-glycero-3-phosphocholine
DOPE - 1,2-dioleoyl-sn-glycero-3-phosphoethanolamine
DOTAP - 1,2-dioleoyl-3-trimethylammonium-propane
DMG-mPEG$_{2000}$ – 1,2-dimyristoyl-sn-glycero-3-phosphoethanolamine-N-[methoxy(polyethylene glycol)-2000]
DSG-mPEG$_{2000}$ - 1,2-distearoyl-sn-glycero-3-phosphoethanolamine-N-[methoxy(polyethylene glycol)-2000]
DSPE - 1,2-distearoyl-sn-glycero-3-phosphoethanolamine
DSPC - 1,2-distearoyl-sn-glycero-3-phosphocholine
EC_{50} – half maximal effective concentration
EIPA – 5-N-ethyl-N-isoproamiloride
EPO – Erythropoietin
FVII – Factor VII serum clotting protein
Gal – galactarate
GAPDH - Glyceraldehyde 3-phosphate dehydrogenase
Glu – glutamic acid
H_{II} – inverted hexagonal
HDL – high density lipoprotein
IDL- intermediate density lipoprotein
LDL – low density lipoprotein
LDLR – low density lipoprotein receptor
LNP – liposomal nanoparticle
mRNA – messenger RNA
PEI – Polyetheleneimine
PNP – Polymeric nanoparticle
Pten - phosphate and tensin homolog
RISC – RNA Induced Silencing Complex
RNAi – RNA interference
siRNA – small interfering RNA
Tar – tartrate
TNS – 2-(p-toluidinyl)naphthalene-6-sulphonic acid
VLDL – very low density lipoprotein

Chapter 1
Introduction

Overview

Virtually all diseases, including cancer, heart disease, diabetes, and the common cold, involve an abnormal expression of proteins. Whether it is the undesirable upregulation of an oncogene, the absence of a tumor suppressor, or the presence of an exogenous viral protein, protein expression often determines the phenotypes observed in individuals suffering from diseases. To that end, many therapeutics have been developed with the intent of eliminating, modifying, or increasing specific proteins in the body. Developing the ability to regulate individual proteins allows for control of the disease symptoms, and in many cases can result in the elimination of the disease itself (Herzog, Cao, & Srivastava, 2010).

Therapeutic Platforms for Disease Treatment

Numerous types of therapeutics have been examined and developed to regulate protein expression in humans. The use of small molecule drugs are the oldest example of protein modification, with many natural compounds being used for medicinal purposes prior to the development of modern medicine (Koehn & Carter, 2005). Small molecules function in many different ways, including protein degradation, inhibition, modification, activation, and upregulation. While many of these small molecule compounds are effective and selective, many more bind to off target proteins or bind to proteins in untargeted cells, resulting in a plethora of side effects (Bender et al., 2007). Furthermore, not all proteins are easily targetable, and small molecules cannot be used to introduce an exogenous protein that is necessary but absent.

An alternative method for protein regulation involves the direct delivery of a therapeutic protein. Insulin and factor IX are two common therapeutic proteins which are directly injected into patients, and are used to treat diabetes and hemophilia respectively (Dewitt, Hirsch, Care, & Pro, 2014; Orthner, Anderson, & Kosow, 2009). However, the application of protein based therapeutics is limited. For cytoplasmic, nuclear, or transmembrane proteins, obtaining the correct cellular distribution is extremely difficult. In addition, because many proteins are non-catalytic in nature or have a short half-life, either large dosages or continuous dosing of the therapeutic protein is required. Direct protein delivery is also not an effective method for eliminating problematic endogenous proteins.

The development of gene therapy provided an alternative method to regulate protein production in cells. Experiments performed *in vitro* demonstrated that by delivering DNA into the nucleus, a cell could be modified to produce a specific protein, with the appropriate post-translational modifications and cellular localization, for the entire lifetime of the cell (Herzog et al., 2010). Translating the work *in vitro* to *in vivo*, however, has proven extremely difficult. Delivery of DNA to cells *in vivo* faced numerous obstacles, including serum nucleases, tissue biodistribution, cellular uptake, endosomal escape, and finally entry into the nucleus (Escriou, Ciolina, Helbling Leclerc, Wils, & Scherman, 1998; Jiao et al., 1992; Tamkovich et al., 2006). Ultimately these barriers have so far proven insurmountable for many therapeutics, and while research on gene therapy continues, relatively few DNA based drugs have demonstrated success in the clinic.

As an alternative to gene therapy, recent research has focused on the development of RNA based therapeutics. Two major types of RNA are currently being developed for

therapeutic use: messenger RNA (mRNA) and small interfering RNA (siRNA). Just as with DNA, mRNA encodes for a specific protein, allowing for selective introduction or up regulation of a target protein, with the necessary post-translational modifications and cellular localization. mRNA also faces many of the same obstacles as DNA for *in vivo* delivery – save one. While DNA requires entry into the nucleus in order to be transcribed, mRNA needs only to enter the cytoplasm for successful translation. The absence of this barrier has proven significant, as preliminary data have shown positive mRNA expression *in vivo* (Kormann et al., 2011; Zangi et al., 2013). One difference in using mRNA rather than DNA is the duration of action; while mRNA is capable of producing a significant amount of protein, mRNA is degraded much more rapidly than DNA. For diseases that require constitutive expression of a protein, this can be a disadvantage, though for some therapeutic applications, a transient protein expression is optimal (Zangi et al., 2013), making an mRNA based therapeutic preferable in those instances.

The discovery of RNA interference (RNAi) has resulted in the generation of a new class of RNA, siRNA (Fire et al., 1998). By synthetically generating double-stranded RNA that is complementary to a segment of an mRNA transcript, scientists can selectively target mRNA for degradation via the RNA Induced Silencing Complex (RISC). Through careful design of the siRNA sequence, an individual protein can be targeted for silencing *in vivo.* Although varying in activity and structure, siRNA delivery faces many of the same obstacles as mRNA delivery (K. a Whitehead, Langer, & Anderson, 2009). Despite these barriers, siRNA based therapeutics have been developed, several of which have begun clinical studies (Allen & Cullis, 2013; Kanasty, Dorkin, Vegas, & Anderson, 2013; Yin et al., 2014).

Barriers to Systemic RNA Delivery

Between the use of siRNA and mRNA, researchers can selectively silence or express virtually any endogenous or exogenous protein; this ability allows scientists to treat a myriad of diseases and disorders with potentially far fewer side effects than by treating them with many of the small molecule drugs that currently dominate the market. Despite their therapeutic potential, however, relatively few mRNA and siRNA based drugs are currently under development. The primary obstacle preventing RNA therapeutics from entering the clinic is not the efficacy of the RNA itself, which has repeatedly demonstrated success *in vitro*, but rather the difficulty of delivering nucleic acid based drugs to the cytoplasm of the diseased cells *in vivo*. There are numerous barriers to the delivery of siRNA and mRNA drugs systemically.

The first obstacle encountered for systemically injected RNA, is plasma stability. Unmodified RNA is rapidly degraded by numerous circulating exonucleases and endonucleases (Figure 1.1a) (Sorrentino, 1998). Certain chemical modifications, such as 2'-fluoro groups and phosphorothioates, have been developed to help stabilize and protect siRNA from nuclease activity (Chiu & Rana, 2003). However, while these modifications can be included in the synthetically constructed siRNA, they are not readily included in mRNA, which is synthesized enzymatically via *in vitro* transcription. Furthermore, while chemically modified siRNA displays a high degree of efficacy, chemically modified mRNA has demonstrated a decrease in efficacy as compared to the unmodified form (Thess et al., 2015). Alternative methods are required to protect mRNA from degradation during circulation.

If the RNA is not degraded during circulation, the next obstacle faced is biodistribution; intravenously injected siRNA is rapidly cleared by the kidneys (K. A. Whitehead et al., 2014), while we have found the majority of unformulated mRNA locates to the liver (Figure 1.1b). While these two tissue types are implicated in numerous diseases, modifying the biodistribution of the RNA to target other tissue types dramatically increases the number of clinical applications available.

Provided that the siRNA or mRNA has localized to the appropriate tissue type, the next obstacle is cellular uptake. Both siRNA and mRNA are heavily charged molecules, and cannot freely diffuse across the hydrophobic region of the membrane (Figure 1.1c). There are numerous methods by which cells take up material from their surrounding environment (macropinocytosis, caveloi mediated endocytosis, clatherin mediated endocytosis, etc.)(Khalil, Kogure, Akita, & Harashima, 2006); however, RNA is not readily taken up into most cell types (Figure 1.1d). Cellular uptake of RNA can be dramatically improved by delivering with a carrier that directly interacts with the cell membrane, or binds to a surface receptor.

Finally, once the RNA is endocytosed, it must exit the endosome and enter the cytoplasm, where siRNA and mRNA bind to RISC or the ribosomal complex respectively (Figure 1.1e). Again, due to the charged nature of the RNA, simple diffusion across the endosomal membrane is virtually impossible; some disruption must occur in order for the RNA to escape. This process if currently not well understood. Failure to exit the endosomal pathway before entering the lysosome results in the exposure to numerous exonucleases and endonucleases, ultimately resulting in the degradation of the RNA (Figure 1.1f).

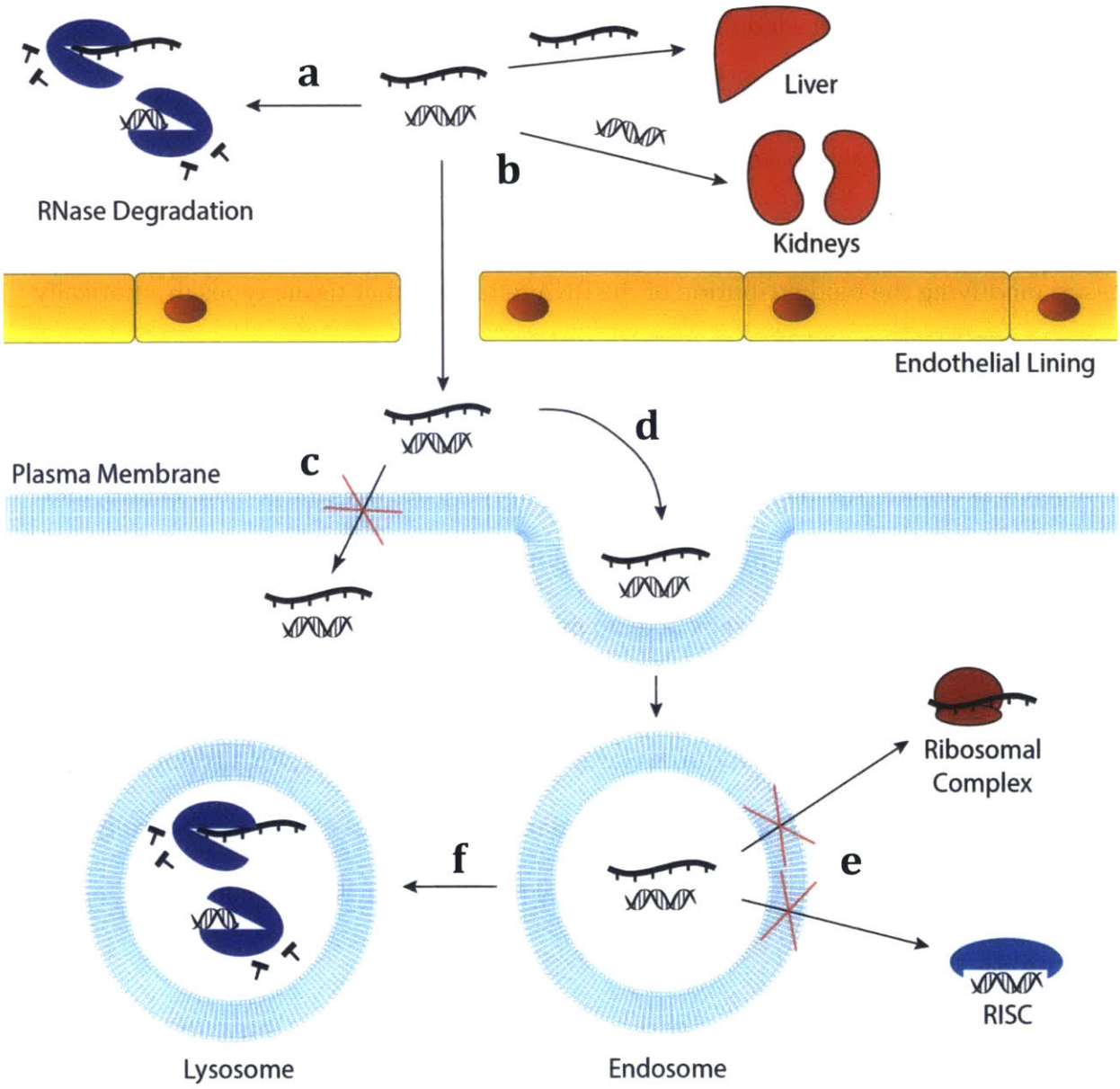

Figure 1.1: Barriers to RNA delivery *in vivo*. (a) Systemically injected RNA face degradation by circulating RNases. (b) Unformulated siRNA localized to the kidneys, while unformulated mRNA distributes to the liver. (c) Due to the high charge density of the RNA, it does not readily diffuse across the plasma membrane. Instead, the RNA must be taken up by an alternative method (d) such as macropinocytosis or endocytocis. (e) mRNA and siRNA must escape the endosome in order to bind to either the ribosomal complex or RISC respectively; diffusion across the endosomal membrane is again impeded by the high charge density of the RNA. (f) Failure to escape the endosome results in transitioning to the lysosome, where the RNA is exposed to RNases, and degraded.

Delivery Vehicles for Systemic RNA Administration

In order to overcome these barriers to RNA delivery *in vivo*, several types of delivery vehicles have been developed. Among these different platforms are viral particles, ligand conjugates, and liposomal nanoparticles. No single delivery method is perfect, but some methods have demonstrated greater practicality than others.

Due to their natural capability to deliver RNA to specific cell types *in vivo*, viruses have been examined as potential delivery vehicles for siRNA and mRNA. While viruses are capable of successfully delivering these compounds, several difficulties reduce their potential for clinical application. Immunostimulation often results in the clearance of viral particles before they have a chance to infect the target cell, as well as generating the risk of creating a potentially lethal cytokine cascade. From a practical standpoint the use of viral therapeutics faces other obstacles, as large scale production of virions can be difficult, especially in replication incompetent strains (Verma & Somia, 1997).

Another method for delivering RNA systemically involves the use of ligand conjugates. Covalent attachment of cellular receptor ligands has been demonstrated to successfully deliver siRNA to specific cell types *in vivo*. (Akinc et al., 2010) The difficulty with using conjugates is that while the ligand may be successful at targeting a specific cell type for cellular uptake, it conveys no mechanism for endosomal escape. As a result, ligand-conjugated siRNA that are endocytosed must survive exposure to nucleases in the lysosome in order to enter the cytoplasm. While extensive chemical modification has created some siRNA conjugates that are capable of surviving these conditions, their use still remains limited. Since mRNA generated through *in vitro* transcription, rather than through direct chemical synthesis like siRNA, it is far more difficult to incorporate the stabilizing

chemical modifications into mRNA backbone. As a result, the mRNA is still vulnerable to degradation by circulating RNases, reducing the potential for the use of direct ligand conjugation for mRNA delivery.

Liposomal nanoparticles (LNPs) have demonstrated tremendous potential for nucleic acid delivery *in vivo*. Structurally, most LNPs consist of a single lamellar or a multilamellar shell around an RNA core (Figure 1.2a). These nanoparticles can be extremely stable in an aqueous environment, even in the presence of negatively charged plasma proteins. This physical barrier serves to protect the RNA from degradation by sterically occluding the nucleases circulating in the blood, allowing for intravenous delivery without requiring any chemical modifications on the RNA. The surface of the liposome can also be modified to evade the immune system, allowing for repeat injections without a loss in efficacy (Akinc et al., 2009).

The size, composition, and charge of the LNP have a notable impact on the biodistribution of the entrapped RNA (Ishiwatari et al., 2012; Sato et al., 2008). While siRNA has a length of only 7.5nm (Schroeder, Levins, Cortez, Langer, & Anderson, 2010), liposomes are much larger, typically 50-200nm in diameter; this increase in size prevents clearance from the kidneys, where the vascular fenestration size is only between 20-30nm (Gaumet, Vargas, Gurny, & Delie, 2008). The fenestration of the endothelial lining for most tissues is even smaller, less than 10nm in size. In contrast the liver (Audouy, Leij, Hoekstra, & Molema, 2002), the spleen, and most tumors generally have larger fenestrations in their vascular system, allowing liposomes to easily penetrate and transfect epithelial cells (Figure 1.2b). The endothelial cells themselves can be a viable tissue target, with several LNPs having been shown to deliver RNA to lung endothelial cells.

In addition to modifying tissue biodistribution, LNPs can also facilitate cellular uptake. Some liposomes are modified with ligands that are capable of binding to proteins on the cell's surface, which in turn allow for either passive or active uptake. Other liposomes bind plasma proteins during circulation, and when the plasma protein binds to a cell surface receptor and is endocytosed, the LNP is taken up as well (Figure 1.2c). Alternatively, it has been theorized that the positive surface charge of the LNP drives cellular uptake by binding to the negatively charged surface proteins and lipids. Regardless of the specific method employed, the presence of the LNP dramatically increases the cellular uptake of the entrapped RNA.

Although there are many potential pathways for the LNP to be taken up, such as macropinocytosis, clatherin dependent endocytosis, and caveolae mediated endocytosis (Khalil et al., 2006), most uptake methods result in the liposome and the entrapped RNA entering the endosomal pathway (Figure 1.2d). There are several theories as to how LNPs aid in RNA escaping the endosome and entering the cytoplasm (Allen & Cullis, 2013) (Figure 1.1e). One theory suggests that the ionizable lipids act as a proton sponge; as the lipids become protonated, additional counter ions are pumped into the endosome causing it to swell and rupture. Another theory suggests that the lipids in the LNP insert into the endosomal membrane, which destabilizes the membrane and allows the RNA to exit into the cytoplasm. Depending on the structure and composition of the LNP, both theories may be applicable to various degrees.

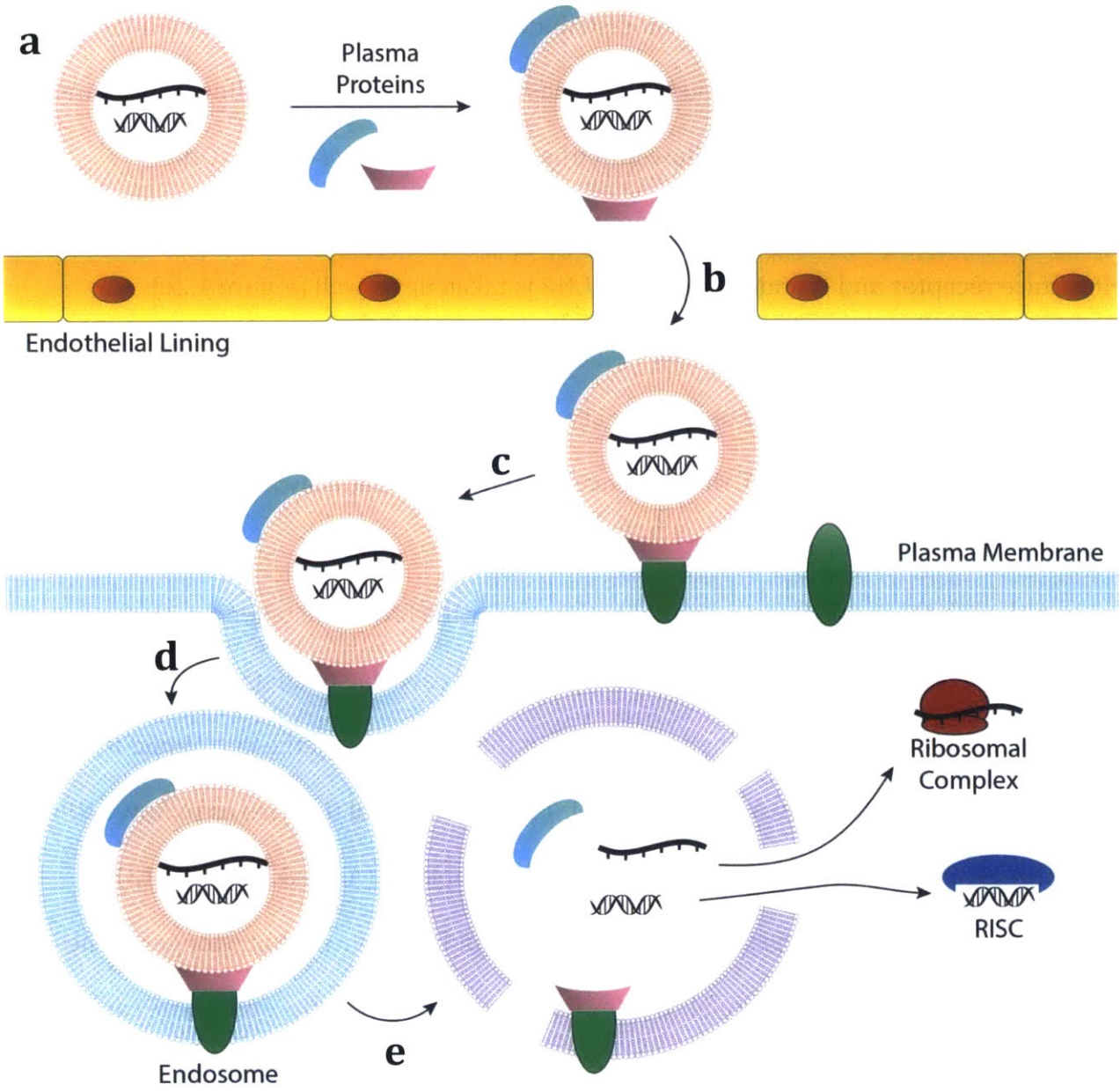

Figure 1.2: Liposomal mediated RNA delivery *in vivo*. (a) The LNP generally consists of a single or multi-lamellar lipid membrane around an RNA core, sterically obstructing access from the circulating RNases. (b) The size of the LNP modulates the biodistribution of the RNA, as few organs have endothelial fenestrations large enough to allow the LNP to pass through. (c) The LNP binds to the surface of the target cell through either electrostatic interactions or through protein mediated interactions. (d) The LNP may be taken up into the cell through multiple pathways, including macropinocytosis, clatherin mediated endocytosis, and caveolae mediated endocytosis. (e) LNPs enhance endosomal escape of RNA by disrupting the endosomal membrane stability.

From a development standpoint, liposomes have many additional benefits. Some liposomes are self-assembling, with the RNA automatically becoming entrapped due to electrostatic interactions with the cationic or ionizable lipids. Physical characteristics, such as particle size and surface charge, are heavily influenced by composition, allowing for LNP formation in a highly reproducible and scalable manner. Since the biodistribution is largely independent of the RNA sequence, liposomes are also very modular, meaning that once an LNP has been developed for a specific cell type, numerous different RNAs can be delivered with the same formulation, ultimately allowing for rapid development of numerous therapeutics for a specific cell type. Liposomes can also be highly stable, retaining their size and entrapment even after multiples months of storage at 37°C (Akinc et al., 2009). This stability allows for easier transportation and storage of the therapeutics, increasing both their shelf life and their ease of access.

Liposomal Concepts Addressed in this Thesis

Due to all of the advantages in using LNPs as a delivery platform for RNA, it is no surprise that they are being actively researched and developed; many siRNA formulated liposomes have already reached clinical trials (M. E. Davis et al., 2010), while many more have demonstrated great success in a pre-clinical setting. But despite the extensive research already done on liposomal delivery of RNA, many obstacles and questions remain.

Toxicity has always been a potential obstacle for LNPs; ionizable and cationic lipids have induced weight loss, cytokine stimulation, and even tissue necrosis at high doses. Early generation lipids demonstrated a relatively high EC_{50} for siRNA delivery, and a narrow therapeutic window; LNPs using the ND-98 lipid, for example, had an EC_{50} of ~2 mg

kg^{-1} for anti-FVII siRNA, with mice manifesting toxicity at a dose of 10 mg kg^{-1} (Akinc et al., 2009). Subsequent generations of lipids have demonstrated a greater increase in efficacy, but the tolerated dose level has remained relatively unchanged. The majority of these second generation lipids have few, if any, labile functional groups, making them difficult for the cells to degrade. This has raised concerns for repeat dosing of LNPs; even if the ionizable lipid is non-immunogenic, and well tolerated at a single dose, evidence has suggested that the lack of degradability may result in accumulated toxicity from repeat dosing. One of the focuses of my research has been on the development of labile or biocompatible lipids, to improve the tolerability of not just a single dose, but of chronic treatment.

Despite the successes in developing LNPs for siRNA delivery *in vivo*, relatively little is known about the structure-function relationship between ionizable lipids and RNA delivery. While many efficacious lipids have been developed, they have been discovered primarily as a part of large library screens (Akinc et al., 2008, 2009; Love et al., 2010; Mahon et al., 2010); no lipids have been successfully designed *ab initio*. Aside from the presence of an amine core and hydrophobic poly-carbon tails, very little is known about what structural motifs are important for RNA delivery. This lack of knowledge significantly reduces the pace at which new and potentially more efficacious compounds can be discovered. Through examination of efficacious and non-efficacious lipids, my research has focused on better understanding the lipid structural motifs important for effective RNA delivery. This knowledge will ultimately allow for more rationally designed lipids in the future, reducing both the time and cost required to develop new delivery agents.

The use of liposomes for RNA delivery has been accomplished primarily with siRNA, thus far. As more mRNA therapeutics are under development, the question arises as to whether LNPs designed for siRNA delivery *in vivo* are also viable for mRNA delivery. While both therapeutics consist of RNA, the difference in molecular size, hybridization, and charge density can potentially alter both the size and structure of the LNP as well as endosomal escape, and overall efficacy. In order to determine whether siRNA optimized LNPs can be used for mRNA delivery as well, we examined the effect of two properties on RNA delivery: the structure of the ionizable lipid, and the composition of the LNP.

Finally, while numerous LNPs have been developed to deliver RNA to hepatocytes *in vivo*, relatively few LNPs exist for delivery to other tissue types. Historically it has been demonstrated that more positively charged nanoparticles have increased biodistribution and efficacy in the lungs. To that end, my research includes efforts to redirect liver-targeted liposomes to the lung through the modification of LNP surface charge. In addition, I examine the role of plasma proteins, profiling the proteins bound to the different LNPs, as well as determining their effect on liposomal efficacy for different cell types.

Chapter 2

Determining the structural motifs required for efficacious ionizable lipids via examination of a degradable, acrylate-based compound library

This chapter contains previously published data:
Whitehead, K. A., Dorkin, J. R., Vegas, A. J., Chang, P. H., *et al.* (2014). Degradable lipid nanoparticles with predictable in vivo siRNA delivery activity. Nature Communications, 5.

Structual Motifs Important to Efficacious Ionizable Lipids

While many efficacious lipids have been developed for siRNA delivery *in vivo*, discovery of these compounds has primarily been achieved through screening large lipid libraries (Akinc et al., 2008, 2009; Love et al., 2010; Mahon et al., 2010). Generating and screening these libraries requires a tremendous amount of time, effort, and resources; furthermore, there is no guarantee that such libraries will contain a compound with improved efficacy or tolerability over the current generation of lipids. The scope and cost of these screens could be dramatically reduced, however, though the implementation of rational design. Establishing which structural motifs aid or hinder in liposomal delivery would allow for the development of smaller lipid libraries while improving the probability of developing a compound with increased efficacy.

Unfortunately, relatively little is known about the structure-function relationship between ionizable lipids and RNA delivery *in vivo*. In order to better examine this relationship, a combinatorial library was designed by Dr. Kathryn Whitehead. This library consisted of 1400 unique compounds, comprised of 280 alkyl-amines (Appendix B), and 5 different tails. The amine cores and lipid tails were combined via Michael addition (Figure 2.1). The relative ease of this synthesis allowed for the generation of such a large library, which ultimately provides more analytical power. In addition, the resulting lipids contain one or more ester groups. Inclusion of an ester groups provides a labile functional group, which can then be hydrolyzed or potentially degraded by the numerous esterases in the body. Thus, in addition to providing information about the correlation between lipid structure and efficacy, we hope to generate a library with better efficacy and improved tolerability over the current generation of lipids.

Combinatorial Library Synthesis and *in vitro* Screening

The 1400 lipids from the combinatorial library were formulated using a previously published composition (Love et al., 2010); the ionizable lipid was combined with 1,2-distearoyl-sn-glycero-3-phosphocholine (DSPC), cholesterol, and 1,2-dimyristoyl-sn-glycero-3-phosphoethanolamine-N-[methoxy(polyethylene glycol)-2000] (DMG-mPEG$_{2000}$) at a molar ratio of 50:10:38.5:1.5 and with an ionizable lipid:siRNA weight ratio of 5:1. For *in vitro* testing, the LNPs were formulated with firefly luciferase siRNA, and applied to HeLa cells expressing both firefly luciferase and *Renilla* luciferase. After treatment, the relative ratio of firefly to *Renilla* luminescence was examined, and 82 compounds demonstrated greater than 50% silencing *in vitro* (Figure 2.2a). Examination of these 82 compounds revealed several structural motifs that were enriched for compared to the initial library. The relative hit rate for a structural motif was determined as the (percentage of compounds with that motif that demonstrated >50% silencing *in vitro*) – (the percentage of compounds with that motif in the original library).

Among the 82 most efficacious compounds from the *in vitro* screen, several structural motifs were over or under represented as compared to the original library. Compounds containing lipid tails that were 12 or 13 carbons long had a relative hit rate increase of 5%, while the C10 tail showed the greatest decrease in hit rate, at -8% (Figure 2.2b). The number of tails in the lipid also demonstrated a correlation with efficacy, with compounds having three or more tails demonstrating a higher hit rate than compounds with only two tails (Figure 2.2c). Various functional groups within the amine core also influenced efficacy, with secondary amines, tertiary amines, alcohols, piperazines, and a

brached core appearing to improve delivery, while ethers, five member rings, and six member rings demonstrated decreased efficacy.

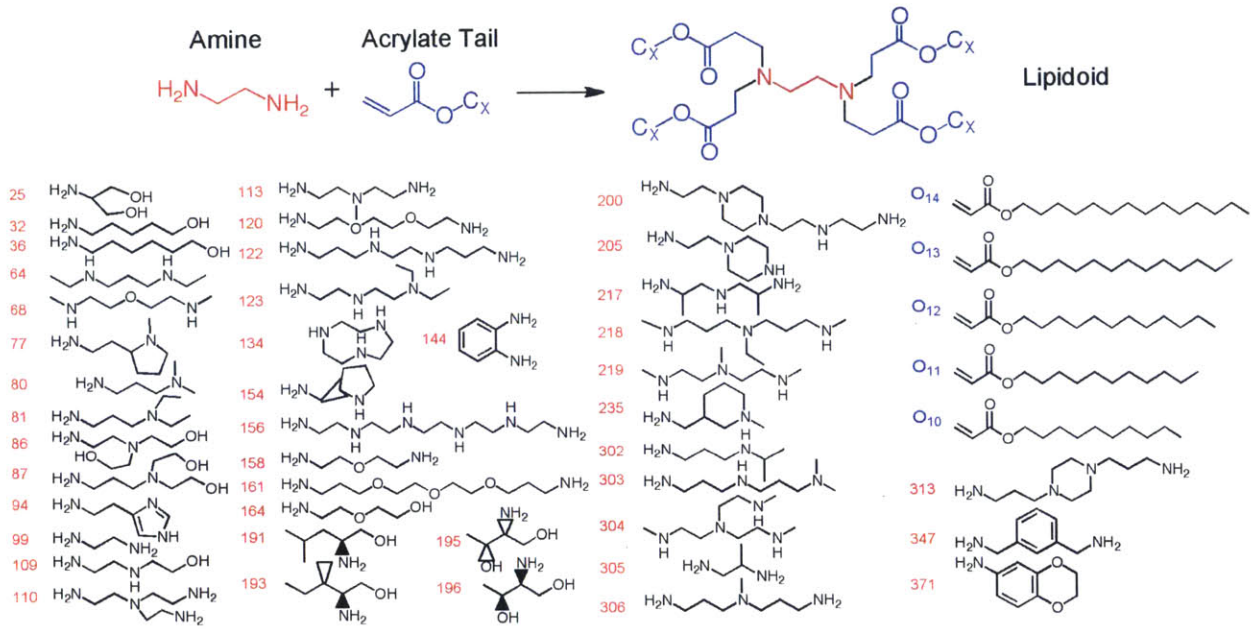

Figure 2.1: Combinatorial library of degradable lipids. A library of ionizable lipids was generated by combining primary and secondary amines with fully saturated poly-carbon acrylate tails via Michael Addition. A portion of the amines used in the library are included, as well as the 5 acrylate tails. (X = 10-14).

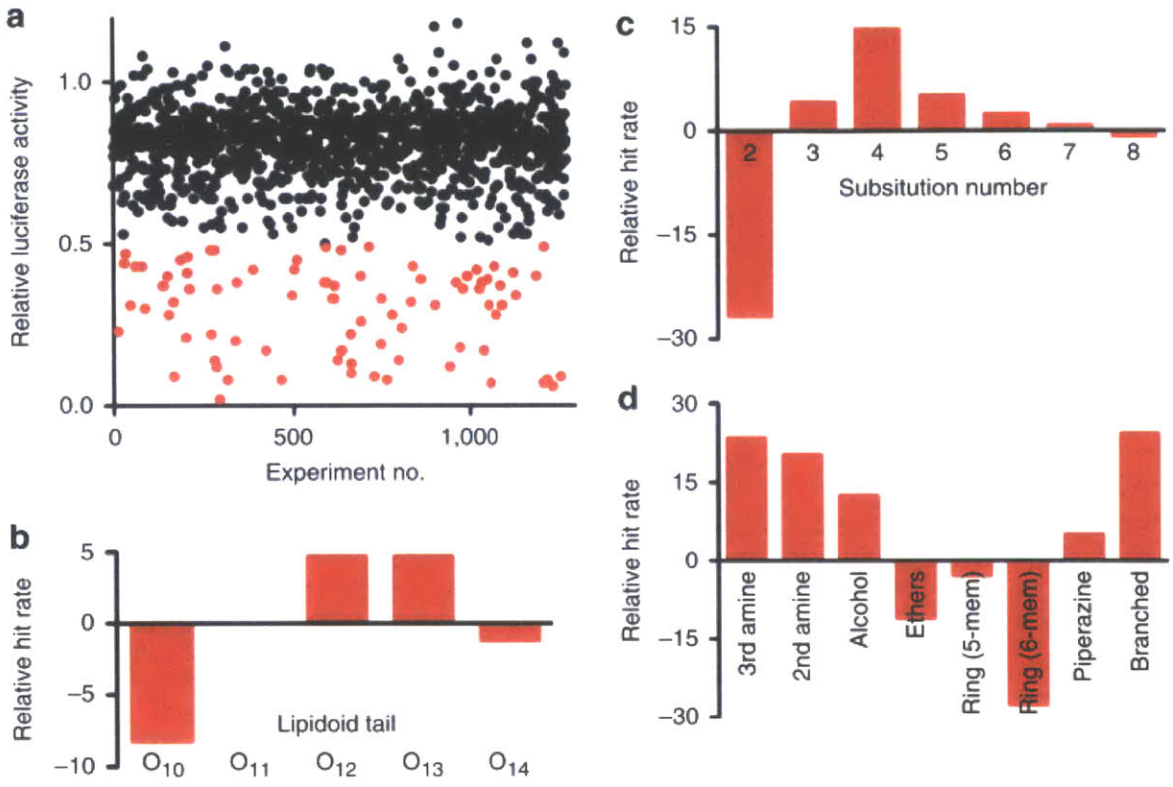

Figure 2.2: *In vitro* LNP efficacy. (a) HeLa cells expressing both firefly and *Renilla* luciferase were treated with LNPs containing anti-firefly luciferase siRNA. 24 hours post administration the relative firefly:*Renilla* luminescence ratio was determined. Compounds demonstrating less than 50% firefly luminescence relative to *Renilla* luminesce are highlighted in red. The relative hit rate of compounds was determined for various structural motifs: (b) the length of their lipid tail, (c) the number of tails in the lipid, and (d) the structure of the amine core.

In vivo Lipid Testing and Formulation Optimization

In order to further evaluate the efficacy of the ionizable lipids, the 82 most efficacious compounds, as well 14 less efficacious compounds, were examined for their capabilities to target hepatocytes for silencing *in vivo*. The LNPs were formulated containing an siRNA sequence that targets protein clotting factor VII (FVII). FVII is produced exclusively by hepatocytes, and therefore any decrease in the observed protein level is a direct indication of siRNA efficacy in hepatocytes; any potential transfection of

alternative tissues is not registered in this assay. In addition, FVII is a secreted protein, which allows for the protein levels to be determined easily, and with minimal invasion, by examining blood samples.

The formulations were injected intravenously at a total siRNA dose of 5 mg kg^{-1}. Of the 96 compounds examined, 15 of them demonstrated >95% FVII silencing two days later (Figure 2.3a). These 15 compounds were subsequently injected at lower doses to determine their EC50s, which determined to range from 0.05 mg kg^{-1} to 2 mg kg^{-1} (Figure 2.3b).

The liposomal formulation was then optimized to determine the maximal level of efficacy. The optimization was performed using the ionizable lipid $304O_{13}$, which had demonstrated an EC50 of 0.1 mg kg^{-1}. Slight variations in the mole percent of DMG-$mPEG_{2000}$ resulted in significant changes in liposomal efficacy, with a 0.25% variation resulting in as much as a three-fold change in EC50. Ultimately the maximal efficacy was observed when using a DMG-$mPEG_{2000}$ mole percent between 0.5% and 1% (Figure 2.3c); the lipid molar ratio of 50: 10.75:38.5:0.75 for the ionizable lipid:DSPC:cholesterol:DMG-$mPEG_{2000}$ was determined to be the considered the optimal formulation for $304O_{13}$, resulting in an EC50 of 0.02 mg kg^{-1} for these LNPs.

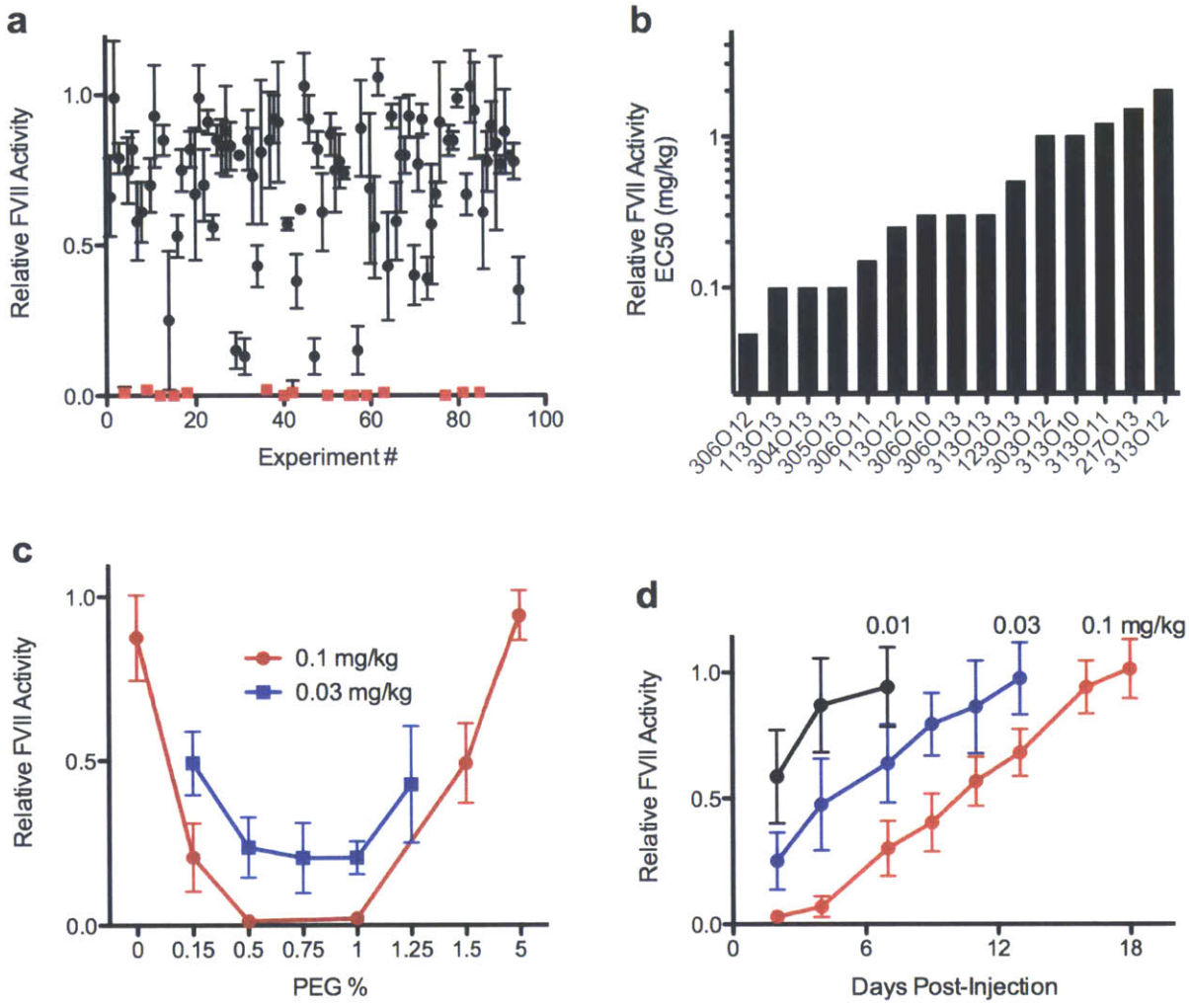

Figure 2.3: *In vivo* LNP efficacy. (a) The 96 most efficacious compounds, as determined from the *in vitro* screen were formulated with anti-FVII siRNA and injected intravenously into mice at a total siRNA dose of 5 mg kg-1. The FVII serum protein levels were determined 48 hours later, and compared relative to a PBS treated group. (b) The 15 top performing ionizable lipids were injected *in vivo* at lower doses to determine their relative EC50s for FVII silencing. (c) The ionizable lipid $304O_{13}$ was formulated with varying mole percents of DMG-$mPEG_{2000}$ and injected intravenously at either 0.1 mg kg^{-1} or 0.03 mg kg^{-1}. (d) The duration of action for the optimized 304O13 LNP was determined for three dose levels: 0.1 mg kg^{-1}, 0.03 mg kg^{-1}, and 0.01 mg kg^{-1}. (Data points represent group mean $\pm$ standard deviation , n=3)

The duration of action was examined for the optimized $304O_{13}$ LNP at three doses: 0.1 mg kg^{-1}, 0.03 mg kg^{-1}, and 0.01 mg kg^{-1}. A single injection of anti-FVII siRNA at a dose of 0.1 mg kg-1 resulted in greater than 95% silencing, with the FVII serum protein levels returning to baseline after 18 days (Figure 2.3d). Regardless of the initial dose, the rate of recovery was comparable.

LNP Biodistribution

In order to determine whether any tissues other than the liver were potentially being transfected by the LNPs, we examined the relative biodistribution of the siRNA. Both formulated and unformulated fluorescently labeled siRNA were injected intravenously. One hour post injection the liver, spleen, kidneys, heart, lungs, pancreas, uterus, ovaries, thymus, muscle, and fat were examined *ex vivo*. The three organs demonstrating the high accumulation of siRNA were the liver, spleen, and kidneys (Figure 2.4a). Unformulated siRNA localized predominantly to the kidneys; 14% of the fluorescence signal was seen in the liver, with 1% in the spleen, and 71% in the kidneys. Formulated siRNA showed dramatically higher levels in the liver and spleen, with 42% of the fluorescent signal seen in the liver, 24% in the spleen, and 18% in the kidneys. Cross sections of the organs were examined to determine the relative localization of the siRNA within the different tissues (Figure 2.4b). A fairly homogenous distribution is observed for the formulated siRNA in the liver, while in the spleen the siRNA appears to be primarily localized to the red pulp. In the kidneys the siRNA seems to permeate the renal cortex; a lack of signal in the rest of the kidney may indicate either difficulty crossing the glomerular basement membrane, or rapid clearance to the bladder once the siRNA passes through the nephron.

Concurrent to examining the biodistribution, we examined the clearance rate of the formulated siRNA, to ensure that the majority of the nanoparticles had been taken up at a one hour time point, and were not in circulation. Fluorescently labeled siRNA was formulated and injected intravenously. Blood was drawn at various time points, and fluorescence in the serum was determined (Figure 2.4c). The earliest observed time point was at 20 seconds, and by 6 minutes only half of the signal remained, demonstrating a rapid clearance of nanoparticles. At one hour post-injection, less than 10% of the initial siRNA remained in circulation, suggesting that the biodistribution observed at a one hour timepoint was indicative of the final nanoparticle distribution.

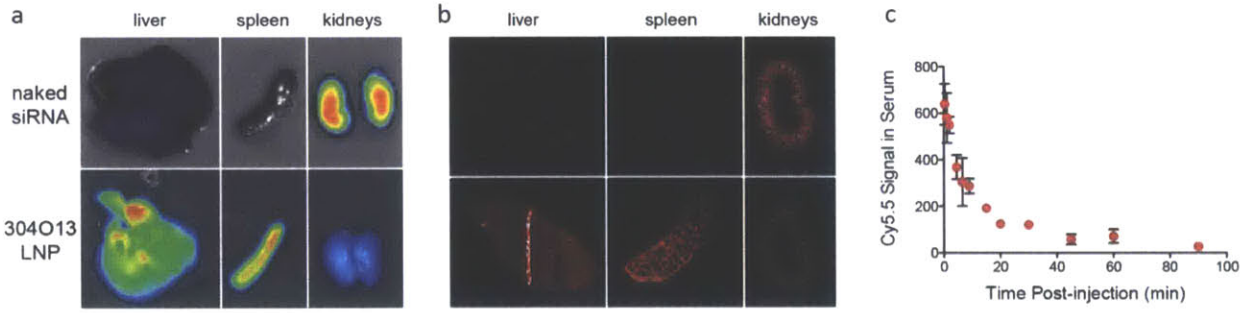

Figure 2.4: LNP biodistribution and pharmacokinetics. (a) Unformulated siRNA (top row) localized primarily in the kidneys (71%), while the LNP formulated siRNA (bottom row) localized primarily to the liver (42%), with some observed in the spleen (24%), and significantly less found in the kidneys (18%). (b) The cross-sections of the tissues reveal disperse distribution of the siRNA in the liver, with splenic siRNA localized primarily in the red pulp, and the siRNA in the kidneys primarily in the renal cortex. (c) (Data points represent group mean $\pm$ standard deviation , n=3)

Ionizable Lipid Structural Analysis

Having successfully optimized the liposomal formulation, and verified the relative tissue targeting of the LNPs, we sought to further investigate which structural motifs of the 96 compounds tested *in vivo*, correlated with a high degree of efficacy (Figure 2.5a). Of

these lipids, 26 (yellow circle) were found to contain O_{13} tails, while 68 of them have 3 or more tails (blue circle), and with respect to the amine core, 44 of them were synthesized from an alkyl-amine containing at least one tertiary amine (red circle). Lipids containing all three properties demonstrated an 88% success rate for a high degree of silencing FVII protein production *in vivo*, while elimination of even one of these criteria resulted in a decrease to only a 17-31% success rate. If two or more of the criteria were not met, FVII silencing was not observed at the tested dose of 5 mg kg^{-1}.

In addition to examining the structural motifs of the individual lipids, the physical characteristics of the formulated LNPs were examined as well. One parameter that demonstrated a strong correlation with efficacy was the pKa of the nanoparticle. The pKa of the LNP has been shown to have a significant effect on the efficacy of the nanoparticle (Jayaraman et al., 2012; Zhang, Fan, Levorse, & Crocker, 2011). Of the LNPs examined, only nanoparticles with a pKa of 5.4 or greater demonstrated a high degree of silencing *in vivo* (Figure 2.5b). When this additional parameter is considered in addition with the three structural motifs previously mentioned, the predictive power becomes even greater; 100% of the compounds that meet all four criteria demonstrated a high level of efficacy *in vivo*.

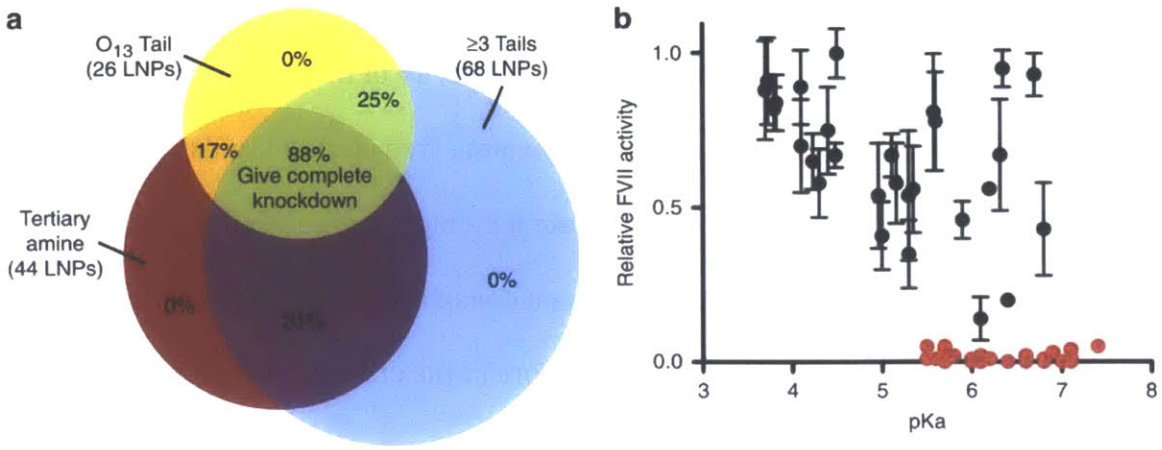

Figure 2.5: Characterization correlating with efficacy. (a) The probability that containing a structural motif will result in >95% silencing *in vivo* at a dose of 5 mg kg^{-1}. (b) The relative *in vivo* FVII silencing of LNPs with respect to their pKa. (Data points represent group mean ± standard deviation , n=3)

Second Generation Library Synthesis and Screening

In order to determine the validity of our hypothesis, a second lipid library was generated. Amine cores containing tertiary amines, and capable of undergoing Michael addition with three or more acrylates, were combined with O_{13} tails to generate a new library of lipids (Figure 2.6a). The lipids were then formulated with anti-FVII siRNA and the pKa was determined. All of the LNPs showed pKa values ≥ 5.4, except for liposomes containing either $509O_{13}$ or $510O_{13}$. We predicted that all of the compounds from the second library, except for $509O_{13}$ and $510O_{13}$, would demonstrate a high degree of silencing *in vivo*. This prediction proved correct; when tested *in vivo* all of the compounds except $509O_{13}$ and $510O_{13}$ demonstrated greater than 95% silencing at a dose of 5 mg kg^{-1} (Figure 2.6b).

As we have demonstrated, we can dramatically improve the probability of synthesizing an efficacious lipid of this type by making sure to include three structural

parameters: the inclusion of a tertiary amine in the amine core, the presence of three or more lipid tails, and using lipid tails that are 13 carbons long. When the initial library of 1400 compounds was generated with no structural parameters, only 15 lipids, roughly 1%, demonstrated a high level of silencing *in vivo*; however, when the second library was designed around these three motifs, greater than 80% of the compounds showed efficient silencing of hepatocytes *in vivo*. When the fourth parameter, the pKa of the LNP, was included, the rate of prediction is raised to 100%. Together, these parameters provide an invaluable tool for the design and screening, markedly reducing the time, cost, and number of animals required to develop new LNPs for therapeutic delivery.

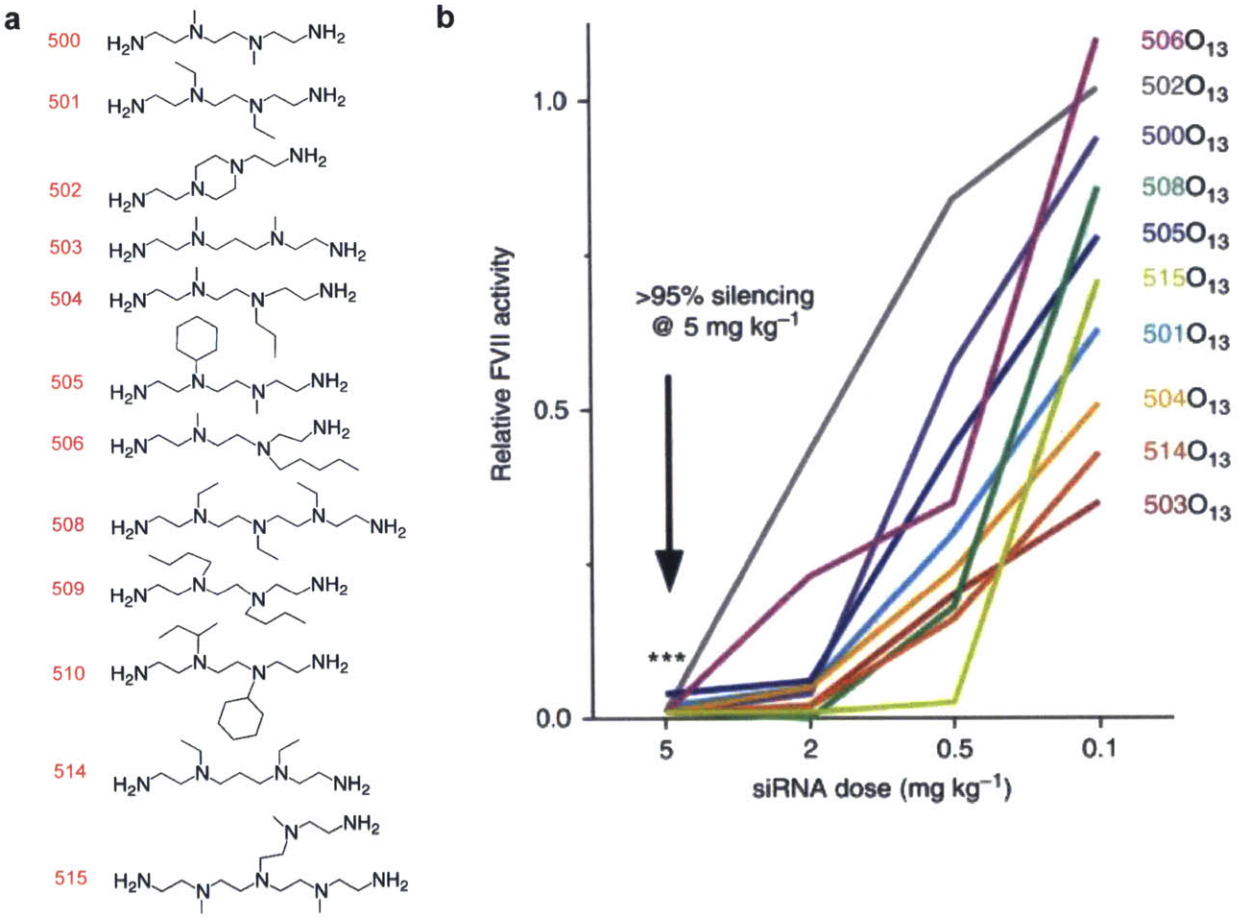

Figure 2.6: The structure and silencing of the rationally designed library. (a) The amine cores combined with O_{13} tails to generate the second library. (b) The dose response curves for the LNPs that fit all four parameters established for high levels of efficacy *in vivo*.

Methods and Materials

Amine-lipid Synthesis. The alkyl-amines for the initial library screen were purchased from Sigma Aldrich, Alfa Aesar, Acros Organics, and CHESS Organics. The acrylates were obtained from Scientific Polymer Products and Hampford Research, Inc. For the 500 series, the alkyl amines were synthesized by reacting secondary amines with sodium cyanide to form nitriles. These nitriles were then reduced to primary amines by using lithium aluminum hydride (Gamage et al., 2001). The amine-lipids were synthesized by combining

the alkyl-amines with the acrylates and stirring for 3 days at 90°C. *In vitro* experiments were conducted using the crude material, while *in vivo* experiments were performed using either crude material, or material that had been purified using a Teledyne Isco Chromatography system.

LNP Formulation. The LNPs were formulated using an ionizable lipid, cholesterol (Sigma Aldrich), DSPC (Avanti Polar Lipids), and DMG-mPEG$_{2000}$ (Alnylam Pharmaceuticals); the lipids were combined at a molar ratio of 50:38.5:(11.5-X):X respectively in 90% ethanol and 10% 10mM sodium citrate buffer, pH 3, comprising the organic phase. Unless otherwise stated in the text, X = 1.5. The aqueous phase consisted of the siRNA dissolved in a solution of 10mM sodium citrate buffer, pH 3. Equal volumes of the organic and aqueous phases were mixed using a microfluidics device (Chen et al., 2012), and immediately diluted with a two-fold volume of 1X PBS, pH7.4. The lipidoid:siRNA weight ratio was 5:1, unless otherwise stated in the text. After formulation the particles were dialyzed against 1X PBS, pH 7.4, for at least 90 minutes.

***In vitro* transfection.** HeLa cells stably modified to express both firefly and *Renilla* luciferase (American Type Culture Collection, Manassas, VA) were seeded in a white 96-well plate at a density of 15,000 cells per well. Cells were transfected at a concentration of 40nM of formulated anti-firefly luciferase siRNA (Dharmacon). Firefly and *Renilla* luciferase were determined using a Dual-Glo Luciferase Assay kit (Promega).

***In vivo* silencing.** All animal experiments were conducted with the approval of the Institutional Animal Care and Use Committee (IACUC). Female C57BL/6 mice at least 6 weeks of age (Charles River Laboratories) were injected intravenously via the tail vein with either PBS, naked siRNA, or siRNA formulated LNPs. The siRNA sequence for FVII provided by Alnylam Pharmaceuticals may be found in Appendix A. Two days post injection blood was obtained from the mouse, and the FVII levels in the serum were determined using a Biophen FVII kit (Aniara Corporation).

Biodistribution. LNPs were formulated with siRNA that had been labeled with Cy5.5 on the 5'-end of the sense strand (provided by Alnylam Pharmaceuticals). Female C57BL/6 mice were injected with the LNPs at a dose of 1 mg kg^{-1} of total siRNA; 1 hour post injection, the mice were euthanized and the organs were removed and imaged using an IVIS system (Calipur Life Sciences).

Blood clearance. LNPs formulated with Cy5.5-labelled siRNA was injected at a dose of 0.5 mg kg^{-1} into female C57BL/6 mice via the tail vein. Blood samples were collected at the various time points via the retroorbital vein, except for the final time point which was collected via a cardiac puncture. The serum was isolated from the samples, and was imaged and quantified using an Odyssey CLx imaging system (LI-COR Biosciences).

Nanoparticle characterization. The total concentration of siRNA and the percent of entrapped siRNA were determined using the Quant-iT RiboGreen RNA assay (Invitrogen).

Particle sizes were determined using a ZETAPals analyzer (Brookhaven Instruments). Zeta potential measurements are acquired on a Zetasizer Nano ZS (Malvern).

pKa measurements. The pKa of the LNPs were determined as previously described (Heyes, Palmer, Bremner, & MacLachlan, 2005). Briefly, solutions of 20mM sodium phosphate, 25mM citrate, 20mM ammonium acetate, and 150mM NaCl were titrated to a series of pHs ranging from 2 to 12. These solutions were aliquoted into a black 96-well flat bottom plate in quadruplicate. The LNPs and TNS were added to each of the wells such the final concentrations were 20μM and 6μM respectively. The fluorescence of each well was determined using a Tecan plate reader and using an excitation wavelength of 322nm and an emission wavelength of 431nm.

Chapter 3

Examining the role of apolipoproteins on efficacy and cellular uptake using novel lipopeptide based LNPs

This chapter contains data previously published:
Dong, Y., Love, K. T., Dorkin, J. R., Sirirungruang, S., *et al.* (2014). Lipopeptide nanoparticles for potent and selective siRNA delivery in rodents and nonhuman primates (vol 111, pg 3955, 2014). *PNAS*, 111(15), 5753.

Overview

While the analysis of the degradable lipid library in Chapter 2 elucidates some of the structural motifs and characteristics important for LNP delivery, it provides limited information as to the mechanism of action. Although historically it has been postulated that hepatocellular delivery of LNPs is primarily size dependent, it has been demonstrated that localization to the liver by nanoparticles <100nm in size is insufficient for the successful transfection of hepatocytes *in vivo* (Santel et al., 2006; Semple et al., 2010). Recent publications have provided evidence that apolipoprotein E is essential for hepatocellular delivery *in vivo* (Akinc et al., 2010; Bisgaier, Siebenkas, & Williams, 1989; Yan et al., 2005), but only a small subset of apolipoproteins and isotypes have been examined thus far. In this chapter we examine a larger subset of apolipoproteins, determining both their effect on hepatocellular delivery, and determine their role in cellular uptake.

The investigation into the apolipoprotein modulated delivery was performed using a novel lipid library developed by Dr. Yizhou Dong. This library was designed around the use of amino acids and dipeptides as the ionizable core of the lipopeptide. By structuring the compound around a biocompatible core, the idea was to create a compound that would be degradable by the cell, thus reducing the toxicity and improving the therapeutic window.

Lipopeptide Iterative Screening

A series of small lipid libraries were generated and tested in an iterative manner in order to reduce the amount of time and resources required to analyze a larger combinatorial library screen. The initial library consisted of only 60 compounds, combining

each of the 20 amino acids with three different lipid tails (Figure 3.1); each lipid tail consisted of a fully saturated twelve carbon long tail with either a terminal aldehyde (A12), acrylate (O12), or epoxide group (E12) to allow for the addition to the amine groups on the lipopeptide core. For the liposomal formulation, the lipopeptides were combined with cholesterol, DSPC, and DMG-mPEG2000 using a lipid molar ratio of 50:38.5:10:1.5, and with a lipid to siRNA weight ratio of 5:1. As with the acrylate-based library, siRNA targeting the serum protein FVII was used for *in vivo* formulation in order to select for liposomes that successfully targeted hepatocytes. Of the initial 60 lipopetides that were examined, only thirteen LNPs demonstrated any siRNA entrapment (Appendix C); the rest of the LNPs were discarded, and were not tested in any further capacity. The thirteen formulations with entrapped siRNA were then injected *in vivo* at a dose of 1 mg kg^{-1}. Of the 13 LNPs injected, only one of the lipopeptides tested, K-E12, demonstrated greater than 50% silencing. (Figure 3.2 series 1)

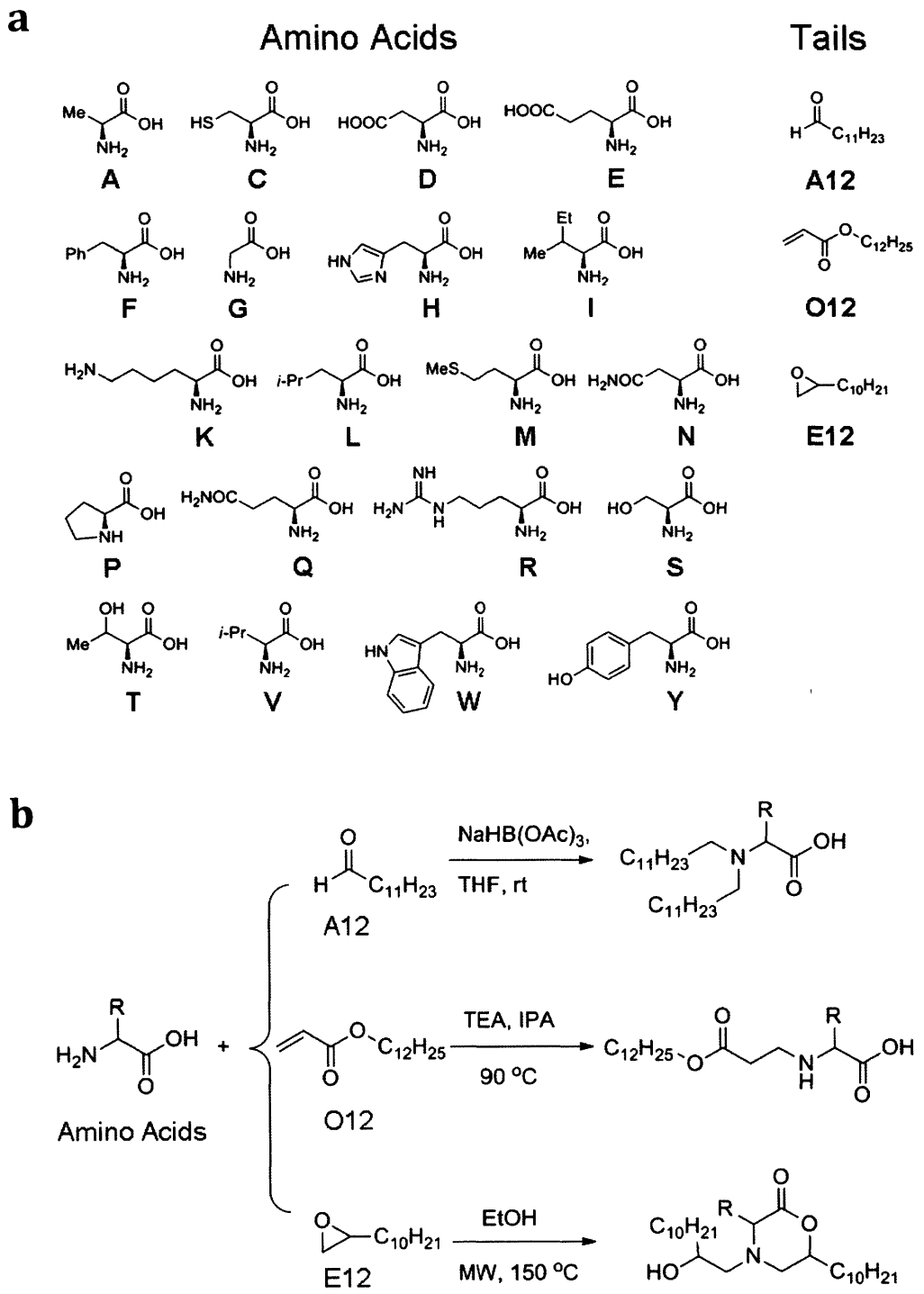

Figure 3.1: Structure and synthesis of lipopeptides. (a) 20 different amino acids and 3 different lipid tails were examined for the initial libraries. (b) Single amino acids were combined with either aldehydes, acrylates, or epoxides to produce the lipopeptides.

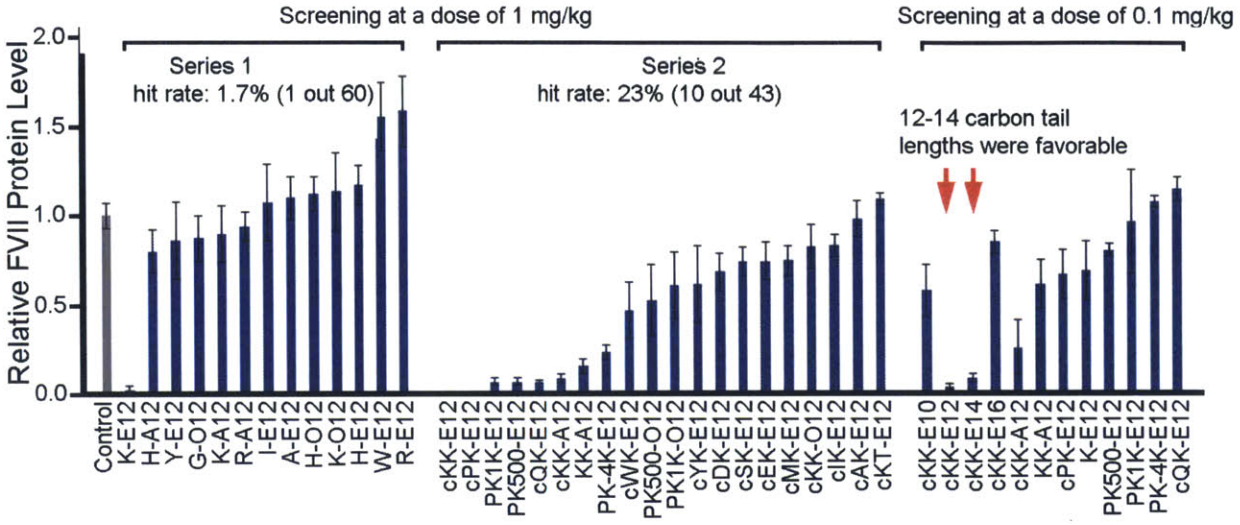

Figure 3.2: Lipopeptide silencing *in vivo*. Lipopeptide formulate anti-FVII siRNAs were injected intravenously in mice. The FVII serum levels were examined 48 hour later and compared relative to a PBS control group. (Dosing was based on entrapped siRNA concentrations; Data points represent group mean ± standard deviation , n=3)

Due to the efficacy of the lysine based lipopeptide, a second library was generated using dipeptide or polypeptide cores containing lysine (Figure 3.3a). For a subset of the dipeptides, a cyclization was performed to produce the diketopiperizine (Figure 3.3b). In total, 43 compounds were generated for the second library, 20 of which were capable of forming stable particles with entrapped siRNA (Appendix C). These LNPs were then injected intravenously at a dose of 1 mg kg^{-1}; 10 of the LNPs injected displayed greater than 50% FVII silencing, with 8 compounds showing more than 80% silencing (Figure 3.2 series 2).

In order to further differentiate between the more efficacious compounds, LNPs demonstrating greater than 80% silencing were re-injected at a dose of 0.1 mg kg^{-1} (Figure 3.2). cKK-E12 demonstrated the greatest degree of silencing, with more than 95% protein

silencing at this dose. The cKK dipeptide was also then combined with lipid tail lengths of C10, C14, and C16 to determine whether the efficacy could be further improved upon, however cKK-E12 demonstrated the maximal degree of silencing. The dose response curve of cKK-E12, demonstrated an EC50 of approximately 0.003 mg/kg (Figure 3.4), making cKK-E12 the most efficacious compound reported for siRNA delivery to date.

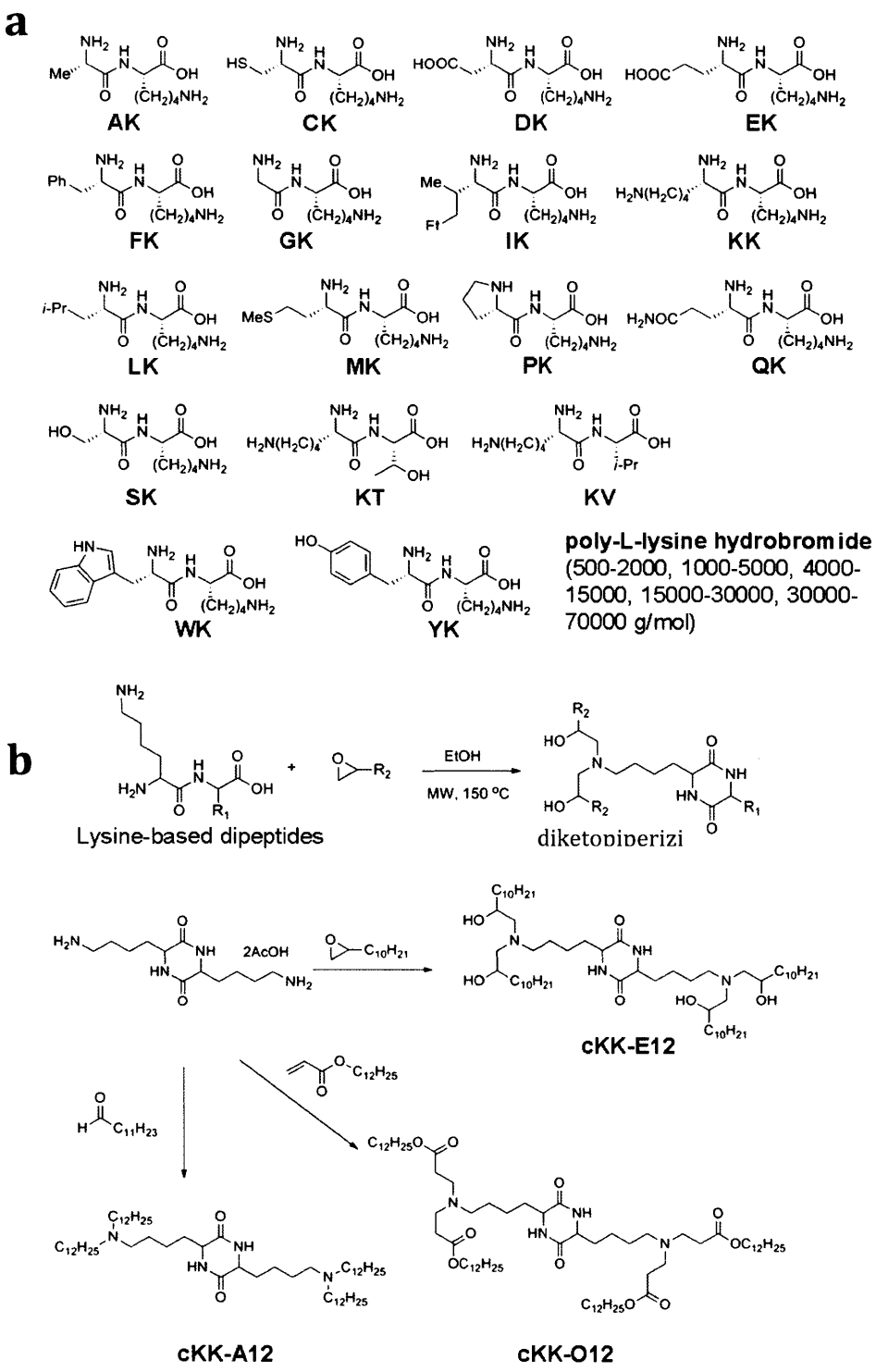

Figure 3.3: Dipeptide and poly-peptide based lipids. (a) For the second library dipeptides containing at least one lysine residue were examined, as well as poly-L-lysines varying in size from 500-70000 g mol^{-1}. (b) A cyclization was performed on the dipeptides to produce the diketopiperizine.

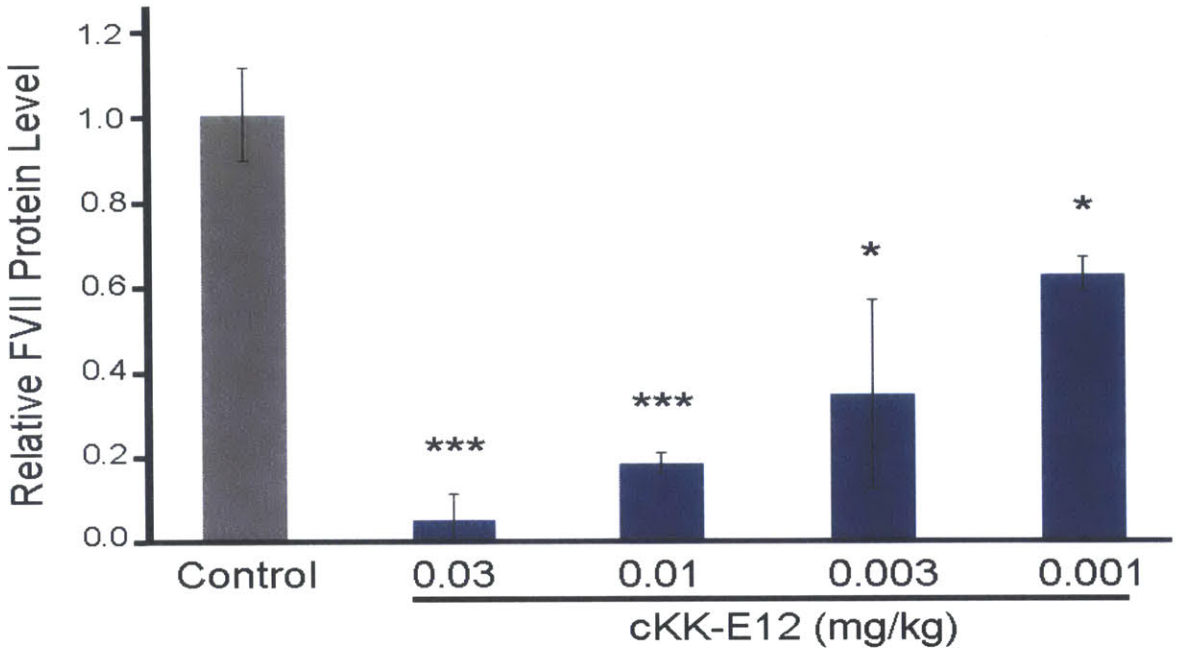

Figure 3.4: Dose response curve for cKK-E12. FVII serum levels were examined 48 hour later and compared relative to a PBS control group. (Dosing was based on entrapped siRNA concentrations; Data points equal group mean ± standard deviation, n= 3 or 4; *, $P < 0.05$; **, $P < 0.01$, ***, $P < 0.005$; t-test, double-tailed)

Lipopeptide Biodistribution

In order to verify that the liver is the primary target of the lipopeptide based LNPs, a biodistribution assay was performed. Both formulated and unformulated Cy5.5-labeled siRNA were injected intravenously, and the fluorescent signals of the tissues were determined *ex vivo* one hour post injection (Figure 3.5). The formulated siRNA demonstrated a greater than 40% increase in liver biodistribution over the unformulated siRNA, with none of the other tissues demonstrating any significant increase in signal.

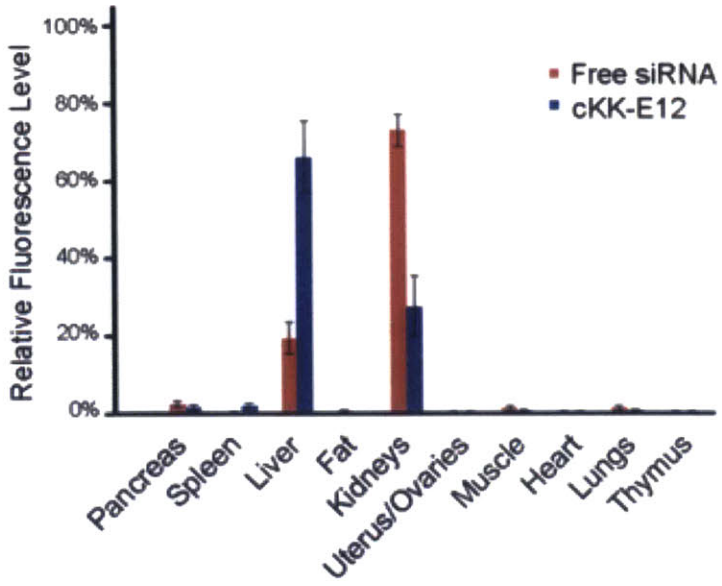

Figure 3.5: siRNA biodistribution. Formulated and unformulated Cy5.5 labeled siRNA were injected I.V. at a dose of 1 mg kg-1. Tissues were examined *ex vivo* 1 hour post injection. (Data points equal group mean ± standard deviation, n= 3)

An orthogonal experiment was performed to verify the tissue specificity of the cKK-E12 based LNPs. The lipopeptide was formulated with a siRNA targeting phosphate and tensin homolog (Pten), which is found in all cell types. The LNPs were injected systemically at a dose of 0.1 mg kg^{-1} entrapped siRNA. The Pten mRNA levels were determined for six tissue types the liver, lung, spleen, kidney, heart, and brain, and were normalized to the mRNA levels of glyceraldehyde 3-phosphate dehydrogenase (GAPDH in those tissues, another ubiquitous protein. Of the six organs examined, only the liver displayed any significant silencing of the Pten (Figure 3.6a). In a subsequent experiment, after an intravenous injection of 0.1 mg kg^{-1} Pten targeted siRNA, the liver was removed, and the hepatocytes, endothelial cells, and immune cells were separated. The relative Pten mRNA levels were detected for each cell type, and again normalized against the GAPDH mRNA levels. The vast majority of Pten silencing occurred in hepatocytes, with no significant

changes in Pten mRNA levels observed for either the endothelial cells or the immune cells (Figure 3.6b).

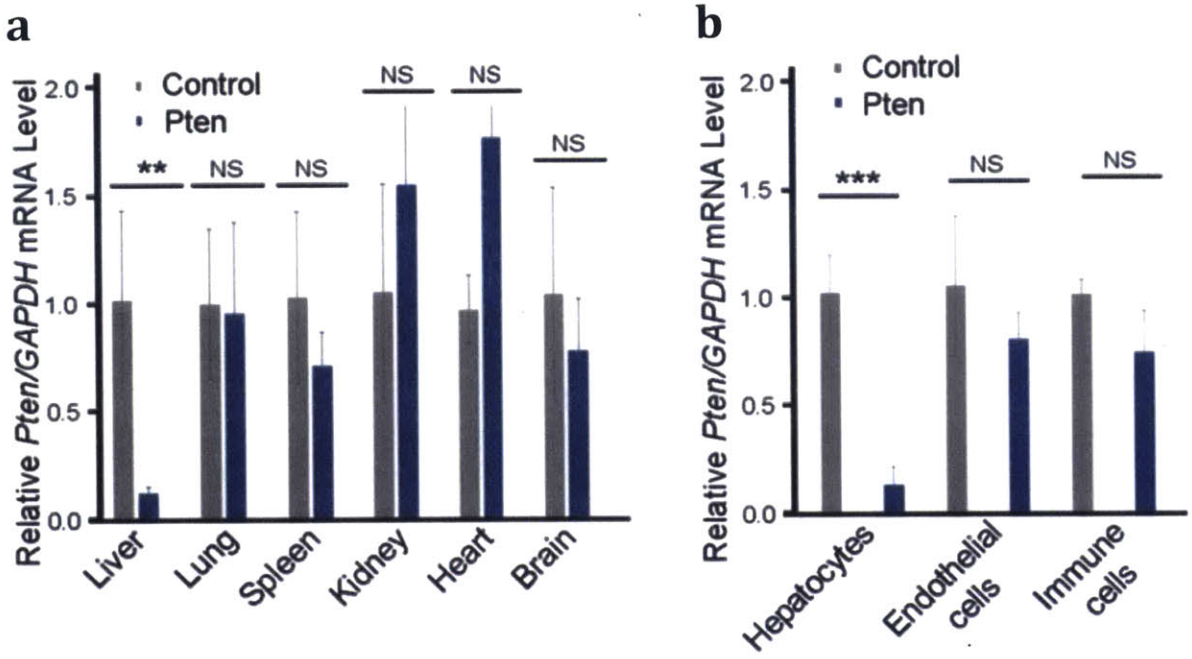

Figure 3.6: Tissue and cellular LNP specificity. (a) cKK-E12 LNPs containing anti-Pten siRNA were injected at a dose of 0.1 mg kg-1. Pten levels were normalized to endogenous GAPDH levels, and graphed relative to control mice injected with formulated anti-luciferase siRNA. (b) The liver tissue of mice treated with formulated anti-Pten siRNA was examined *ex vivo* to determine the relative silencing in each cell type. (Data points equal group mean ± standard deviation, n= 3 or 4; *, $P < 0.05$; **, $P < 0.01$, ***, $P < 0.005$; t-test, double-tailed)

The Effect of Apolipoproteins on LNP Cellular Uptake and siRNA Expression

To examine whether the presence of lipoproteins modifies the efficacy of the LNPs, an anti-firefly luciferase siRNA was formulated with cKK-E12 and incubated with one of eleven different lipoproteins. The LNP was then added to HeLa cells expressing both firefly and *Renilla* luciferase, and the relative expression levels were determined 24 hours later. With the exception of apolipoprotein (Apo) B none of the apolipoproteins resulted in any

decrease in cell viability. While less than 20% luciferase silencing was observed for LNPs co-incubated with apolipoproteins A-I, A-II, or H, about 30% silencing was observed for the three isoforms of ApoC, and approximately 70% silencing was observed for all four isoforms ApoE (Figure 3.7). ApoE aids in the clearance of lipoprotein remnants (Yan et al., 2005), including Chylomicrons, VLDL, IDL, and LDL, providing a potential mechanism of action for hepatocellular uptake of the LNP.

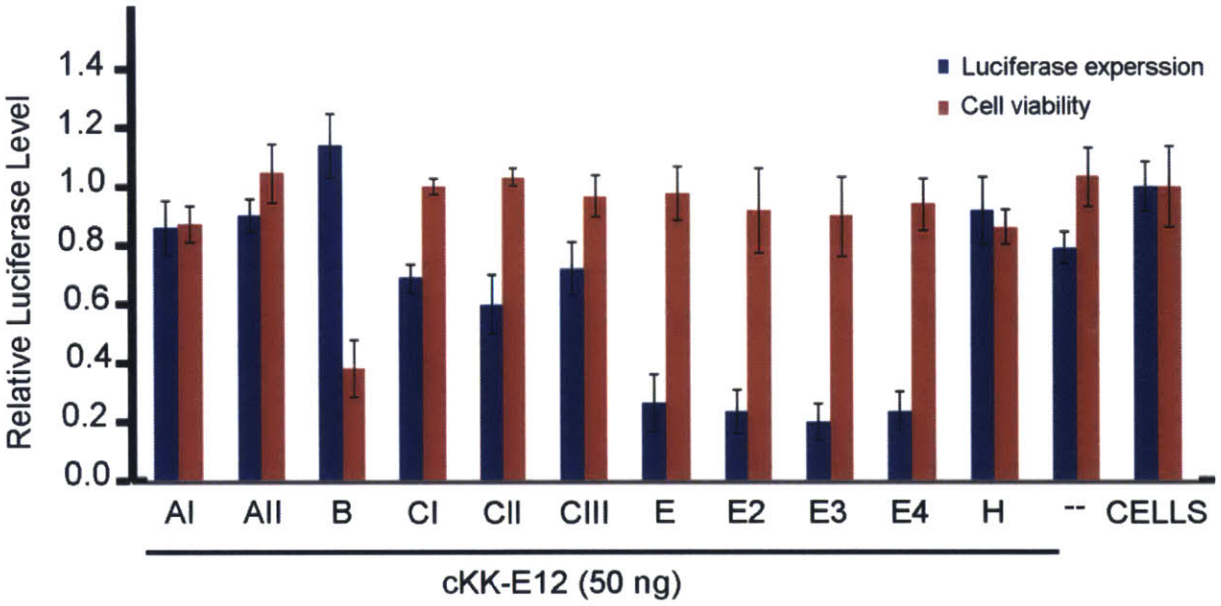

Figure 3.7: Lipoprotein effect on LNP silencing. LNP formulated anti-firefly luciferase was applied to HeLa cells expressing firefly and *Renilla* luciferase, with or without the presence of apolipoproteins. The ratio of firefly luminescence to *Renilla* luminescence was determined and compared relative to untreated cells. (Data points equal group mean ± standard deviation, n=4)

To observe the effect that ApoE has on cellular uptake and localization, cells were treated with cKK-E12 formulated Alexa-647-labeled siRNA either with or without ApoE. While some siRNA can be observed in the cells treated without ApoE, far greater signal is observed in cells where ApoE is present (Figure 3.8a). In order to determine the method of

cellular uptake, LNPs containing the fluorescently labeled siRNA were incubated with ApoE and one of three fluorescently labeled cellular uptake markers: dextran, CTX-B, or transferrin. Dextran is a fluid-phase uptake marker, indicative of macropinocytosis, while CTX-B is a marker for clatherin mediated endocytosis, and transferrin is a marker for cavleolae mediated endocytosis. Co-localization of the siRNA with one of the cellular uptake markers indicates a potential route of entry. HeLa cells were examined under the three conditions, and subsequent imaging demonstrated the greatest co-localization of siRNA with dextran, suggesting that the LNPs are taken up by macropinocytosis (Figure 3.8b). In order to confirm the mechanism of cell uptake, LNPs containing Alexa-647-labeled siRNA were again co-incubated with ApoE, and were applied to cells either alone, or in the presence of either dynasore, a dynamin inhibitor, or 5-N-ethyl-N-isoproamiloride (EIPA), a macropinocytosis inhibitor. While cells incubated with LNPs and ApoE demonstrated siRNA uptake, addition of either dynasore or EIPA dramatically reduced cellular uptake; this provides additional evidence to suggest that the mechanism of action for ApoE mediated LNP uptake is in fact macropinocytosis.

LNP Delivery in ApoE and LDLR Knockout Mice

To determine whether ApoE effects LNP delivery to hepatocytes *in vivo*, LNPs containing anti-FVII siRNA were injected in wild-type mice, as well as ApoE knockout mice, and low density lipoprotein receptor (LDLR) knockout mice. ApoE is a constituent of lipoprotein remnants *in vivo*, including very low density lipoporteins (VLDL), intermediate density lipoproteins (IDL), and low density lipoproteins, (LDL). Previous research had indicated the LDLR as important for LNP delivery to hepatocytes (Akinc et al., 2010), which

is why the LDLR knockout strain was selected for testing. Greater than 80% silencing was observed for the LNPs injected into wild-type mice, however no silencing was observed in ApoE knockout mice, providing additional evidence that ApoE is essential for the lipopeptide efficacy *in vivo*. (Figure 3.9) Silencing for the LDLR knockout mice, however, demonstrated the same level of silencing as the wild-type mice, indicating that either LDL particles containing ApoE are not the primary mediator for LNP uptake *in vivo*, or that the uptake pathway for the LNPs is redundant, relying on multiple ApoE containing lipoproteins for cellular uptake *in vivo*.

Through the iterative use of library screens, we were able to successfully generate a lysine based lipopeptide that, when formulated in an LNP, demonstrates siRNA delivery capability to the hepatocytes equal to, or greater than anything currently published. Analysis of the mechanism of action highlights the important role that lipoproteins play on cellular uptake and expression of LNP formulated siRNA. ApoE, and to a lesser extent ApoC, aid in the cellular uptake and expression of the LNPs. *In vivo*, ApoE is found on lipoprotein remnants of chylomicrons, VLDL, IDL, and LDL, while ApoC is found primarily on HDL, chylomicrons, and VLDL. This suggests that either VLDL or chylomicrons may aid in hepatocellular delivery of the lipopeptide nanoparticle. This evidence is supported by the silencing data from wild type, ApoE knockout, and LDLR knockout mice. While the loss of ApoE resulted in a concurrent loss in hepatocellular silencing, mice that lacked the LDL receptor showed silencing levels comparable to that of wild type mice. This emphasizes that ApoE is required for LNP delivery of siRNA to the liver, while suggesting that the lipoprotein remnant involved is not LDL, but rather chylomicrons, VLDL, or IDL particles.

While the lipoprotein binding may aid in delivery in multiple ways, it is clear that lipoprotein binding is important for cellular uptake. Imaging techniques have demonstrated that ApoE is required for cellular uptake, and that the internalization proceeds through a macropinocytosis pathway.

By better understanding the role that endogenous lipoproteins play on cellular uptake and liposomal efficacy, we can potentially alter the biodistribution and expression of the RNA formulated LNPs through modulating their composition and surface chemistry to increase, or decrease, binding to various serum proteins.

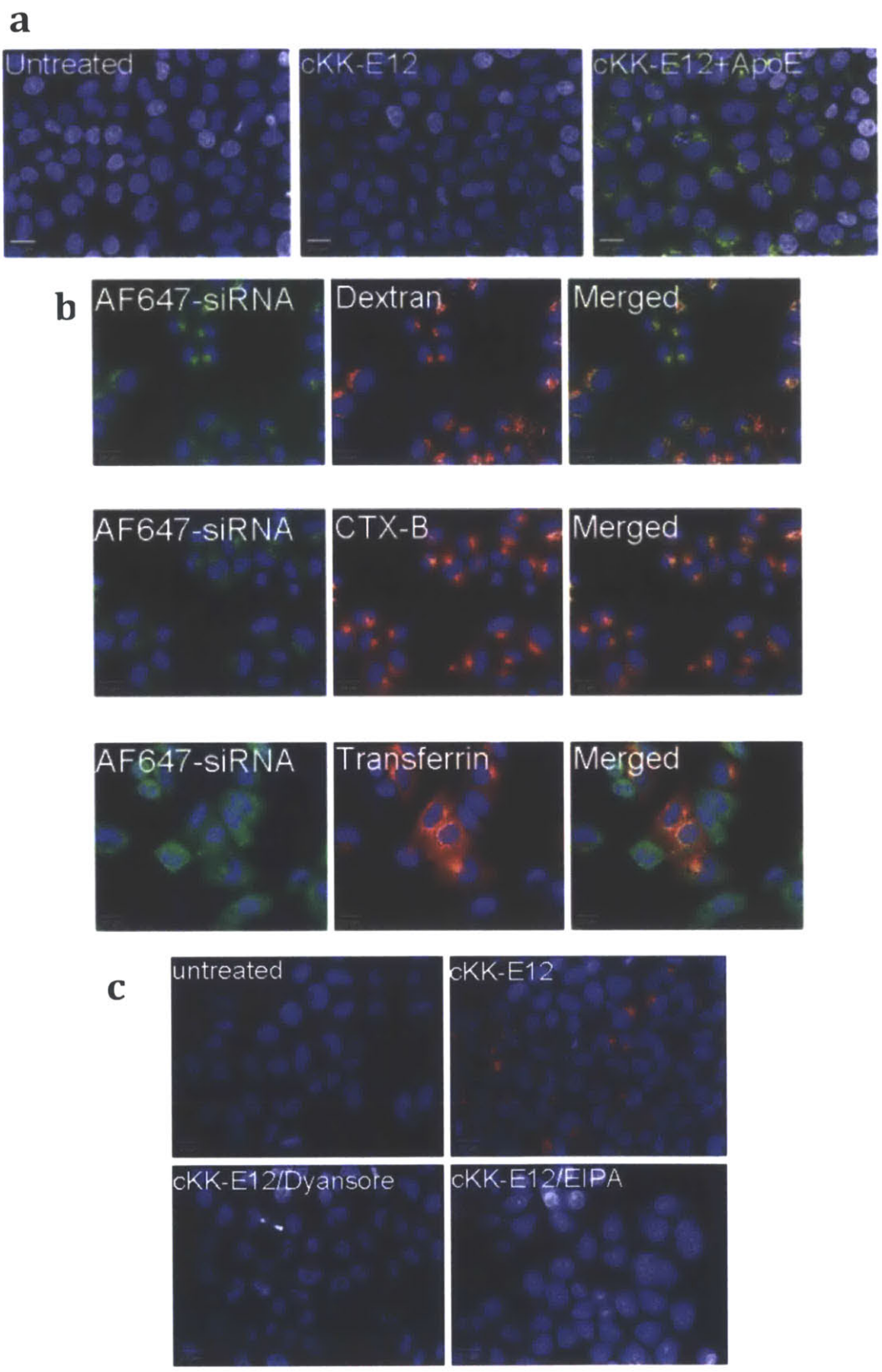
a
Untreated
cKK-E12
cKK-E12+ApoE
b
AF647-siRNA
Dextran
Merged
AF647-siRNA
CTX-B
Merged
AF647-siRNA
Transferrin
Merged
c
untreated
cKK-E12
cKK-E12/Dyansore
cKK-E12/EIPA

Figure 3.8: LNP cellular uptake *in vitro*. (a) Co-administration of LNPs containing fluorescently labeled siRNA and ApoE resulted in an increase in cellular uptake, as compared to administration without ApoE. Nuclei stained with Hoescht. (b) Formulated fluorescently labeled siRNA was co-incubated with ApoE and either fluorescently labeled Dextren, CTX-B, or Transferrin. Nuclei stained with Hoescht. (c) HeLa cells were treated with ApoE co-incubated with LNPs containing fluorescently labeled siRNA either alone or in the presence of Dynasore or EIPA. Untreated cells were included as a negative control. Nuclei were stained with Hoescht. (scale bar = 20 μm)

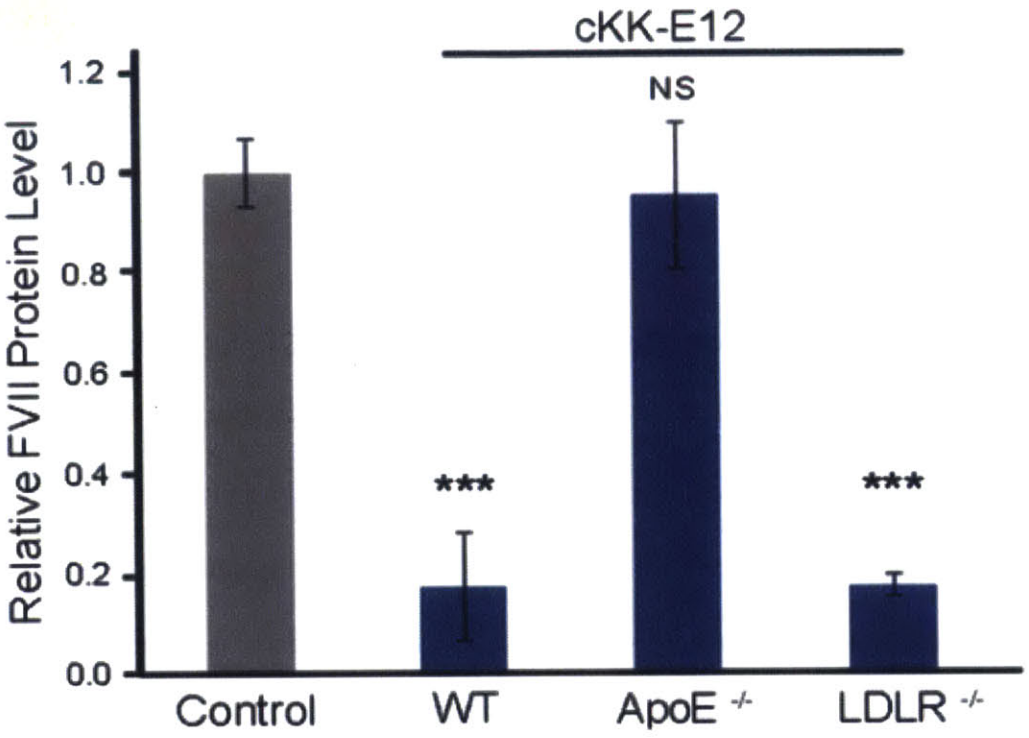

Figure 3.9: Silencing in wild type (WT), ApoE knockout and LDLR knockout mice. Mice were injected intravenously with formulated anti-FVII siRNA, and their FVII serum levels were compared 48 hours later. Mice lacking ApoE demonstrate a significant loss in silencing, while mice lacking the LDL receptor showed silencing comparable to wild type mice. (Data points equal group mean ± standard deviation, n = 3; ***P < 0.005; NS, not significant; t test, double- tailed). Control, PBS; WT, wild type)

Methods and Materials

General procedures for lipopeptide synthesis. To generate the aldehyde based lipopeptides, the amine cores were dissolved with the aldehyde tails at a molar ratio of 1:3 in THF. Sodium triacetoxyborohydride was added to the solution and allowed to stir for

three days at room temperature. The final product was purified via flash column chromatography (Isco Combiflash systems). The acrylate based lipopeptides were generated by combining the amine cores with the acrylate tails in a 1:3 molar ratio and dissolving them in isopropanol or acetonitrile with triethyl amine. The solution was stirred for 2 days at 90°C and purified via flash column chromatography. For the synthesis of epoxide based lipopeptides, the amine cores and epoxide tails were dissolved in ethanol at a molar ratio of 3:1 and irradiated in a microwave oven (Biotage Initiator) at 150°C for 5 hours. The reaction mixture was then purified by flash chromatography.

Liposomal Formulation. LNPs were formulated using a 50:10:38.5:1.5 lipid molar ratio of lipopeptide:DSPC:cholesterol:DMG-mPEG$_{2000}$, at a 5:1 lipopeptide to siRNA ratio. The lipids were dissolved in an ethanol solution, while the siRNA was dissolved in a 10mM citrate buffer, pH 3. Using a microfluidics device the lipids and siRNA were combined in a 1:1 volume ratio, and the subsequent mixture was immediately diluted in a 1:2 volume ratio with PBS, as has previously been described (Chen et al., 2012). The siRNA sequences for FVII, luciferase, Pten, and GFP-Alexa-647 provided by Alnylam Pharmaceuticals can be found in Appendix A.

***In vivo* LNP delivery in mice.** All experiments involving animals were appoved by the IACUC and in accordance with local, state, and federal regulations. Female C57BL/6 mice (Charles River Labs, 6 to 8 weeks, 18-22 grams), *apoE-/-* mice (Jackson Laboratories, C57BL/6 background, 6 to8 weeks old, 18-22 grams) and *LDLR-/-* mice (Jackson Laboratories, C57BL/6 background, 6 to 8 weeks old, 18-22 grams) were injected

intravenously via the tail vein for all systemic administrations. Mice were anaesthetized using isofluorane and blood was obtained using a retroorbital bleed. Serum was obtained from the samples using serum separator tubes (BD biosciences). FVII protein levels were determined using a chromogenic assay (Biophen FVII, Aniara Corporation). Mice used for the control groups were injected with 1X PBS.

Analyzing mRNA levels in tissues. Mice were sacrificed via CO2 asphyxiation 48 hours post injection. The lungs, liver, heart, and kidneys were removed and immediately frozen in liquid nitrogen. The frozen tissues were pulverized and the tissue lysates were prepared using Tissue and Cell Lysis buffer (Epicentre) supplemented with 0.5 mg ml^{-1} Proteinase K (Epicentre). mRNA levels were determined using a branched DNA assay (QuantiGene 2.0 Reagent System, Affymetrix). mRNA levels were compared to endogenous GAPDH mRNA levels, and normalized to PBS injected control groups.

Cellular Internalization Assays. HeLa cells were seeded at 1.5 x 10^4 cells per well in a black 96-well plate (Greiner Bio-one). Cells were incubated with 50ng of formulated Alexa-647-labeled siRNA with or without 1μg of ApoE per well for 3 hours. Incubation time for the labeled markers varied based on their internalization rates. Oregon Green Dextran (300 μg mL^{-1}, marker for macropinocytosis) was co-incubated for 3 hours, Alexa 488 labeled Transferrin (1 μg mL^{-1}, marker for clatherin mediated endocytosis) was co-incubated for 15 minutes, and Alexa 488 labeled Cholera Toxin B (10μg mL^{-1}, marker for caveolae mediated endocytosis) was co-incubated for 30 minutes with the LNPs. Cells were washed, fixed, and counterstained in OPTIMEM containing Hoscht (2 μg mL^{-1}) for nuclei

identification. Cell imaging was performed with an automated spinning disk confocal microscope (OPERA, Perkin Elmer) with a 40X objective. 20 fields from each well were examined to eliminate bias and provide a statistically significant number of cells for analysis.

***In vitro* transfection with apolipoproteins.** HeLa cells expressing firefly and *Renilla* luciferase were seeded in a white opaque 96-well plate (Corning). The following day the cells were transfected with 50ng of formulated anti-firefly luciferase siRNA; all treatments were done in quadruplicate. Apolipoproteins (Fitzgerald Industries) were incubated with LNPs for 5 minutes before addition to the cells. After 24 hours incubation at 37°C, 5% CO_2, cells were analyzed for luciferase expression using Dual-Glo assay kits (Promega). To visualize cellular uptake, LNPs were formulated with Alexa-Fluor 647-labeled siRNA and incubated with HeLa cells for 3 hours. Cells were then fixed in 4% paraformaldehyde, permeabilized with 0.1% saponin and stained with Hoescht. All images were acquired using a spinning disc confocal microscope (OPERA, Perkin Elmer), and data were analyzed using Acapella Software (Perkin Elmer).

Chapter 4

Optimizing LNPs for mRNA delivery to the liver

This chapter contains previously published data:
Kauffman, K. J., Dorkin, J. R., *et al.* (2015). Optimization of Lipid Nanoparticle Formulations for mRNA Delivery in Vivo with Fractional Factorial and Definitive Screening Designs. *Nano Lett.*, 15 (7300-7306).

Formulation Optimization Parameters

While a considerable amount of work has been performed developing LNPs for siRNA delivery, only recently have lipid nanoparticles been investigated as possible *in vivo* delivery vectors for mRNA. Although the structural compositions of siRNA and mRNA are very similar, differences in their size, charge density, chemical modifications, and strand hybridization can have a dramatic effect on their physical properties (Janas, Janas, & Yarus, 2006; Vlassov, Khvorova, & Yarus, 2001). Because of these differences, liposomal formulations that have been optimized for siRNA may not be optimal for mRNA. In order to determine which liposomal characteristics, if any, vary for mRNA and siRNA delivery, we took a liposomal formulation developed for siRNA delivery, and attempted to optimize it for mRNA delivery by varying both the lipid composition and lipid molar ratio.

The formulation selected for optimization was developed for siRNA delivery to hepatocytes, with a lipid composition of C12-200, DSPC, cholesterol, and DMG-mPEG2000 in a 50:10:38.5:1.5 molar ratio, and a 5:1 weight ratio of C12-200 to siRNA (Table 1, original formulation). This formulation has been demonstrated to successfully deliver anti-FVII siRNA to hepatocytes *in vivo* with an EC50 of only 0.01 mg kg^{-1} in mice (Love et al., 2010). While many parameters influence the efficacy of the liposome, we chose to focus on three in particular: the structure of the phospholipid in the formulation, the molar ratio of the lipid composition of the LNP, and the weight ratio of C12-200 to the mRNA.

The phospholipid's structure influenced the formation and stability of the lipid membrane. Phospholipids with a large polar head group and fullly saturated lipid tails tend to be more cylindrical in shape (Figure 4.1a), and are capable of stacking together in in flat sheets to form lipid bilayers, resulting in the more stable lamellar phase (Figure 4.1b)

(Deamer, Leonard, Tardieu, & Branton, 1970). Lipids with a small polar head groups and unsaturated tails are more conical in shape (Figure 4.1c), and tend to organize in inverted micellar structures, comprising the less stable inverted hexagonal (H_{II}) phase (figure 4.1d) (Takahashi, Sinoda, & Hatta, 1996). While inclusion of phospholipids promoting the lamellar phase can increase liposomal stability during circulation, the inclusion of phospholipids promoting the (H_{II}) phase can destabilize both the liposomal membrane and the endosomal membrane, markedly increasing the release of RNA from the nanoparticle into the cytoplasm (Zhigaltsev, Maurer, Wong, & Cullis, 2002). In order to examine the effect of the phospholipid structure on the efficacy of the nanoparticle, four phospholipids were included in the library: 1,2-distearoyl-sn-glycero-3-phosphocholine (DSPC), 1,2-dioleoyl-sn-glycero-3-phosphocholine (DOPC), 1,2-distearoyl-sn-glycero-3-phosphoethanolamine (DSPE), and 1,2-dioleoyl-sn-glycero-3-phosphoethanolamine (DOPE). (Figure 4.2) Of the four lipids, DSPC is the most cylindrical in nature, due to the relatively large head group of the phosphocholine and the presence of fullly saturated tails; the lipid in the group that is least cylindrical and most conical in nature is DOPE, due to the relatively small size of the phosphoethanolamine group and the kinked nature of the unsaturated tails, with the structure of DOPC and DSPE falling somewhere in between the two.

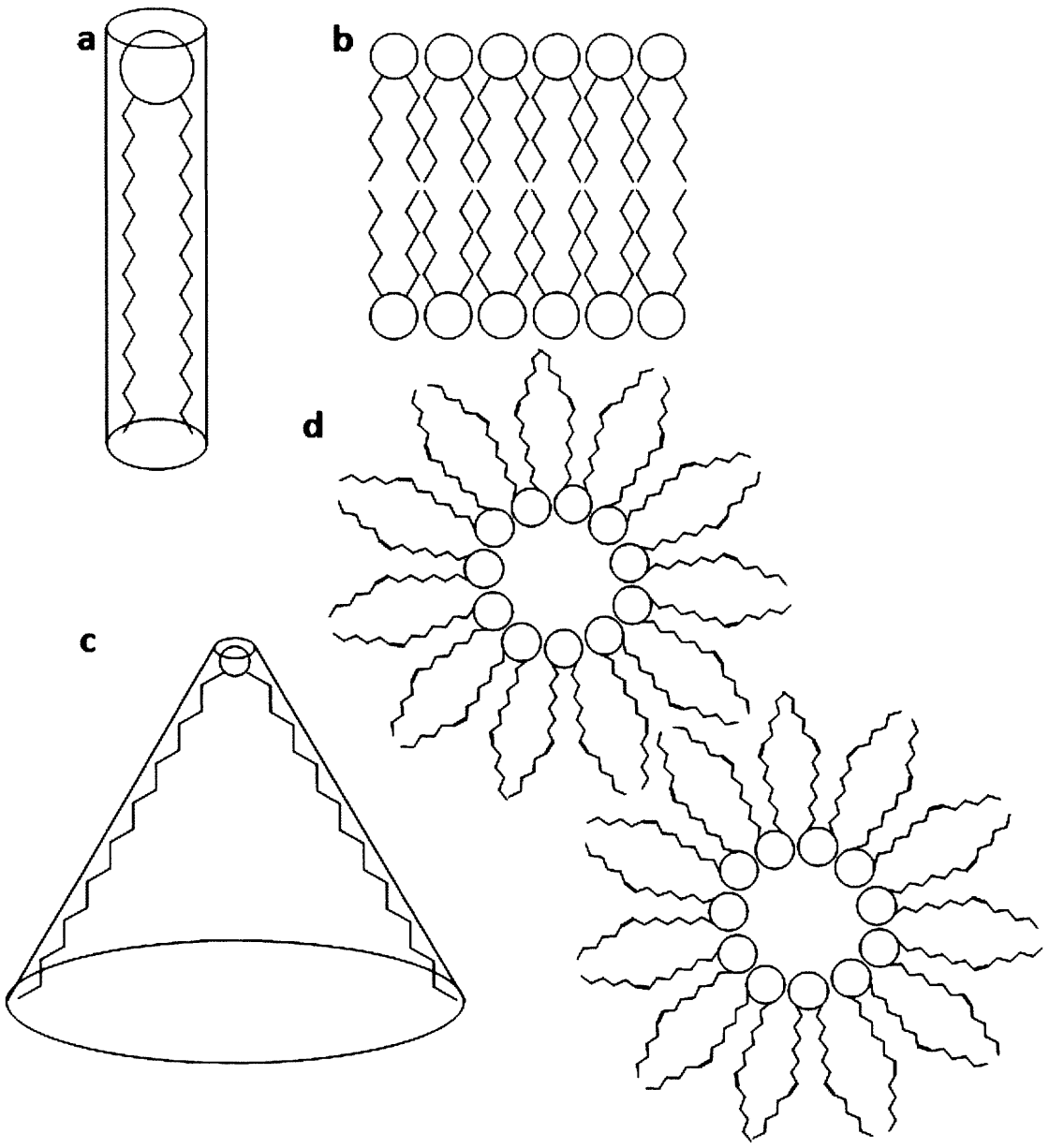

Figure 4.1: Phospholipid structure and membrane formation. (a) A cylindrical phospholipid tends to organize in the more stable (b) lamellar phase. (c) A conical lipid promotes the formation of the less stable (d) inverted hexagonal phase.

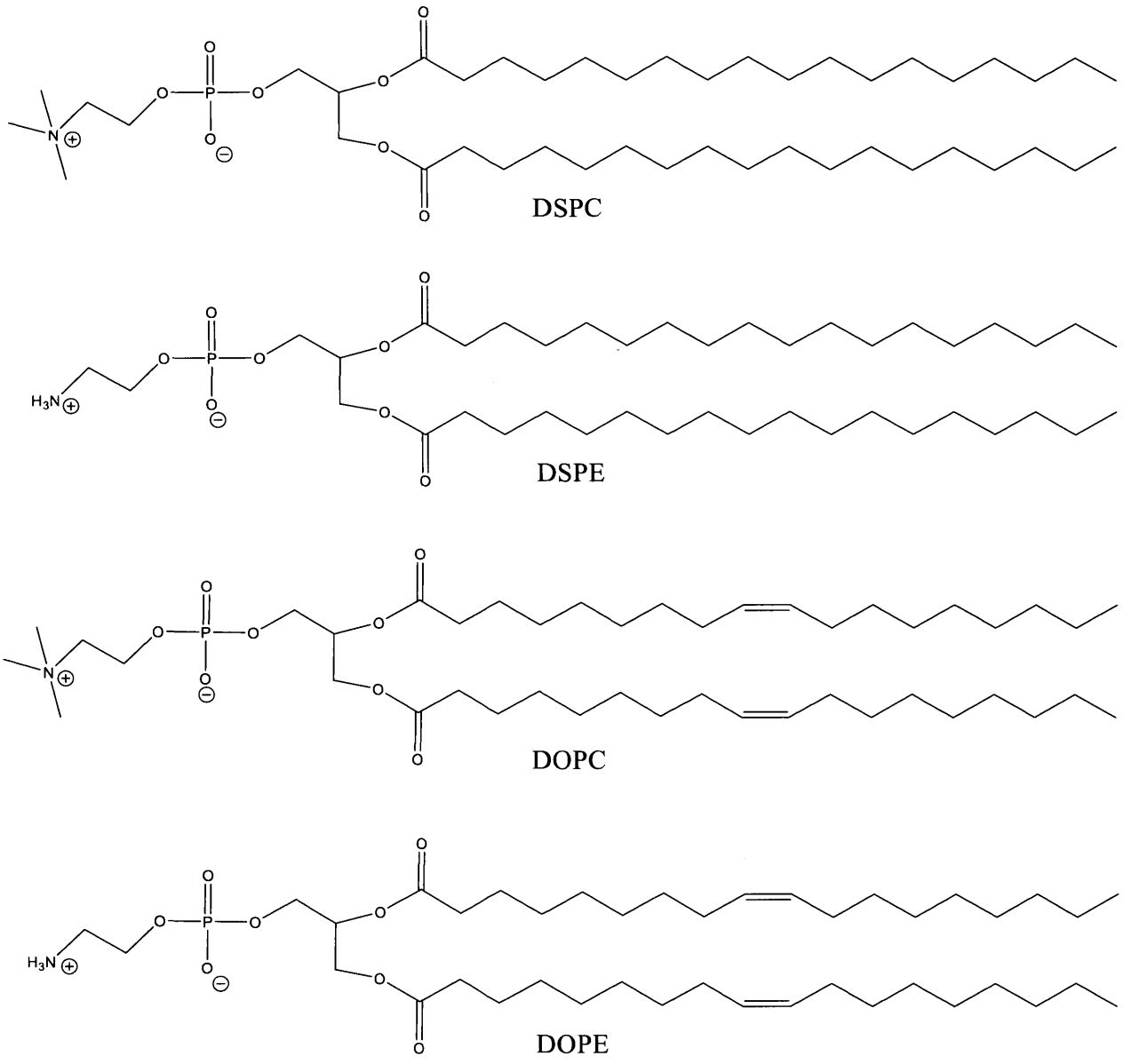

Figure 4.2: Phospholipid Structure. Four phospholipids were examined for optimized mRNA delivery. The phospholipids vary in structure, with DSPC having the most cylindrical shape and DOPE having the most conical shape.

Modulating the lipid molar ratio of the formulation can markedly alter the efficacy of LNPs through a variety of ways. Varying the mole percent of the lipid-anchored PEG can

change the size and circulation time of the LNPs (Bao et al., 2013; Belliveau et al., 2012) as well as reduce hemolysis and clearance by the immune cells (Kanasty et al., 2013). Even a small change in the molar percentage of the lipid-anchored PEG can have a profound effect on the efficacy, with less than a 0.5% difference capable of altering the EC_{50} by an order of magnitude (K. A. Whitehead et al., 2014). The molar percentage of cholesterol can have a dynamic role on membrane stability, promoting either the lamellar or H_{II} phase, depending on concentration (Takahashi et al., 1996). This in turn can have a significant effect on drug encapsulation and release from the LNP (Zhigaltsev et al., 2002).

In addition to varying the phospholipid structure and lipid molar ratio, we chose to examine the effect of altering the ionizable lipid to RNA weight ratio. Increasing this ratio has been demonstrated to improve efficacy to a point, after which diminishing returns are observed (Akinc et al., 2009). Since much of the toxicity stems from the lipid dose of the formulated therapeutic, it is important to establish the minimal lipid to RNA ratio that maximizes the efficacy of the formulation in order to ensure the largest therapeutic window.

Due to the number of parameters being modified for the optimization process, testing a complete combinatorial library would be impractical. Previous experiments have shown a poor correlation between *in vitro* and *in vivo* data (K. A. Whitehead et al., 2012), suggesting that to find the optimized LNP for mRNA delivery, all of the formulations would need to be examined *in vivo*. Testing such a large number of LNPs *in vivo* is financially prohibitive, and extraordinarily time consuming. As an alternative to testing every combination individually, we elected to use a statistically relevant design of experiment (DOE) to determine which parameters positively affect the efficacy while using significantly

fewer data points. By using fractional factorial and definitive screening designs, we can still determine the most significant first order and second order effects to establish an optimized LNP for mRNA delivery.

To evaluate the efficacy of mRNA delivery to hepatocytes, mRNA coding for human erythropoietin (EPO) was selected. EPO is naturally synthesized and secreted by the kidneys into the blood stream, where its primary role is to upregulate red blood cell production in the bone marrow. Human EPO mRNA was chosen as the target mRNA for several reasons. Since EPO is a secreted protein, the relative degree of mRNA delivery can be readily determined by examining the EPO levels in the serum. Human EPO is also structurally different enough from endogenous murine EPO such that serum levels of human EPO can be determined by an enzyme-linked immunosorbent assay (ELISA) without signal interference from endogenous murine EPO. EPO also has relevance as a therapeutic protein, capable of treating patients suffering from anemia.

LNP Parameter Screening in vivo

In order to establish a baseline of efficacy from which to optimize, EPO mRNA was formulated using the siRNA optimized LNP composition (Table 4.1). The LNPs were injected intravenously at a dose of 15ug of total RNA per mouse, and at six hours post injection, the EPO protein level in the serum was determined to be 963 $\pm$ 141 ng mL^{-1}.

For the initial library, fourteen formulations were examined within a given range of parameters (Table 1, Library A and Appendix D). The specific formulation conditions within the given parameter space were selected by generating a $3^4 \times 2^2$ definitive screening design, using 4 three-level quantitative factors (C12-200 to RNA weight ratio, C12-200

mole %, phospholipid mole %, and DMG-mPEG2000 mole %) and 2 two-level qualitative factors, one for the phospholipid tail group (disteroyl versus dioleoyl), and one for the phospholipid head group (phosphocholine versus phosphoethanol amine). Of the fourteen LNPs in Library A, two of them produced EPO levels higher than that of the original formulation: formulation A-02 with an EPO level of 6445 $\pm$ 1237 ng mL^{-1}, and A-09 with an EPO level of 2072 $\pm$ 302 ng mL^{-1} (Figure 4.3a).

Table 4.1: Composition parameters for each of the formulation libraries tests

	Lipid mole percent					
	C12-200	Phospho-lipid	Cholesterol	DMG-$mPEG_{2000}$	C12-200: RNA	Phospho-lipid
siRNA optimized formulation	50	10	38.5	1.5	5	DSPC
Library A	40-60	4-16	29.5-55.5	0.5-2.5	2.5-7.5	DSPC, DOPC, DSPE, DOPE
Library B	30-40	16-28	28.5-51.5	2.5-3.5	7.5-12.5	DSPC, DOPE
Library C	35	16	46.5	2.5	5-25	DOPE
mRNA optimized formulation	35	16	46.5	2.5	10	DOPE

From Library A, several parameters were modified or eliminated to generate Library B (Table 1). Of the four phospholipids tested, DSPE was eliminated as a possibility as it proved insoluble at a concentration relevant for formulation, and DOPC was eliminated, as no formulation containing that phospholipid demonstrated any improvement over the original LNP; only DSPC and DOPE were examined in the second library. Since both A-02 and A-09 contained both lipid molar percentages and a C12-200 to

RNA weight ratio that were at the edge of the conditions tested, the parameters were shifted to follow the trends.

Using these boundry criteria an L18-Taguchi fractional factorial design (Rao, Kumar, Prakasham, & Hobbs, 2008) was used to generate the formulations in Library B (Appendix D). Of the eighteen formulations in Library B, eleven demonstrated efficacy higher than that of the original formulation (Figure 4.3b). The single strongest predictor of efficacy was the inclusion of DOPE, with all of the formulations containing DOPE outperforming the formulations containing DSPC (Figure 4.3c). In addition, a second order effect between the presence of DOPE and increasing the weight ratio of C12-200 to RNA was observed. In order to further examine this second order effect, a third and final library, Library C, was generated, using the same lipid composition and molar ratio as formulation B-26, while varying the lipid to RNA weight ratio (Table 4.1). The efficacy of the formulations can be seen to increase proportionally with the C12-200 to RNA weight ratio, until a weight ratio of 10 to 1 is achieved (Figure 4.3d). Beyond this point, no significant increase in efficacy is observed. Due to the potential for increased toxicity for higher levels of lipid doses, the C12-200 to RNA weight ratio of 10 to 1 was selected as the optimal ratio, making formulation C-35 the optimized formulation for mRNA delivery *in vivo*. The formulation C-35 contains C12-200, DOPE, Cholesterol, and DMG-mPEG$_{2000}$ at a molar ratio of 35:16:46.5:2.5 with a C12-200 to mRNA weight ratio of 10:1. At a dose of 15 μg of mRNA injected intravenously, this results in an EPO serum level of 7065 ± 513 ng mL^{-1}, seven times higher than the original siRNA optimized formulation.

a

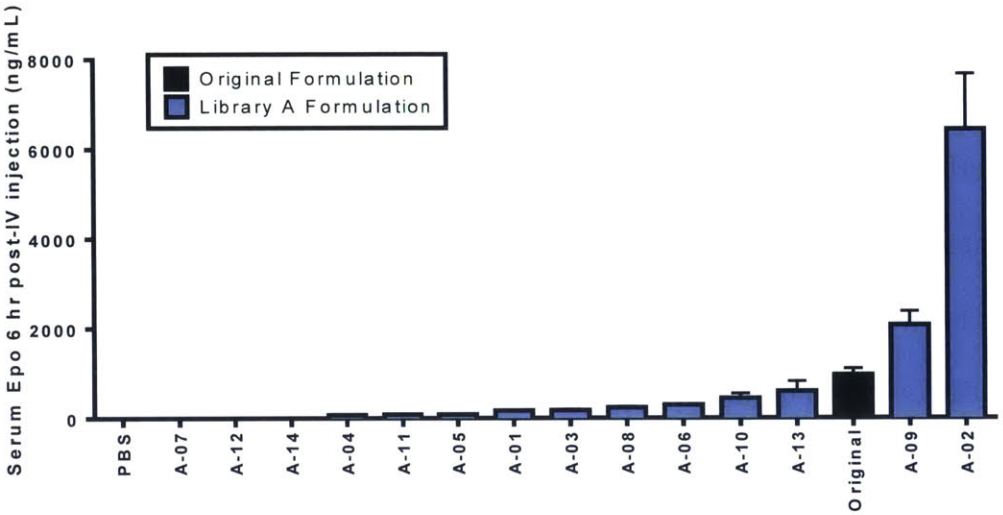
Serum Epo 6 hr post-IV injection (ng/mL)
8000
6000
4000
2000
0
Original Formulation
Library A Formulation
PBS
A-07
A-12
A-14
A-04
A-11
A-05
A-01
A-03
A-08
A-06
A-10
A-13
Original
A-09
A-02

b

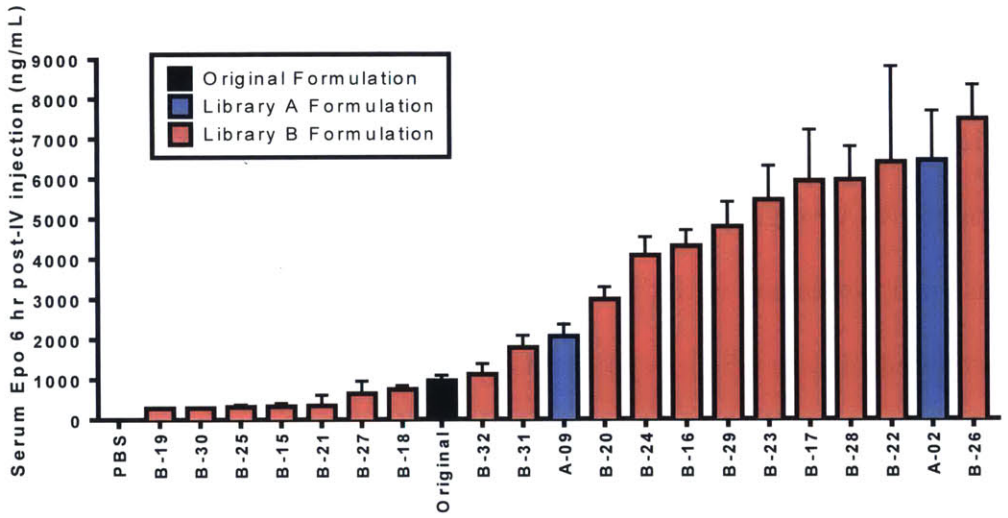
Serum Epo 6 hr post-IV injection (ng/mL)
9000
8000
7000
6000
5000
4000
3000
2000
1000
0
Original Formulation
Library A Formulation
Library B Formulation
PBS
B-19
B-30
B-25
B-15
B-21
B-27
B-18
Original
B-32
B-31
A-09
B-20
B-24
B-16
B-29
B-23
B-17
B-28
B-22
A-02
B-26

c

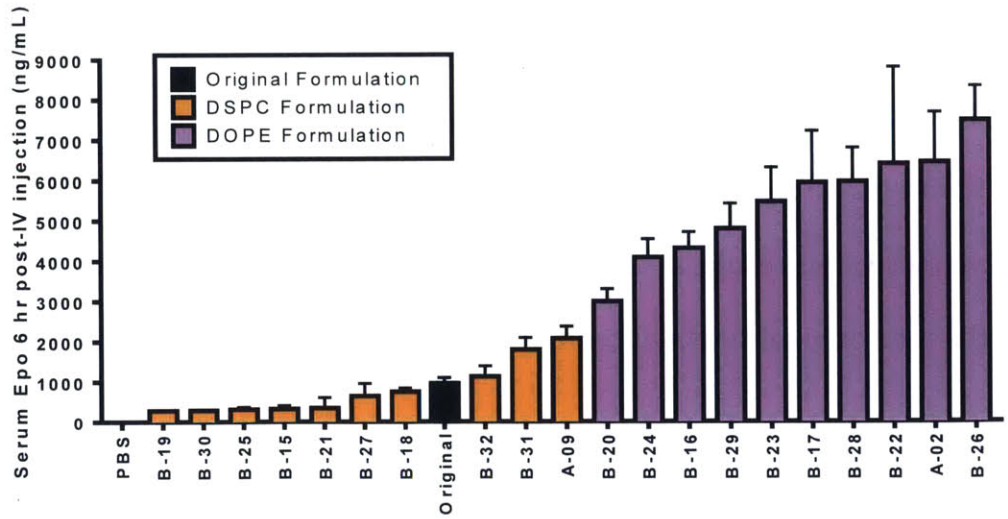
Serum Epo 6 hr post-IV injection (ng/mL)
9000
8000
7000
6000
5000
4000
3000
2000
1000
0
Original Formulation
DSPC Formulation
DOPE Formulation
PBS
B-19
B-30
B-25
B-15
B-21
B-27
B-18
Original
B-32
B-31
A-09
B-20
B-24
B-16
B-29
B-23
B-17
B-28
B-22
A-02
B-26

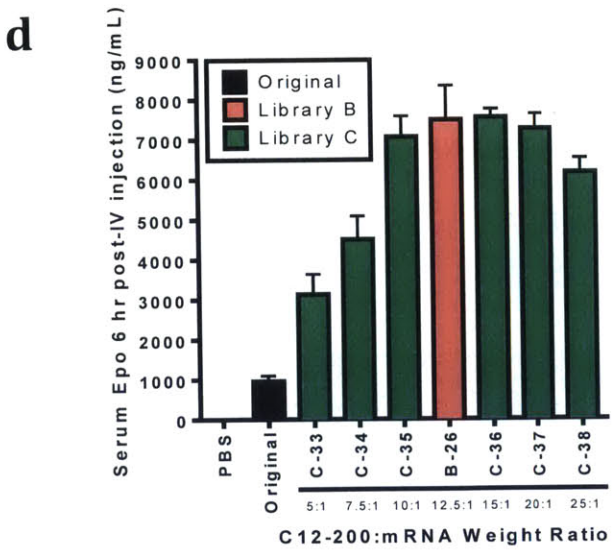

Figure 4.3: EPO expression across LNP parameters. (a) Of the 14 liposomal formulation in Library A two of them outperformed the original formulation for EPO production. (b) 11 of the 18 formulations in Library B demonstrated higher efficacy than the original formulation, with all of the DOPE containing formulations outperforming the DSPC formulations (c). (d) The efficacy of the LNPs increases as the weight ratio increases, up to a C12-200 to mRNA ratio of 10:1, after which point the efficacy remains constant. (Data points equal group mean ± standard deviation, n=3)

Formulation Efficacy Across RNA Sequence and Mouse Strain

Having established an optimized formulation for EPO mRNA delivery, we wanted to verify that such a formulation was not sequence specific. To that end, both the siRNA optimized LNP and the C-35 parameters were formulated using luciferase mRNA and injected intravenously at a dose of 15 ug per mouse. Luciferase mRNA was chosen, both because of the relative ease of detecting the protein, and because of its size; the length of the luciferase mRNA is approximately twice that of EPO mRNA (2148 nucleotides versus 1077 nucleotides), allowing us to examine whether optimized formulation is affected by the size of the RNA cargo. Six hours post injection the organs were isolated and the luminescence was examined. Of the eight organs examined, the liver showed the greatest

signal, with some slight signal seen in the pancreas and spleen (Figure 4.4). The luminescence produced by the liver treated with the C-35 formulation was approximately three fold greater than that of the liver treated with the siRNA optimized formulation, providing evidence that our optimized LNP is not mRNA sequence specific.

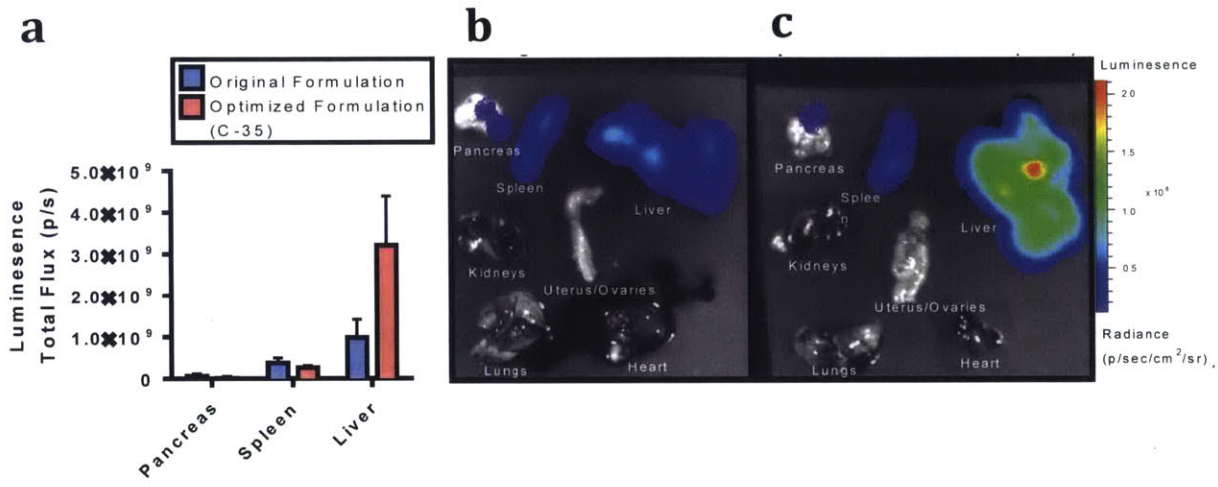

Figure 4.4: Luciferase expression and tissue distribution. (a) Luciferase mRNA displayed significantly higher expression levels in the liver with the C-35 optimized formulation as compared to the siRNA optimized formulation. (Data points equal group mean ± standard deviation, n=3)

In order to examine the mechanism of action for the LNP delivery, the C-35 LNP composition was formulated with luciferase mRNA and injected intravenously into three different mouse strains, wild type, LDLR$^{-/-}$, and ApoE$^{-/-}$, at a dose of 7.5 μg per mouse (Figure 4.5). As was observed with the lipopeptide LNPs in chapter 3, efficacious LNP delivery to the liver is heavily dependent on the presence of ApoE; virtually no luminescence was observed in the ApoE knockout mice as compared with the wild type mice. Due to the variation in the data, the expression level in the LDLR knockout mice does not appear to be significantly different as compared to the wild type strain; however, while we cannot say whether or not the efficacy of the LNP is partially dependent on the LDL

receptor, the relatively high luminescence in the LDLR$^{-/-}$ mouse liver as compared to the ApoE$^{-/-}$ mouse liver strongly suggests that the efficacy is not solely dependent on the LDL receptor.

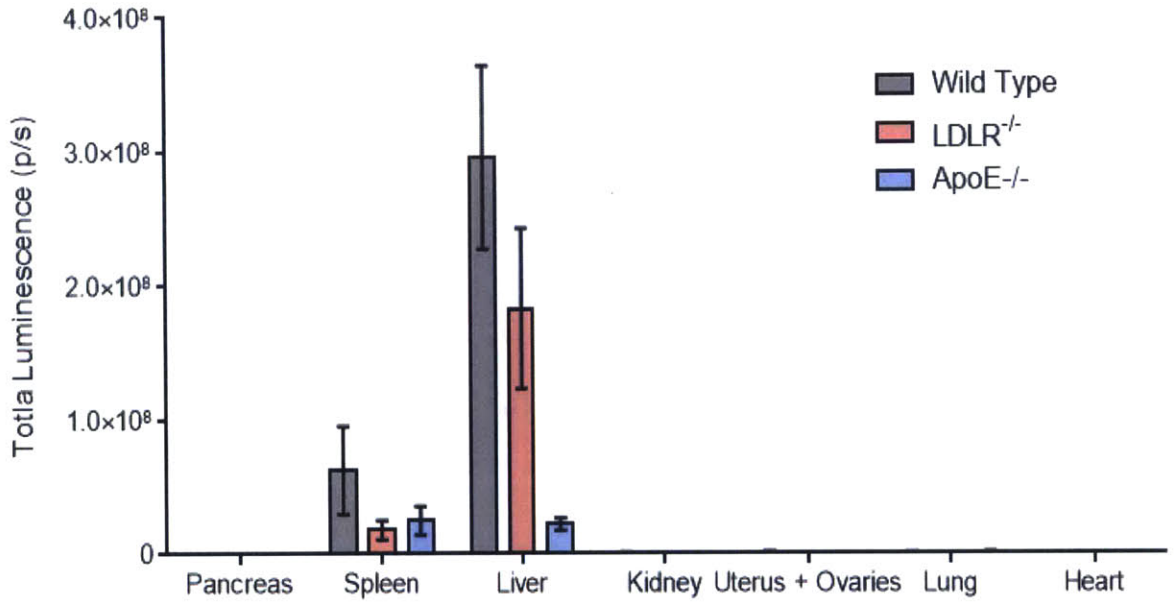

Figure 4.5: Tissue luminescence across mouse strains. Total luminescence was determined *ex vivo* in eight different tissues six hour post intravenous injection of 7.5 μg of C-35 formulated luciferase mRNA. Both wild type mice an LDLR knockout mice demonstrated high levels of luminescence in the liver as compared to the ApoE knockout mice with showed little luciferase expression. (Data points equal group mean ± standard deviation, n=4)

Since the formulation C-35 was optimal for mRNA delivery we wanted to test it with siRNA delivery to determine whether the LNP showed improved efficacy regardless of the RNA composition, or whether it was in fact mRNA specific. Both the mRNA and siRNA optimized LNPs were formulated with anti-FVII siRNA and injected intravenously at three doses; seventy-two hours later, the FVII levels were determined, and we found that relative serum levels of the proteins were comparable at each time point for the two formulations

(Figure 4.6). While C-35 displayed a dramatic increase in mRNA expression levels *in vivo*, it appeared to offer no advantage over the original formulation for siRNA delivery.

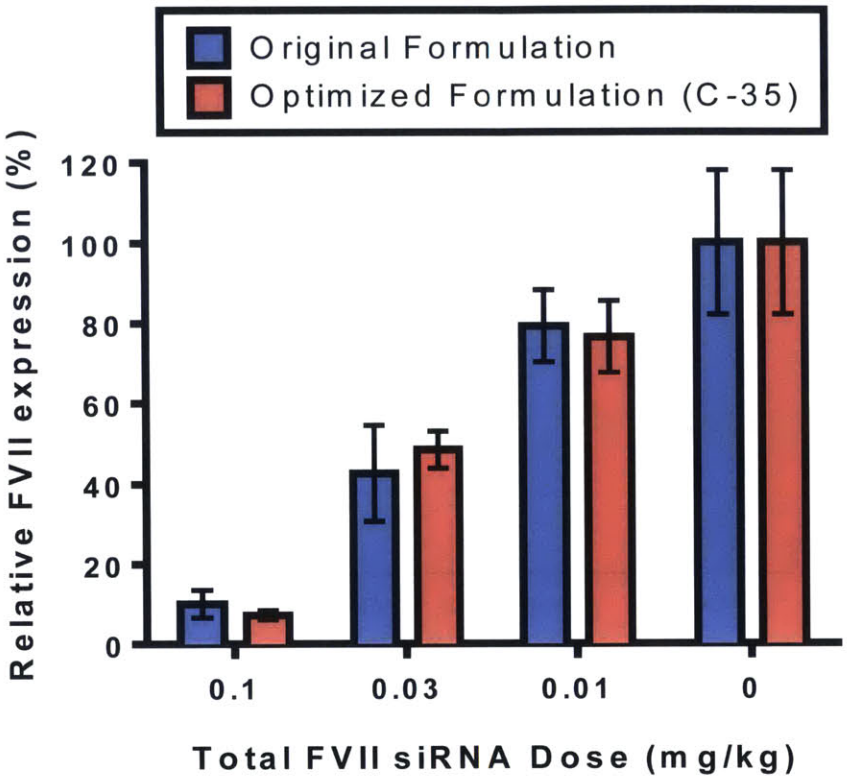

Figure 4.6: FVII silencing *in vivo*. The siRNA optimized formulation and the mRNA optimized formulation displayed identical silencing *in vivo*. (Data points equal group mean ± standard deviation, n=3)

The two formulations are similar in many ways, but there are some significant differences which may explain the observed differences between siRNA and mRNA delivery. Structurally, mRNA is much larger than siRNA, with the EPO mRNA approximately 50 times larger than the anti-FVII siRNA, which affects the RNA entrapment efficiency (EE); the siRNA optimized formulation demonstrated an mRNA EE of only 24%, while the C-35 formulation demonstrated almost double the degree of entrapment, with an EE of 43%.

Delivering more mRNA into the cell may contribute to a higher degree of efficacy, but it isn't the only factor; formulation B-30 demonstrated the highest EE with 60%, but the EPO expression was extremely low at 293 ± 13 ng mL^{-1}. Another potential explanation for the difference in efficacy is membrane stability, and the tendency of the LNP to promote a lamellar to H_{II} phase transition. Both the inclusion of the conical lipid DOPE and the increase in total lipid:RNA weight ratio may contribute to the destabilization of the endosomal membrane, allowing the larger mRNA molecules to escape. This may also explain why no difference in efficacy is observed between the two formulations for siRNA delivery. The siRNA optimized LNP is capable of sufficiently destabilizing the endosomal membrane to allow siRNA to escape into the cytoplasm, and further destabilization by the mRNA optimized LNP does not alter the number of siRNA molecules entering the cytoplasm.

While the optimized liposomal formulations for siRNA and mRNA are similar in many ways, the LNPs developed for siRNA delivery *in vivo* cannot be directly applied to mRNA delivery without structural modification and optimization. Due to the structural differences between siRNA and mRNA, changes must be made to the liposomal composition to increase the relative entrapment, as well as improve in endosomal escape. While several parameters have been elucidated in this experiment, including the lipid molar ratio, lipid to RNA weight ratio, and the phospholipid structure, additional experiments will be required to examine the possible effect of other parameters, including the effect of varying the chain length of the PEG group, and determining the optimal ionizable lipid to use.

Method and Materials.

Liposomal formulation. C12-200 (Alnylam Pharmaceuticals), a phospholipid, cholesterol (Sigma), and DMG-mPEG2000 (Avanti Polar Lipids), were dissolved in ethanol and combined in the molar ratios stated above. DSPC (Avanti Polar Lipids), DSPE (Avanti Polar Lipids), DOPC, (Avanti Polar Lipids), and DOPE (Avanti Polar lipids) were used as the different phospholipids in the experiments. An aqueous solution comprised of RNA dissolved in 10 mM citrate buffer (pH 3) was combined with the lipid solution in a 3:1 ratio, using a microfluidics device (Chen et al., 2012). The mRNA for EPO and luciferase were provided by Shire, and the anti-FVII siRNA was provided by Alnylam Pharmaceuticals. All RNA sequences may be found in Appendix A. The liposomal formulations were then dialyzed against 1X PBS at 4C for 2 hours using a 20,000 molecular weight cutoff Slide-A-Lyzer cassette (Life Technologies).

LNP characterization. The RNA entrapment efficiency was determined by using a Quant-iT RiboGreen RNA assay (Invitrogen) (Heyes et al., 2005). Particle size and PDI of the LNPs were measured via dynamic light scattering Zetasizer Nano ZS (Malvern).

Animal Experiments. All animal studies were approved by the MIT IACUC, and followed all local, state, and federal regulations. All female mice were used: C57BL/6 mice (Charles River Labs, 18-22 grams), B6.129S7-Ldlrtm1Her/J (Jackson Laboratories, 18-22 grams), and B6.129P2-apoetm1unc/J (Jackson Laboratories, 18-22 grams). LNPs were injected intravenously into the tail vein. Blood samples were obtained from the tail vein, and serum was removed from the samples using serum separation tubes (BD Biosciences). EPO

protein levels were measured using an ELISA (Human Erythropoietin Quantikine IVD ELISA Kit, R&D systems). FVII protein levels were determined using a chromogenic assay (Biophen FVII, Aniara Corporation) and were normalized to control mice injected with PBS. For tissue imaging, 6 hours after being injected intravenously with formulated luciferase mRNA, mice were injected I.P. with 130μL of D-luciferin (Perkin Elmer) at a concentration of 30 mg mL^{-1}. Fifteen minutes after administration of the D-luciferin, the mice were sacrificed and the liver, spleen, pancreas, kidneys, uterus, ovaries, lungs, and heart were removed and their tissue luminescence was determined using an IVID imagine system (Perkin Elmer). The images were analyzed using LivingImage software (Perkin Elmer).

Statistics. The Design of Experiment (DOE) was constructed, and the data were analyzed, using JMP software (SAS). Statistical significance was defined as having a *p*-value less than 0.05. Library A was designed using a $3^4 \times 2^2$ definitive screening, with 4 three level quantitative factors (C12-200:RNA weight ratio, C12-200 mole %, phospholipid mole %, and PEG mole %) and with 2 two-level qualitative factors for the phospholipid head group (phosphocholine versus phosphoethanolamine) and the phospholipid tail groups (distearoyl versus dioleoyl). For Library B, a $3^4 \times 2^1$ L-18 Taguchi fractional factorial design was used, with the same 4 three level quantitative factors, but with only one two-level qualitative factor (DSPC versus DOPE).

Chapter 5

Examining the efficacy of ionizable lipids for both siRNA and mRNA delivery

Ionizable Lipid Library Design

While liposomal formulations optimized for siRNA are capable of delivering mRNA *in vivo*, we clearly demonstrate in the previous chapter that alterations to the liposomal composition are essential for maximal mRNA expression. This raises the question as to whether ionizable lipids that have been developed for siRNA delivery are also optimal for mRNA delivery. Although we have demonstrated that C12-200 is capable of delivering both siRNA and mRNA to the liver, it was originally selected because of its capability of delivering siRNA to hepatocytes *in vivo* (Love et al., 2010) and may not be optimal for mRNA delivery. In order to determine whether the relative efficacy of ionizable lipids is comparable for siRNA and mRNA, a new lipid library was developed to be screened with both siRNA and mRNA.

This novel lipid library was designed by Dr. Yizhou Dong, and was based around a class of Poly(glycoamidoamines) (PGAAs), compounds which have previously been used for DNA delivery *in vitro* (M. Davis et al., 2004; Y. Liu & Reineke, 2010; McLendon, Fichter, & Reineke, 2010; Prevette, Lynch, & Reineke, 2010). Like the highly efficacious transfection reagent PEI, these polymers have a high number of amine groups to promote nucleic acid binding, cell uptake, and endosomal escape. PEI, however, is extremely cytotoxic, due in part to its inability to be degraded by the cell, ultimately limiting its potential for clinical use. PGAAs have demonstrated low cytotoxicity because of their capability to be degraded though aminolysis. Due to their success in delivering nucleic acids *in vitro*, and because of their low toxicity, the PGAAs were considered an optimal candidates for the amine core of a new class of ionizable lipids, the Poly(glycoamidoamine)-lipid brushes (PGAALBs). While PGAAs have demonstrated the capability of delivering nucleic acids to cells *in vitro*, they

have shown little success with systemic delivery *in vivo.* The addition of lipid tails to the polymer cores provides a hydrophobic moiety, which has been demonstrated to improve polymeric nanoparticle serum stability (Eltoukhy, Chen, Alabi, Langer, & Anderson, 2013) and also allows for co-formulation with hydrophobic excipients to generate more efficacious LNPs.

A combinatorial library of PGAALBs were synthesized by varying three components: a sugar moiety, a polyethylamine segment, and a lipid tail (Figure 5.1). Three sugar molecules were included in the library: tartrate (Tar), galactarate (Gal), and glutamic acid (Glu). These sugars were combined with polyethylamine segments ranging from 2-5 repeats to comprise the polymer core of the PGAALBs, and were synthesized via a previously published method (Y. Liu, Wenning, Lynch, & Reineke, 2004). Lipid tails were then added to the polymer core using an epoxide ring opening (Love et al., 2010); four fully saturated lipid tails were examined, 10,12,14, and 16 carbons long in length. Nomenclature for these particles consists of combining the sugar abbreviation with the number of amine repeats, followed by the length of the carbon tail. For example, a PGAALB consisting of tartrate, a polyethylamine segment with 4 repeats, and a lipid tail 12 carbons long would be abbreviated as TarN4C12.

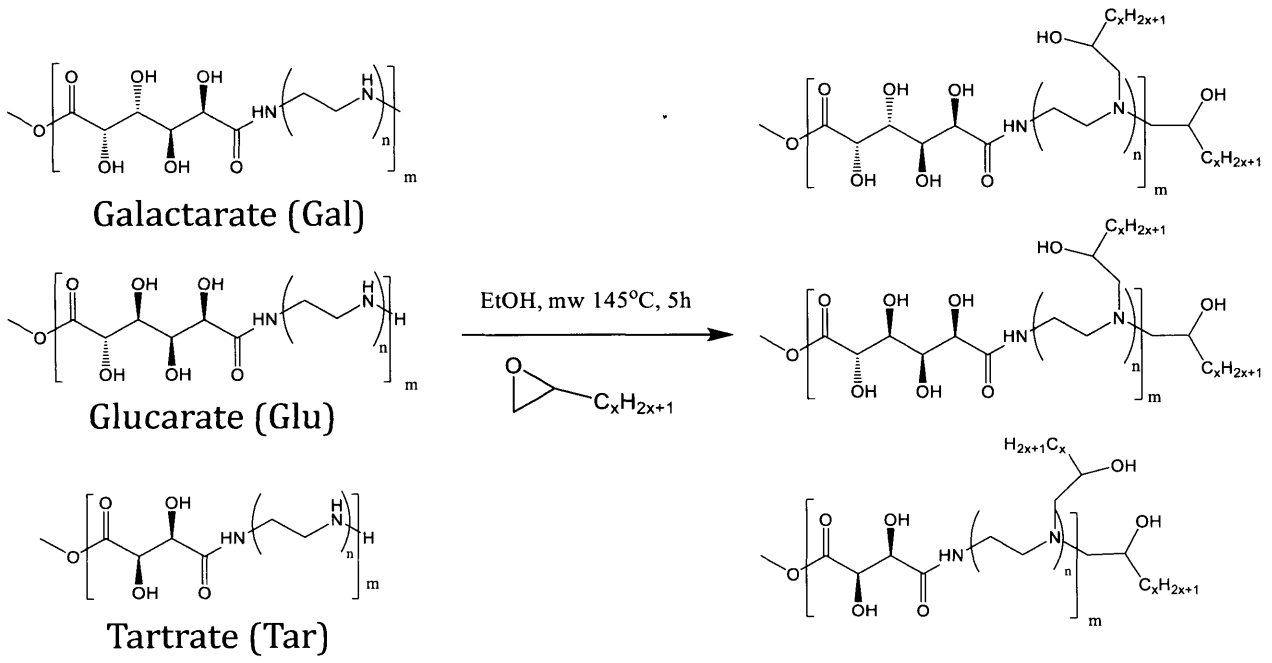

Figure 5.1: Poly(glycoamidoamine)-lipid brush composition. Three sugar backbones were examined, Galactarate (Gal), Glucarate (Glu), and Tartrate (Tar). Four different lengths of amine repeats were examined (n=2-5), and four different epoxide tail lengths were examined (x=8, 10, 12, and 14). The number of core repeats was held constant (m≈10).

Ionizable Lipid Screen with siRNA and mRNA

Initial attempts to formulate PGAALBs with siRNA resulted in particle aggregation, and were unsuitable for injection. In order to generate more stable nanoparticles, cholesterol, DSPC, and DMG-PEG2000 were added to the formulation. The lipid ratio selected was based on the lipid ratio previously published for C12-200 nanoparticles delivering siRNA to hepatocytes (Love et al., 2010). However, due to the wide variation in molecular weight of the PGAALBs, we decided to maintain a specific weight ratio for the lipids, rather than a molar ratio. The original C12-200 formulation consisted of a lipid molar ratio of 50:10:38.5:1.5 for C12-200:DSPC:Cholesterol:DMG-mPEG$_{2000}$ which corresponds to a lipid weight ratio of 68:9:18:5. This weight ratio was used for the PGAALB

nanoparticles, with the polymer brushes replacing the C12-200 (Table 5.1). The PGAALB to siRNA weight ratio was also held constant at 5:1. Anti-FVII siRNA formulated nanoparticles were then injected intravenously at a dose of 0.3 mg kg^{-1}, and the FVII serum levels were determined 48 hours later.

When the FVII protein levels are examined, several trends are observed. As the length of the amine core increases and as the length of the lipid tails decrease, we see a decrease in FVII serum protein levels, with the N5C10 compounds demonstrating greatest degree of protein knockdown; more than 90% silencing is observed (Figure 5.2a). Minimal difference in efficacy is observed among the three sugars used; while galactarate appears significantly more efficacious that glutamic acid or tartrate for N4C14, and significantly more efficacious than tartrate for N4C16, this trend is not consistent among the other groups.

Table 5.1: Formulation composition for siRNA and mRNA LNPs.

	Lipid weight ratio					
	Polymer Brush	Phospho-lipid	Cholesterol	DMG-mPEG$_{2000}$	Phospho-lipid	Polymer Brush to RNA wt. ratio
siRNA	68	9	18	5	DSPC	5
mRNA	50	20	20	10	DOPE	10

For formulations containing EPO mRNA we elected to use a lipid composition based upon the C12-200 formulation optimized for mRNA delivery, discussed in chapter 4. The lipid weight ratio of 50:20:20:10 for PGAALB:DOPE:Cholesterol:DMG-PEG$_{2000}$ was selected (Table 5.1), with a PGAALB to mRNA weight ratio of 10:1. A small pilot experiment confirmed that this formulation composition demonstrated a higher mRNA expression with

the PGAALBs as compared to the formulation composition optimized for siRNA delivery. LNPs were formulated with EPO mRNA and injected intravenously at a dose of 0.3 mg kg^{-1}.

As with the siRNA based formulations, the efficacy of the LNPs increases both as the length of the amine core increases, and as the length of the lipid tails decrease, with the highest EPO serum levels found using the N5C10 based PGAALBs, having values ranging from 680-1180 ng mL^{-1} (Figure 5.2b). The use of different sugar moieties in the PGAALBs also has little effect on the overall EPO expression, as was observed with siRNA delivery. Of the three sugars the tartrate based compounds demonstrated higher EPO expression for several of the conditions, but this trend is not consistent for all groups.

These experiments provide valuable supporting evidence that relative efficacy for ionizable lipids is the same for both siRNA and mRNA delivery. These data help to alleviate the need to re-screen previous lipid libraries that have been developed for siRNA delivery before using them for mRNA. Despite the promising results, this trend still needs to be confirmed across other types of ionizable lipids in order to ensure that it isn't a result specific to PGAALBs. Combined with the previous chapter, these experiments provide valuable information about the differences and similarities of siRNA and mRNA delivery to hepatocytes *in vivo.* While many of the LNPs that have been developed for siRNA may ultimately be translated for mRNA delivery, important screens with the ionizable lipids of interest will be necessary in order to ensure the maximal efficacy is obtained.

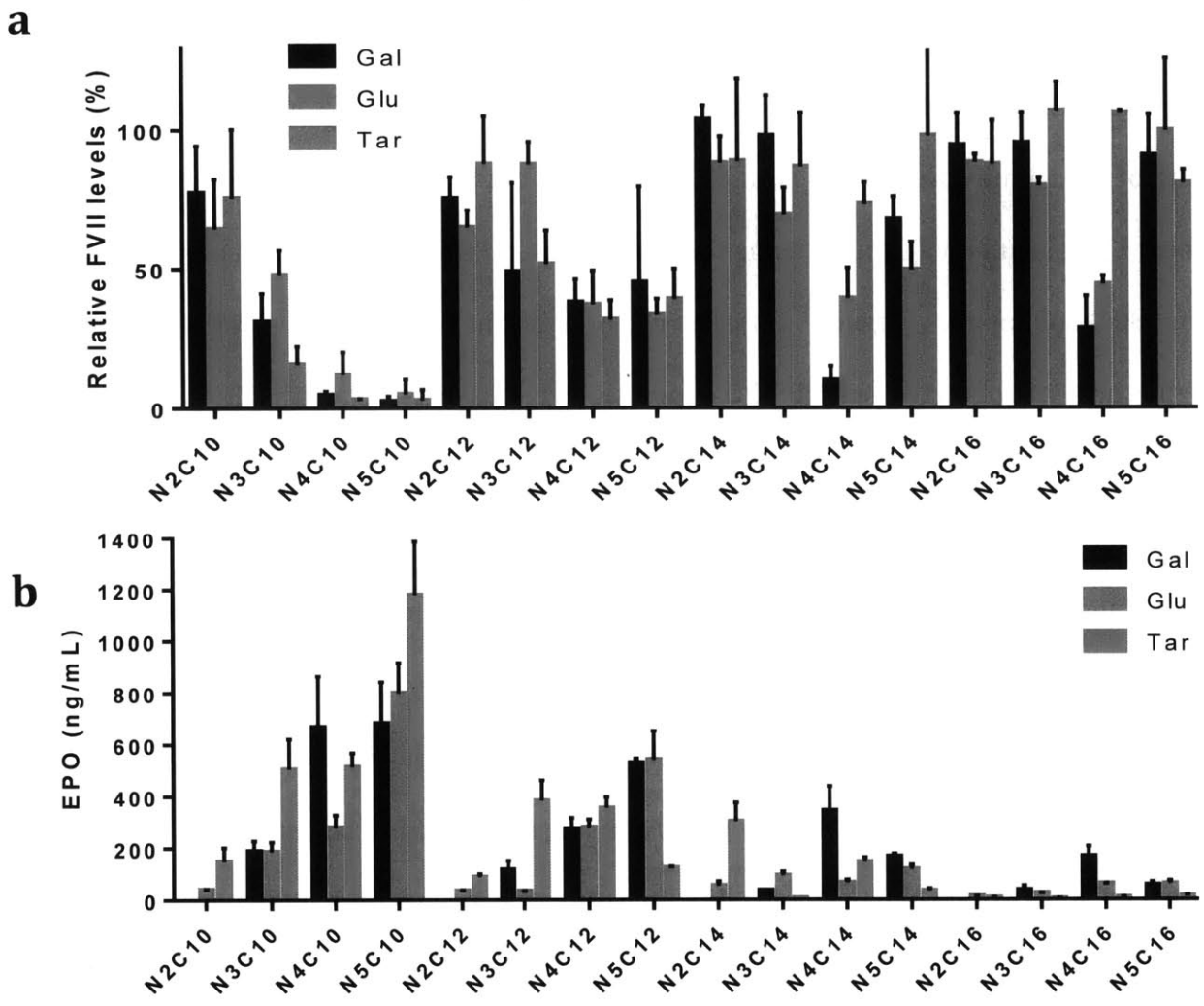

Figure 5.2: PGAALB *in vivo* efficacy. (a) Relative FVII serum levels of mice 48 hours after being dosed with 0.3 mg kg^{-1} of formulated anti-FVII siRNA. FVII levels compared to a PBS injected control group. (b) EPO serum levels of mice 6 hours after being dosed with 0.3 mg kg^{-1} of formulated EPO mRNA. (Data represented as mean $\pm$ standard deviation, n=3)

Methods and Materials

General procedures for Polymer Brush synthesis. Poly(glycoamidoamines) (PGAAs) were synthesizes using methods previously reported (Y. Liu et al., 2004). Lipid tails containing termilan epoxides were added to PGAAs via amine mediated ring openings. A solution of PGAA and lipid tails in ethanol were combined at a ratio of 1.5:1 of epoxides:amines; this solution was then irradiated in a microwave oven at 140°C for 5 hours and subsequently purified via flash chromatography.

Formulation procedures. Liposomes were formed using a microfluidic device as was previously described (Chen et al., 2012). Liposomes formulated for siRNA delivery were comprised of PGAALB, DSPC (Avanti Polar Lipids), cholesterol (Sigma Aldrich), and DMG-PEG2000 (Avanti Polar Lipids) in a 68:9:18:5 weight ratio, with a PGAALB to RNA ratio of 5:1. Liposomes formulate for mRNA delivery were comprised of PGAALB, DOPE (Avanti Polar Lipids), cholesterol, and DMG-PEG2000, with a PGAALB to RNA ratio of 10:1. The lipids were dissolved in ethanol. For both siRNA and mRNA type formulations, the RNA was dissolved in 10mM citrate buffer, pH 3.0. The ethanol and aqueous solutions were combined in a 1:1 ratio in the microfluidics device, and immediately diluted two fold by PBS. Formulations were dialyzed for a minimum of 2 hours against 1X PBS, pH 7.4, using Slide-A-Lyzers (Pierce Thermo Scientific).

Liposomal Characterization. RNA concentration and RNA entrapment were determined using a RiboGreen assay (Life Technologies). Particle sizes were determined using a Zetasizer Nano ZS (Malvern).

***In vivo* delivery in mice.** All procedures were approved by the MIT Institutional Animal Care and Use Committee (IACUC) and complied with local, state, and federal regulations. Female C57BL/6 mice, between 18-24 grams were used for all *in vivo* experiments. LNPs were injected intravenously via the tail vein at a dose of 0.3 mg/kg total RNA (including both entrapped and unentrapped RNA). For mice injected with FVII siRNA, blood samples were taken after 48 hours; for mice injected with EPO mRNA, blood samples were taken 6 hours post injection.

Protein analysis. Serum samples were obtained using serum separation tubes (BD Biosciences). FVII protein levels were determined using a chromogenic assay (Aniara). EPO levels were determined using an ELISA (R&D Biosciences)

Chapter 6

Determining the lipoprotein involvement for LNP delivery to the liver versus to the lungs

Liposomal Biodistribution Overview

In the previous chapters we have repeatedly demonstrated our capability to deliver siRNA and mRNA to the liver, using a myriad of ionizable lipids and formulation compositions. Indeed, the field as a whole has had great success in systemic nucleic acid delivery to the liver (Albanese, Tang, & Chan, 2012; Audouy et al., 2002; Semple et al., 2010; Zimmermann et al., 2006). However, while there are many diseases that can be treated by delivering RNA to hepatocytes, we must be able to develop new LNPs capable of targeting other tissue types in order to fully realize the potential of siRNA and mRNA as therapeutics.

Historically it has been postulated that LNPs primarily target the liver due to their size; the majority of liposomes are between 50 and 150 nanometers in diameter, making penetration of the endothelial lining difficult for most organs. The liver is one of the few organs with a larger endothelial fenestration size, roughly 150-175nm nanometers in diameter, (Takakura, Mahato, & Hashida, 1998; Wisse, De Zanger, Charels, Van Der Smissen, & McCuskey, 1985) which allows the LNPs to penetrate the tissue and intercalate among hepatocytes. After the liver, LNPs have demonstrated most success in delivering oligonucleotides to the lung (Audouy et al., 2002; Dahlman et al., 2014; F. Liu, Qi, Huang, & Liu, 1997; Santel et al., 2006). Delivery to the lung is performed, not by generating smaller particles that are capable of crossing the endothelial lining, but by creating larger particle aggregates that become caught in the capillaries of the lung. Some of the LNPs that have had the greatest success in targeting the lung have been those that are positively charged during circulation. It is hypothesized that the positively charged LNPs form aggregates in the presence of negatively charged plasma proteins (Albanese et al., 2012) and these aggregates are then large enough to become lodged in the capillary beds in the lungs. Given

this hypothesis, providing a positive charge to an otherwise neutrally charged or negatively charged LNP could allow us to redirect the biodistribution from the liver to the lungs.

While efficient biodistribution of LNPs to the target tissue is necessary for successful delivery of nucleic acids, it is by no means sufficient. In fact, many nanoparticles are capable of intercalating into the liver, but only a small subset is capable of efficient transfection of these cells (Santel et al., 2006; Semple et al., 2010). Recent research focusing on this important discrepancy has suggested that plasma protein binding may affect the efficacy of the LNP. Indeed, nanoparticles have demonstrated an affinity for lipoproteins to bind to their surfaces, creating a corona of protein and lipids during circulation (Hellstrand et al., 2009; Monopoli, Aberg, Salvati, & Dawson, 2012). Neutrally charged liposomes have shown dependence on apolipoprotein E (ApoE) for hepatocellular uptake *in vivo* (Akinc et al., 2010; Yan et al., 2005), while vitamin A labeled LNPs have been reported to bind circulating retinol-binding protein, leading to the nanoparticles' uptake *in vivo* by the liver and pancreatic stellate cells (Ishiwatari et al., 2012; Sato et al., 2008). In Chapters 2 and 4 of this thesis we show how several of our own LNPs are ApoE dependent, for cell uptake and expression *in vivo.* As we develop LNPs for lung delivery, we intend to examine and compare the plasma binding proteins interaction with the liver targeted LNPs, to gain insight as to the active role these proteins play in targeted tissue delivery.

The ionizable lipid-like material C12-200 is an ideal candidate to test our hypothesis, as it has clearly demonstrated efficient capability to deliver siRNA and mRNA to the liver, but to date has shown no capability of delivering RNA to the lungs. By formulating C12-200 with additional cationic lipids we intend to modulate its biodistribution, redirecting the LNPs to transfect the lungs, rather than the liver. If

successful this would allow for the rapid development of lung targeted liposomes, as the extensive library of liver targeting LNPs could be utilized to deliver RNA to the lungs through a series of formulation modifications, rather than the expensive and time consuming development of lung-specific ionizable lipids.

Biodistribution of Charge Variant LNPs

In order to examine the role of surface charge on plasma protein binding as well as tissue localization, we examined liposomes that were structurally similar but electrostatically different. To accomplish this, LNPs containing C12-200, cholesterol, and DSG-mPEG$_{2000}$ were formulated along with a combination of the amphipathic lipids DODAP and DOTAP (Figure 6.1). DODAP and DOTAP are structurally identical, except for the substitution of their terminal amines; DODAP has an ionizable tertiary amine, while DOTAP has a constitutively positively charged quaternary amine. Four discrete formulations were generated using molar ratios of 3:0, 2:1, 1:2, and 0:3 of DODAP to DOTAP (labeled LNP1-LNP4) and, when formulated with mRNA, the zeta potentials of the nanoparticles are -5.5, 0.7, 7.4, and 12.1 mV, respectively (Table 6.1).

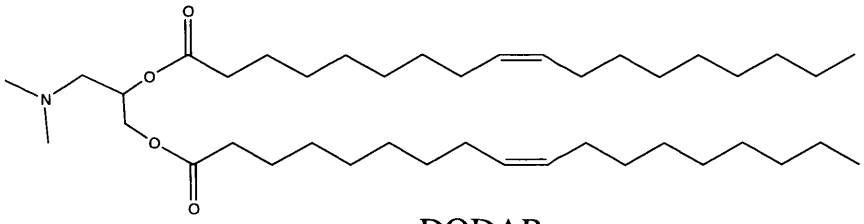

DODAP

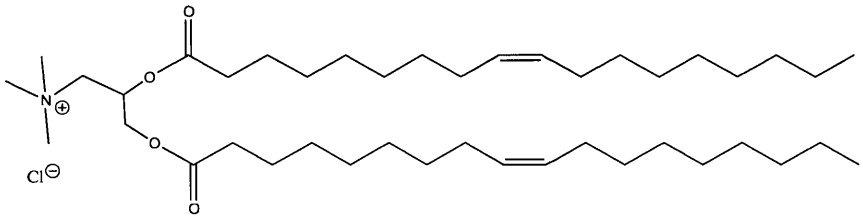

DOTAP

Figure 6.1: Amphipathic lipids DODAP and DOTAP. The two lipids are structurally identical except for the substitution of the amine; DODAP contains an ionizable tertiary amine, while DOTAP contains a quaternary amine, providing it with a constitutive positive charge.

Table 6.1: Liposomal composition and surface charge.

	Lipid Mole %					
	Ionizable Lipid	Cholesterol	DSG-mPEG$_{2000}$	DODAP	DOTAP	Zeta Potential (mV)
LNP1	30	30	1	39	0	-5.49
LNP2	30	30	1	26	13	0.746
LNP3	30	30	1	13	26	7.44
LNP4	30	30	1	0	39	12.1

To study the differences in biodistribution of these LNPs, they were formulated using fluorescently labeled mRNA and injected intravenously into mice. After one hour, organ fluorescence levels were examined *ex vivo*. A stepwise change in tissue localization was observed, with negative and neutral LNPs displaying increased localization to the liver

relative to positively charged LNPs, which saw an increase in localization to the lungs (Figure 6.2a). In order to determine whether this change in organ distribution correlated with a change in cellular transfection capabilities, the LNPs were formulated with luciferase mRNA and were again administered intravenously. Six hours post injection the tissues were examined *ex vivo* for luminescence activity. As the surface charge of the LNP became more positive, a decrease in liver luminescence was observed concurrent with an increase in lung luminescence (Figure 6.2b). No luminescence was observed for unformulated mRNA injected intravenously.

Having successfully redirected LNPs to the lungs, we proceeded to determine which cell types were being affected. Fluorescence-activated cell sorting (FACS) was performed on lung tissue from mice that were injected with LNP4 formulated fluorescently labeled mRNA (Figure 6.3a). Approximately 90% of the Lung endothelial cells demonstrated cellular uptake of the mRNA, as well as 40% of the immune cells analyzed, though virtually no epithelial cells displayed any fluorescent activity. To determine the relative expression rates of the different lung cells, mice were injected with LNP4 formulated luciferase mRNA, and the cells were again separated via FACS (Figure 6.3b). The endothelial cells demonstrated the greatest relative luminescence, but interestingly lung epithelial cells showed greater luminescence than the immune cells, despite the relatively low rate of mRNA uptake by the epithelial cells.

Changing the relative percentage of DODAP and DOTAP successfully resulted in the redistribution of LNPs containing C12-200, but it was unknown as to whether this methodology was applicable to a broader range of ionizable lipids. In order to determine whether modifying the charge composition of the LNPs had broader applications, we

examined two additional ionizable lipids, $503O_{13}$ and cKK-E12 (Figure 6.4). The three ionizable lipids differ with respect to amine cores, lipid tail lengths, number of lipid tails, and lipid tail linkages. The ionizable lipids were formulated with either DODAP or DOTAP, using the 30:30:1:39 molar ratio of ionizable lipid:cholesterol:DSG-$mPEG_{2000}$:phospholipid. The biodistribution of the fluorescently labeled mRNA is comparable regardless of the ionizable lipid used; all three DODAP formulations demonstrated greater than 60% fluorescence in the liver and 10% or less signal in the lungs, while all three DOTAP formulations show approximately 50% signal in liver and 25% or greater signal in the lungs (Figure 6.5a).

The three ionizable lipids also demonstrate similar degrees of relative transfection efficiency. Mice treated with luciferase mRNA formulated using the DODAP formulation had greater than 40% of the tissue luminescence in the liver and less than 1% in the lungs, while the DOTAP formulated luciferase mRNA demonstrated less than 20% of luminescence in the liver and between 45% and 65% of luminescence in the lung (Figure 6.5b). The similarities in the relative biodistribution and expression of the mRNA using the three structurally different ionizable lipids provides evidence that the observed effects are not specific to C12-200, but are more broadly applicable to similar LNPs.

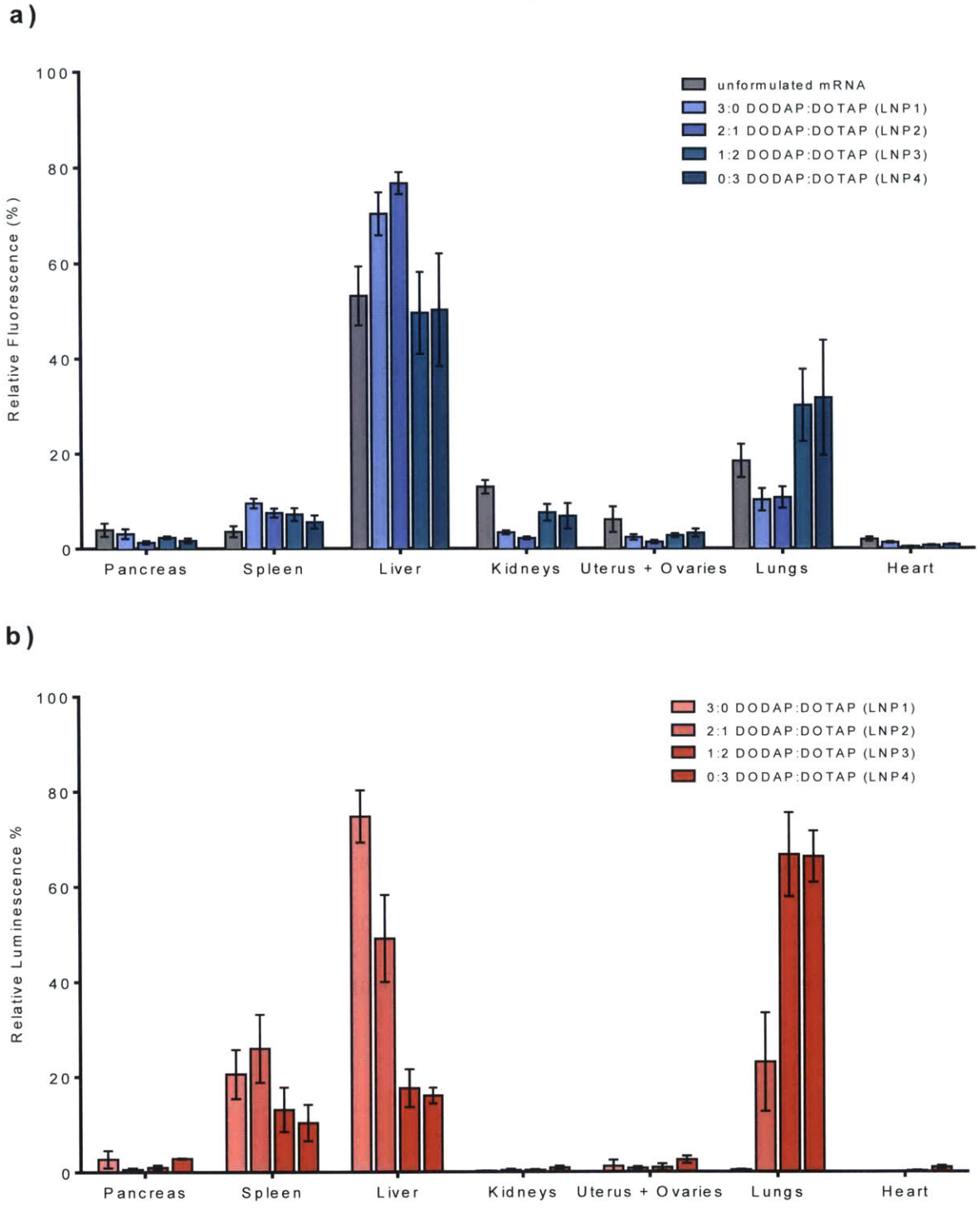

Figure 6.2: Biodistribution of LNP formulated mRNA. (a) Fluorescence readings were taken *ex vivo* one hour after an intravenous injection of 15μg of LNP formulated fluorescently labeled mRNA. The tissue fluorescence was normalized to the total fluorescence to provide the relative biodistribution to each organ. (b) Luminescence

readings were taken from multiple organs *ex vivo* 6 hours after an intravenous injection of 15μg of LNP formulated luciferase mRNA. The luminescence of each organ was normalized to the total luminescence in order to provide the relative organ expression. (Data presented as mean ± standard deviation; n=4)

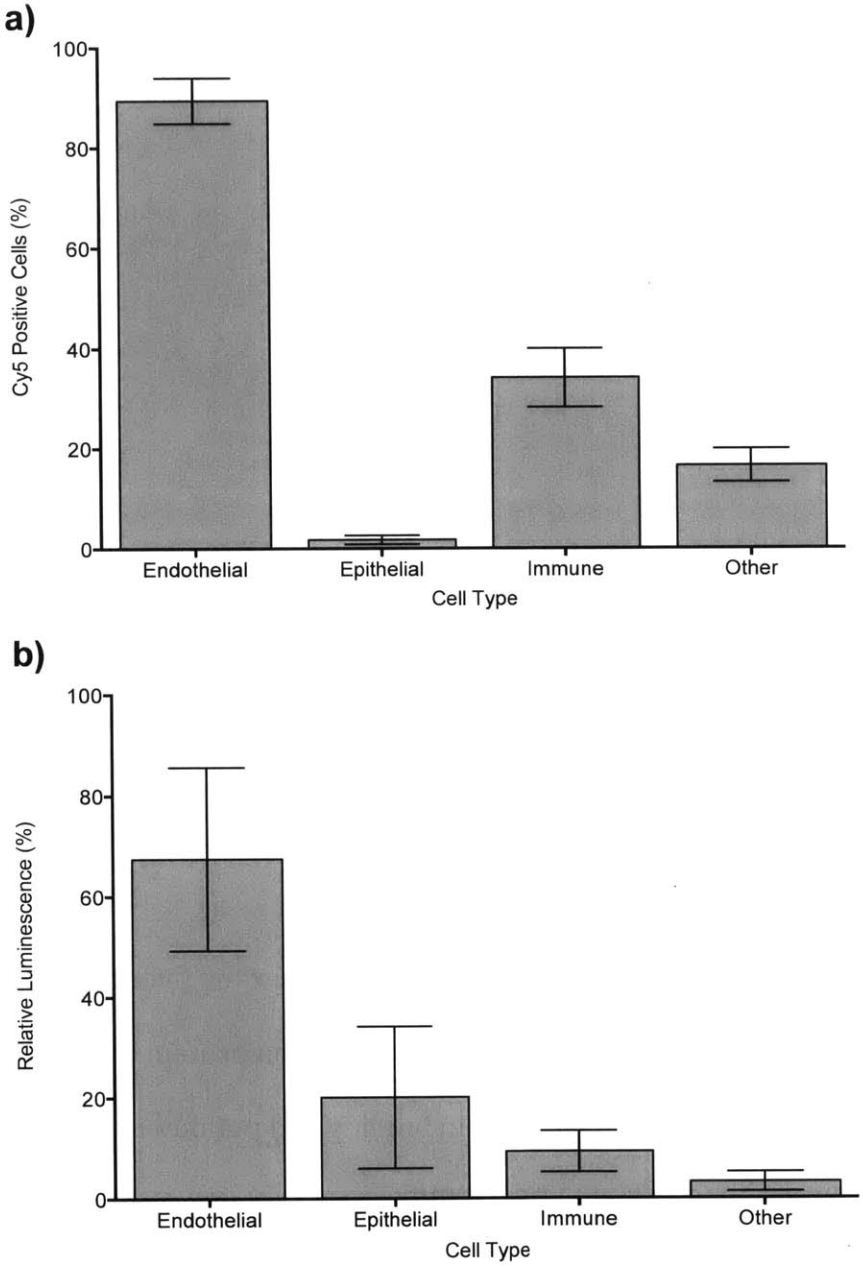

Figure 6.3: Luciferase expression by cell type in the lungs. FACS was performed 6 hours post injection of 15μg of either (a) fluorescently labeled mRNA or (b) luciferase mRNA. Endothelial cells, immune cells, and epithelial cells were separated using the cell surface markers CD-31, CD-45, and EpCAM respectively. Cellular luminescence was divided by the

cell count for each group, and normalized to the total luminescence. (Data presented as mean ± standard deviation; n=4)

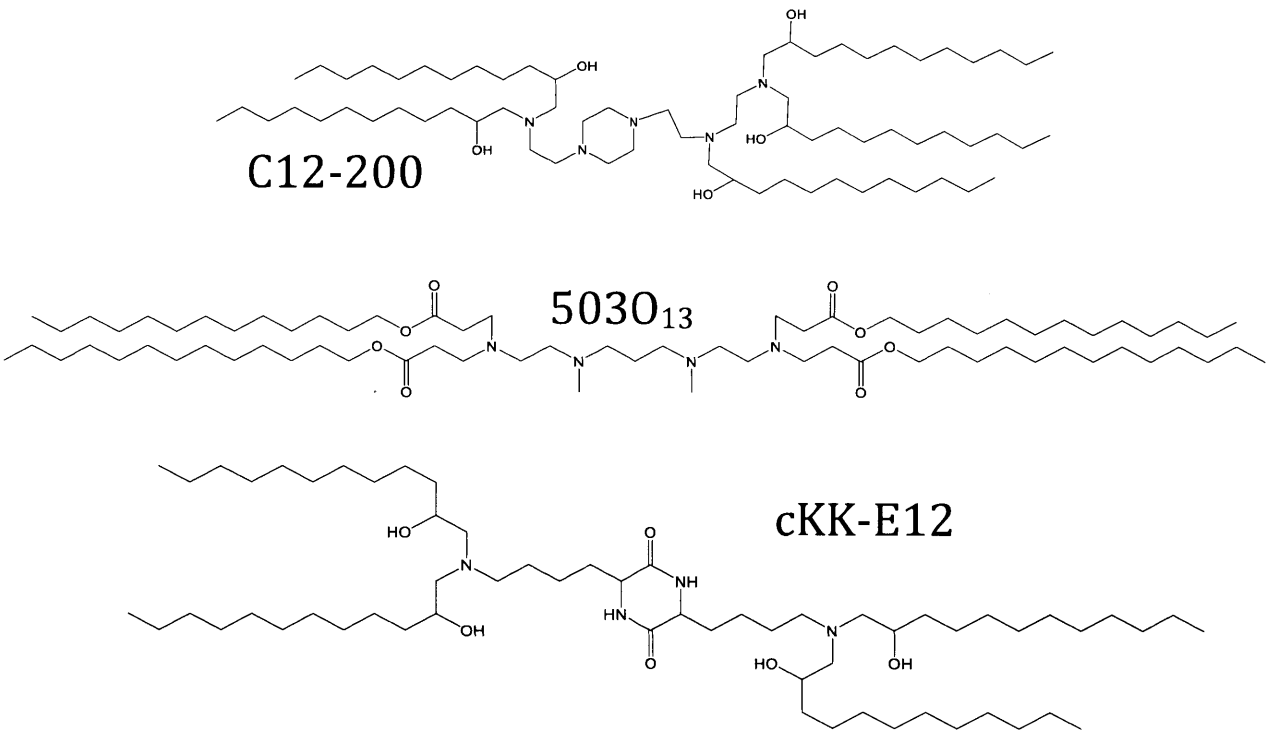

Figure 6.4: Ionizable lipids. The ionizable lipids C12-200, 5030$_{13}$, and cKK-E12 have all demonstrated efficacious siRNA delivery *in vivo*, but are structurally different with respect to the amine core structure, lipid tail length, and the structure of the amine core-lipid tail linker.

Liposomal Plasma Protein Binding Profile

Having successfully generated LNPs that could be directed to either the liver or the lungs, the next step was to assess any potential differences in their plasma protein coronas. To elucidate these differences, we performed an LNP protein binding and pulldown assay. LNP1-4 were formulated containing a biotin labeled DSG-mPEG$_{2000}$ and a fluorescently labeled phospholipid. The LNPs were then incubated with mouse plasma and exposed to streptavidin-labeled magnetic beads. The unbound plasma proteins were removed, and remaining corona proteins were separated via SDS-PAGE. In order to ensure an equal

loading of LNPs, the loading volumes were first normalized to the relative fluorescence intensity of the labeled phospholipid. Coomassie staining of the gel revealed several discrete bands, which were identified via mass spectrometry (Figure 6.6, Appendix E).

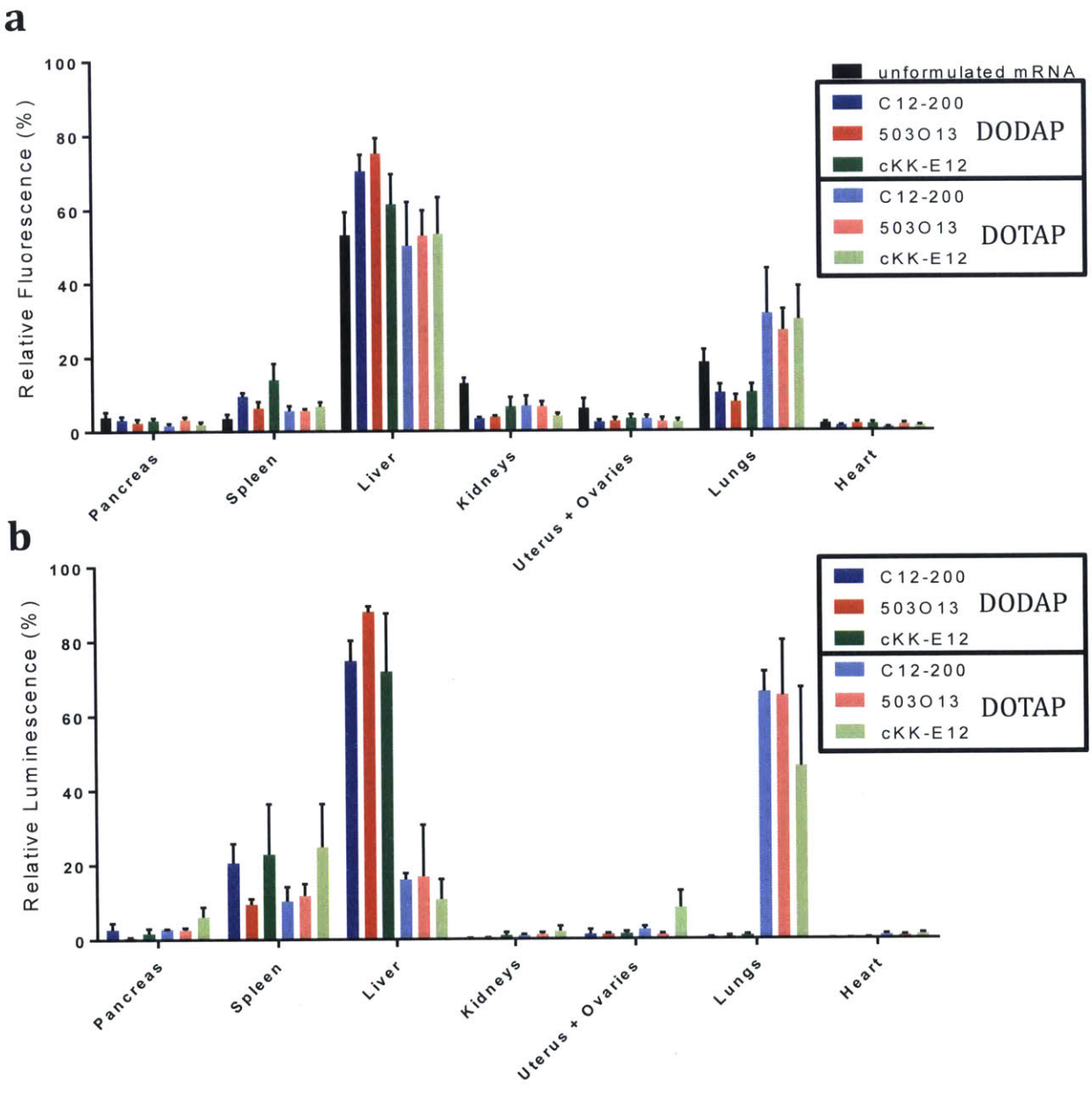

Figure 6.5: Biodistribution and expression across ionizable lipid types. Liposomal formulations containing DODAP or DOTAP are similar in their (a) biodistribution or (b)

tissue expression independent of which ionizable lipid is used. (Data presented as mean ± standard deviation; n=4)

Once identified, the relative protein levels were determined via Western blots (Figure 6.7). The plasma proteins ApoB-100 and ApoE were found to be associated with negatively charged LNPs at much greater levels than neutral or positively charged LNPs. ApoA1 binding levels remained fairly consistent among the four formulations, while fibrinogen and serum albumin demonstrated increased association to positively charged nanoparticles, as compared to neutrally or negatively charged particles.

To verify whether or not the presence of plasma results in microaggregation of the LNPs, a turbidity assay was performed. The formation of aggregates can be determined by examining the increase in light scattering over time (Lauraeus, Holopainen, Taskinen, & Kinnunen, 1998). The turbidity of LNP1 and LNP4 in PBS with and without mouse plasma was examined over a one hour time period, with the particles incubated at 37°C. An increase in turbidity was observed only when LNP4 was co-incubated with mouse plasma; experiments with either LNP4 alone or plasma alone displayed no aggregation, while those using LNP1 demonstrated no increase in turbidity with or without the presence of plasma (Figure 6.8).

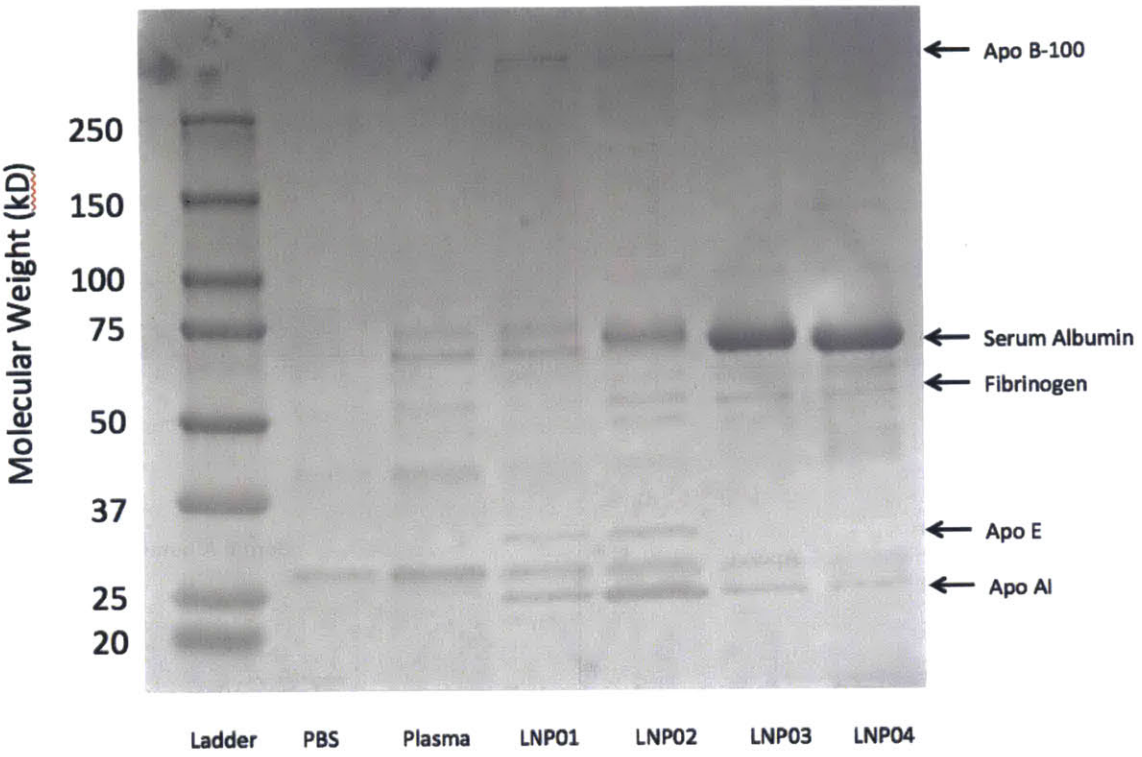

Figure 6.6: Protein binding profile for LNPs. Liposomes were incubated in mouse plasma for one hour at room temperature prior to purification by solid support. The LNPs and all bound proteins were subsequently run on SDS-PAGE. The proteins were imaged via Coomassie staining and the labeled bands were identified via mass spectrometry. (Plasma samples pooled from n=5 mice.)

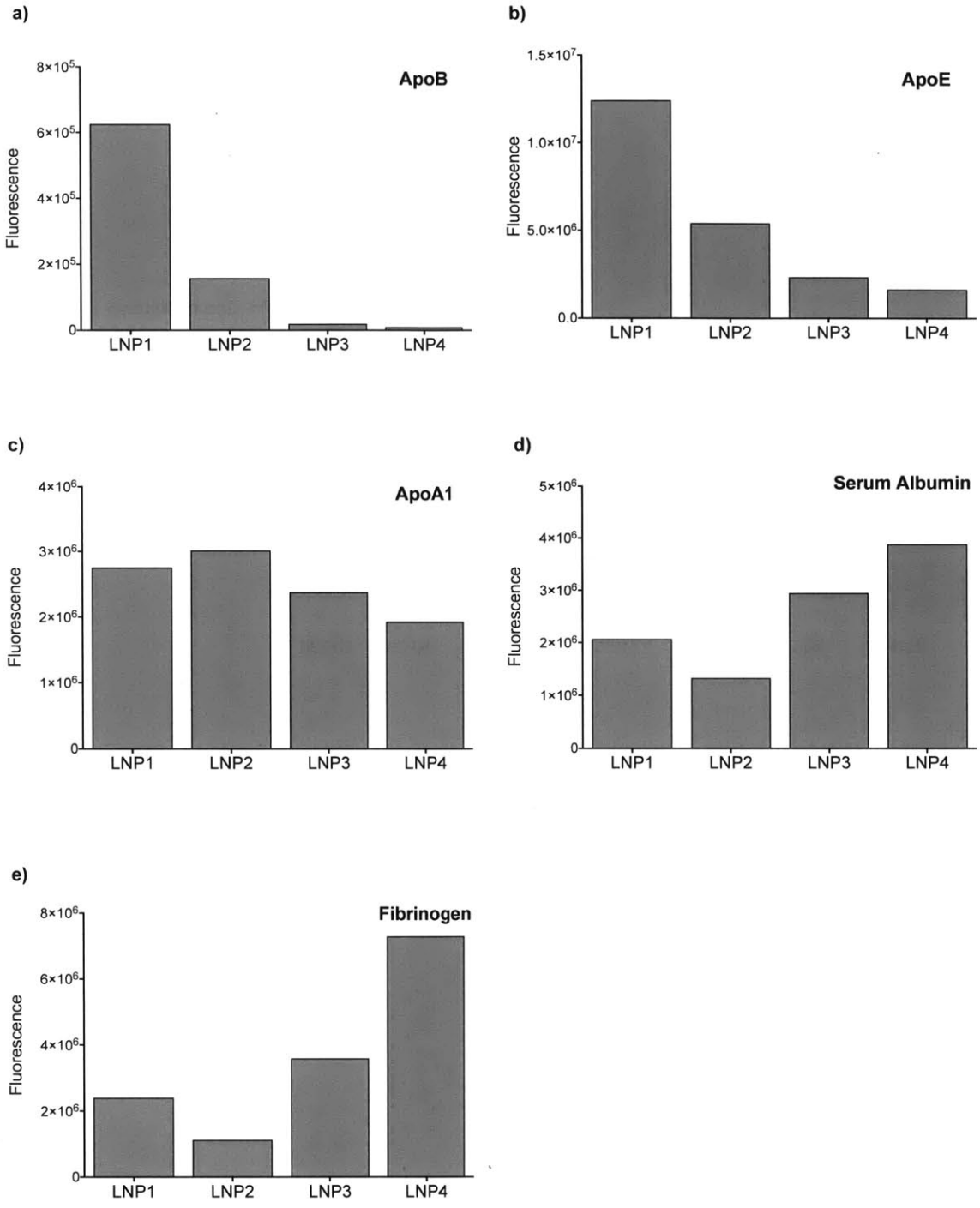

Figure 6.7: Relative protein binding levels. The protein binding intensity for (a) ApoB-100, (b) Apo-E, (c) ApoA1, (d) fibrinogen, and (e) serum albumin. The western blots were imaged using an Odyssey CLx Imager, and band intensity was analyzed using ImageStudio. (Plasma samples pooled from n=5 mice.)

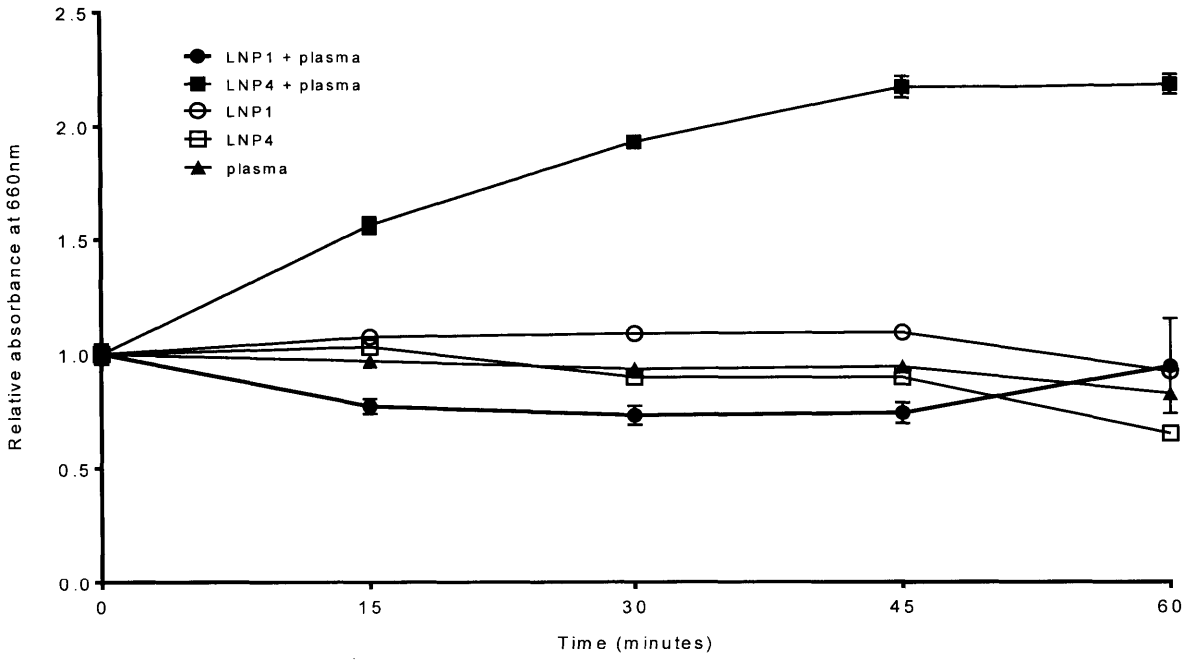

Figure 6.8: Turbidity of LNPs incubated with or without plasma. Liposomes were incubated for one hour at 37°C with or without the presence of mouse plasma. Every fifteen minutes the turbidity of the samples was obtained by recording the light scattering at 660nm. The turbidity values were normalized to the absorbance of the sample at time zero. (Data presented as mean ± standard deviation; n=4 for liposomal conditions, n=8 for pure plasma samples)

Having identified the proteins comprising the coronas around the nanoparticles, the next step was to determine whether any of them played an active role in the transfection efficiency of the LNPs. The transfection capabilities of LNP1 and LNP4 were examined *in vitro* using primary hepatocytes and primary lung endothelial cells. LNP1 and LNP4 were formulated with luciferase mRNA, and then incubated in either serum-free media or media containing FBS, HDL, LDL, IDL, VLDL, chylomicrons, serum albumin, or fibrinogen. After a one hour incubation at 37°C, the various mixtures were added to the primary cell lines, and luminescence was examined twenty-four hours later (Figure 6.9). Hepatocytes treated with LNP1 demonstrated the greatest relative increase in luciferase expression when incubated

with VLDL, with 8-fold higher luminescence as compared to LNP1 combined with FBS. Co-administration with IDL and LDL demonstrated the next greatest improvement in efficacy with a greater than 3-fold increase in luminescence. No specific condition appeared to substantially increase the relative luminescence of the endothelial cells treated with LNP1 (Figure 6.9a). For hepatocytes treated with LNP4, co-administration with the various proteins did not appear to improve mRNA expression; all of the treatment groups displayed a reduction in efficacy as compared to the nanoparticle incubated with FBS. However, when lung endothelial cells were treated with LNP4, a 5-fold increase in luminescence was observed for nanoparticles combined with HDL (Figure 6.9b).

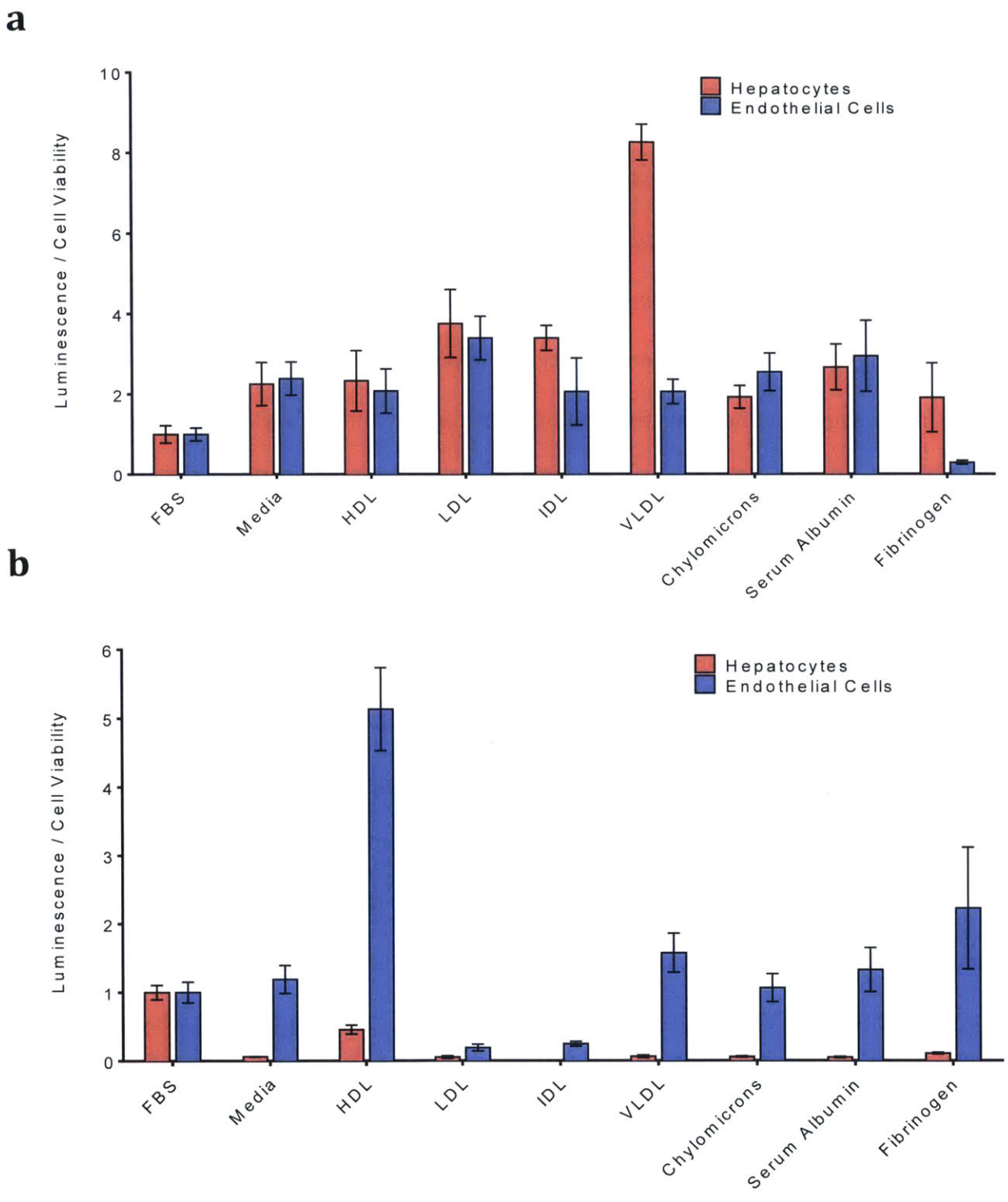

Figure 6.9: *In vitro* luminescence of LNP transfected cells. Primary mouse hepatocytes and endothelial cells were transfected with either **a)** LNP1 or **b)** LNP4 formulated luciferase mRNA. Luminescence was determined twenty-four hours post treatment and normalized to cell viability. (Data presented as mean ± standard deviation, n=4)

Discussion

We were able to modulate the surface charge of LNPs by formulating them with DODAP and DOTAP, lipids that are structurally similar but vary in amine substitution and charge. When injected intravenously a difference in biodistribution was observed, with the more positively charged nanoparticles displaying a 20% decrease in liver localization and a 20% increase in lung localization relative to the more negatively charged liposomes. Despite this significant change, the majority of the positively charged LNPs were still present in the liver at a one-hour time point, with roughly 50% of LNP4 nanoparticles localizing to the liver as compared to the 30% present in the lungs. However, when the efficacy of the liposomal nanoparticles was examined *in vivo*, the change in organ expression was far more significant. As the formulations increased in positive charge, the relative liver luminescence decreased by greater than 50% with the relative lung luminescence increasing by the same amount. That the relative protein expression levels changed more dramatically than the tissue localization suggests that the change in biodistribution does not solely account for the difference in tissue transfection efficacy.

As the surface charge of the liposomes changes, so does the protein composition in the nanoparticles' coronas. The more negatively charged LNPs bind ApoB-100, the major protein constituent of VLDL, IDL, and LDL (Packard et al., 2000), and ApoE, which promotes the clearance of lipoprotein remnants (Yan et al., 2005). Liposomal binding to VLDL, IDL, and LDL particles may promote the hepatic uptake of negatively charged LNPs through VLDL receptor and LDL receptor mediated endocytosis. Conversely, the lack of ApoB-100 and ApoE binding to the more cationic liposomes may indicate their inability to bind to VLDL, IDL, or LDL. The subsequent lack of VLDL or LDL receptor mediated uptake

may explain the loss of hepatic transfection capabilities despite the still predominant biodistribution of the cationic LNPs to the liver.

While the cationic nanoparticles do not bind ApoB-100 or ApoE to a significant degree, they do bind to more negatively charged plasma proteins. Both serum albumin and fibrinogen are heavily negatively charged, and ApoA1 is the major constituent of HDL, which has a greater negative surface density than either LDL or VLDL (Sparks, Chatterjee, Young, Renwick, & Pandey, 2008). A charge dependent interaction between the cationic LNPs and the plasma resulted in increased turbidity observed *in vitro*. *In vivo,* this could correspond to microaggregation of the nanoparticles during circulation, which then become lodged in capillary beds, as previous experiments have shown (McLean et al., 1997). Injecting the LNPs intravenously ensures that the nanoparticles initially encounter capillary beds in the lungs, as opposed to other tissues, resulting in the observed change in biodistribution (Audouy et al., 2002). However, aggregation of the cationic nanoparticles does not appear to solely account for the endothelial transfection efficiency. When the cationic LNPs were applied to endothelial cells *in vitro*, the presence of HDL dramatically increased the relative transfection efficiency, as compared to co-administration with either fibrinogen or serum albumin. As mentioned, the binding of a lipoprotein may improve cellular uptake via receptor-mediated endocytosis, with HDL binding to endothelial cell surface receptors such as endothelial lipase or scavenger receptor class B type-I (Zannis et al., 2015). While HDL binding may be necessary for endothelial transfection efficiency, it alone is not sufficient. The negatively charged LNPs also showed binding to ApoA1, comparable to that of the cationic liposomes, but they demonstrate little or no capability of transfecting lung endothelial cells *in vivo*. There are several possible explanations for this

discrepancy; the lipoprotein mediated hepatocellular uptake may be favored, or there may be insufficient exposure of the HDL bound LNPs due to a lack of microaggregation. Microaggregation of the cationic nanoparticles may even work in a cooperative manner with HDL-mediated receptor binding by increasing the avidity of the LNP to the endothelial cell's protein receptors (Albanese et al., 2012).

Methods and materials

C12-200 was generously provided by Alnylam Pharmaceuticals. The lipids 1,2-distearoyl-*sn*-glycero-3-phosphoethanolamine-N[methoxy(polyethylene glycol)-2000] (ammonium salt) (DSG-PEG2000), 1,2-dioleoyl-3-trimethylammonium-propane (chloride salt) (DOTAP), 1,2-distearoyl-sn-glycero-3-phosphoethanolamine-N-[biotinyl(polyethylene glycol)-2000] (ammonium salt) (DSG-PEG2000-biotin), and 1,2-dioleoyl-sn-glycero-3-phosphoethanolamine-N-(lissamine rhodamine B sulfonyl) (ammonium salt) (DOPELRBS) were purchased from Avanti Polar Lipids. 1,2-dioleoyl-3-dimethylammonium-propane (DODAP) was synthesized as described below. $503O_{13}$ was synthesized as described in (Whitehead 2014 Nature communications) Luciferase mRNA was generously provided by Shire, and Cyanine 5 (Cy5) labeled luciferase mRNA was purchased from TriLink BioTechnologies. Mice used in the experiments were C57BL/6 females, 17-20 grams in weight, obtained from Charles River Laboratories; all animal use was approved by the MIT Committee on Animal Care.

Formulations The LNPs were generated using a microfluidics device, as previously described (Chen et al., 2012). Briefly, the lipids were dissolved in ethanol and combined to form the organic phase. The aqueous phase consisted of the mRNA dissolved in 10mM citrate buffer pH 3.0. The organic and aqueous phases were then combined at a 1:3 volume ratio in a microfluidics device. The resulting LNPs were then dialyzed for 2 hours against 1X PBS at stored at 4°C until used. LNP1-4 were formulated using a lipid molar ratio of 30:39:30:1 for C12-200:amphipathic lipid:cholesterol:DSG-PEG200. The amphipathic lipid molar ratios were 39:0, 26:13, 13:26, and 0:39 of DODAP:DOTAP for LNP1-4 respectively. The C12-200 lipid to mRNA weight ratio was held constant at 10:1, and the nanoparticles were formulated with an mRNA final concentration of 0.1 mg/mL prior to dialysis. LNP5 and LNP6 used the same lipid molar ratios as LNP1 and LNP4, replacing the C12-200 with 503O13; a 10:1 weight ratio of 503O13:mRNA was also used. The zeta potentials and particle sizes for the LNPs were determined using a Zetasizer (Malvern); mRNA entrapment levels were determined using a Ribogreen assay (Life Technologies). (Table S1) Liposomal characterization data can be found in Appendix F.

Biodistribution For fluorescent imagining, mice were injected intravenously (IV) via the tail-vein with 15μg of formulated Cy5 labeled mRNA, n=4. After 1 hour the mice were sacrificed, and the pancreas, spleen, liver, kidneys, uterus and ovaries, lungs, and heart were removed. The tissues were then imaged on an IVIS instrument (Perkin Elmer) using an excitation wavelength of 640nm and an emission wavelength of 680nm. For luminescence images, mice were injected IV via the tail-vein with 15μg of formulated luciferase mRNA, n=4. After six hours the mice were injected IP with 130μL of 30mg/mL of

luciferin (Perkin Elmer) and were left for 10 minutes to allow dissemination of the substrate before being sacrificed. The pancreas, spleen, liver, kidneys, uterus and ovaries, lungs, and heart were removed and the luminescence was measured using an IVIS instrument.

Pulldown Assay For the pulldown assay, the LNPs were formulated in the same method listed above, at a ratio of 30:39:29:1:1 for the lipids C12-200:amphipathic lipids:cholesterol:DSG-PEG2000-biotin:DOPELRBS. Mouse plasma was obtained fresh from C57BL/6 mice, using plasma separator tubes (BD Microtainer) containing EDTA. A solution of 10mM Tris-HCl, 1mM EDTA, and 150mM NaCl was used as the wash buffer. Steptavidin labeled magnetic beads (Thermo Scientific Pierce) were washed 3 times for 3 minutes each prior to use.

The LNPs were incubated in 50% plasma at room temperature for 1 hour on a rotisserie mixer. The negative controls of a 50% plasma solution without LNPs and a PBS control were included. The mixtures were then added to streptavidin labeled magnetic beads and incubated again at room temperature for 1 hour on a rotisserie mixer. After incubation, the remaining solution was removed, and the beads were washed 3 times for 5 minutes each in wash buffer. Laemmli sample buffer (LSB) was then added to the beads and heated at 95°C for 5 minutes prior loading on a 4-20% acrylamide gel (Bio-Rad). The fluorescence of DOPELRBS in the sample was determined using an excitation wavelength of 555nm and an emission wavelength of 588nm and used to ensure equal lipid loading on the gel. For mass spectrometry, the gel bands were subsequently provided to the MIT Koch Institute

Biotechnology Center for analysis. For Western blots, the gels were transferred and stained using primary antibodies against ApoA1 (RayBiotech), ApoB (abcam), ApoE (Calbiochem), Serum albumin (abcam), and Fibrinogen (abcam). Secondary antibodies were obtained from LI-COR Biosciences, and read using an Odyssey imager. Data analysis was processed using Image Studio Software (LI-COR Biosciences).

In vitro luciferase expression Mouse primary lung endothelial cells (Cell Biologics) were plated in gelatin coated 96 well plates at a density of 10,000 cells/well. Primary hepatocytes were isolated from C57BL/6 mice as follows. The mice were euthanized, and then the livers were perfused sequentially through the hepatic portal vein: first with 25mLs of solution A (1X PBS, 10mM HEPES, 0.005% KCl (w/v), 5mM glucose, 200μM EDTA, pH adjusted to 7.4) and then with 25mL of solution B (1X PBS, 30mM HEPES, 0.005% KCl (w/v), 5mM glucose, 1mM $CaCl_2$, and 500μg/mL collagenase)(Collagenase from Clostridium histolyticu from Sigma Aldtrich).(Tosh 2010 Mouse cell culture) After perfusion the liver was removed and added to vial containing solution B where it was cut up and allowed to incubate at 37°C for 30 minutes. The cells were then transferred through a 70μm nylon filter and washed three times with hepatocyte media (Corning), pelleting the cells at 40g for 1 minute. After washing the cells two more times in media, they were plated on a 96 well collagen coated plate (VWR) at a density of 15000 cells per well. Cells were incubated overnight and treated the following day.

The LNPs were incubated with the media and lipoproteins for 30 minutes at 37°C prior to addition to the cells. In addition to being incubated with pure media (Cell Biologics for endothelial cells, Corning for hepatocytes) LNPs were also incubated media combined with FBS (Life Technologies), HDL (Millipore), LDL (Millipore), VLDL (Millipore), IDL (Athens Research & Technology Inc.), Chylomicrons (Athens Research and Technology Inc.), Serum albumin (Sigma), and Fibrinogen (Millipore). For each sample containing luciferase mRNA, 100ng of mRNA was added in 150μL media. After 24 hours, the cell viability was determined using a MultiTox Fluor Multiplex Cytotoxicity Assay (Promega) and the luminescence was determined using a Bright Glo assay (Promega). Imaging was preformed using a Tecan Infinite M200 Pro.

Flow Cytometry for Biodistribution LNP4 was formulated with Cy5-labelled firefly luciferase mRNA and injected into four mice via the tail vein at 15 ug total mRNA. After 6 hr, mice were sacrificed and perfused with 1x PBS. The lungs were collected and digested with DNAse, collagenase I, and collagenase XI for 60 minutes at 37°C, and a single cell suspension was generated by passing through a 70μm nylon filter. The following antibodies were added to the single cell suspension: CD31 (clone MEC13.3), EpCAM (clone G8.8) and CD45 (clone 30-F11) at a 1:300 dilution in PBS containing 1% BSA and 2mM EDTA. Flow cytometry was performed with an LSR Fortessa (BD Biosciences), and the data were analyzed using FlowJo (Treestar Inc., Portland, USA). Endothelial cells were identified as CD31+, EpCAM-, CD45-, epithelial cells as CD31-, EpCAM+, CD45-, and immune cells as CD31-, EpCAM-, CD45+.

Cell Sorting for Luciferase Expression

LNP4 was formulated with firefly luciferase mRNA and injected into four mice via the tail vein at 15 ug total mRNA. An antibody-labelled single cell suspension of lung cells was prepared as described above. Cells were sorted into endothelial (CD31+, EpCAM-, CD45-), epithelial (CD31-, EpCAM+, CD45-), immune (CD31-, EpCAM-, CD45+), and negative (CD31-, EpCAM-, CD45-) cell populations with a FACSAria (BD Biosciences). The sorted populations were centrifuged (350 g, 5 min) and the supernatant was removed. To the cell pellet, 200 uL of Dual-Glo Luciferase Reagent (Promega) was added to lyse the cells. The lysate luminescence was read on a spectrophotometer (Tecan Infinite M200 PRO) and normalized to the cell count of each population. In control mice injected with 200 uL of PBS, negligible luminescence was measured.

Turbidity To examine the aggregation of nanoparticles the LNPs were incubated in either PBS or a solution of 20% mouse plasma. Particles were incubated for 1 hour at 37°C, with a reading taken every 15 minutes. Turbidity was measured as absorbance at 660nm, with PBS included as a blank. Imaging was performed using a Tecan Infinite M200 Pro.

References

Akinc, A., Goldberg, M., Qin, J., Dorkin, J. R., Gamba-Vitalo, C., Maier, M., ... others. (2009). Development of lipidoid-siRNA formulations for systemic delivery to the liver. *Molecular Therapy : The Journal of the American Society of Gene Therapy*, *17*(5), 872–9. http://doi.org/10.1038/mt.2009.36

Akinc, A., Querbes, W., De, S., Qin, J., Frank-Kamenetsky, M., Jayaprakash, K. N., ... Maier, M. a. (2010). Targeted delivery of RNAi therapeutics with endogenous and exogenous ligand-based mechanisms. *Molecular Therapy : The Journal of the American Society of Gene Therapy*, *18*(7), 1357–64. http://doi.org/10.1038/mt.2010.85

Akinc, A., Zumbuehl, A., Goldberg, M., Leshchiner, E. S., Busini, V., Hossain, N., ... others. (2008). A combinatorial library of lipid-like materials for delivery of RNAi therapeutics. *Nature Biotechnology*, *26*(5), 561–9. http://doi.org/10.1038/nbt1402

Albanese, A., Tang, P. S., & Chan, W. C. W. (2012). The effect of nanoparticle size, shape, and surface chemistry on biological systems. *Annual Review of Biomedical Engineering*, *14*, 1–16. http://doi.org/10.1146/annurev-bioeng-071811-150124

Allen, T. M., & Cullis, P. R. (2013). Liposomal drug delivery systems: From concept to clinical applications. *Advanced Drug Delivery Reviews*, *65*(1), 36–48. http://doi.org/10.1016/j.addr.2012.09.037

Audouy, S., Leij, L., Hoekstra, D., & Molema, G. (2002). In Vivo characteristics of cationic liposomes as delivery vectgors for gene therapy. *In Vivo*, *19*(11).

Bao, Y., Jin, Y., Chivukula, P., Zhang, J., Liu, Y., Liu, J., ... Yu, L. (2013). Effect of PEGylation on biodistribution and gene silencing of siRNA/lipid nanoparticle complexes. *Pharmaceutical Research*, *30*(2), 342–351. http://doi.org/10.1007/s11095-012-0874-6

Belliveau, N. M., Huft, J., Lin, P. J., Chen, S., Leung, A. K., Leaver, T. J., ... Cullis, P. R. (2012). Microfluidic Synthesis of Highly Potent Limit-size Lipid Nanoparticles for In Vivo Delivery of siRNA. *Molecular Therapy — Nucleic Acids*, *1*(8), e37. http://doi.org/10.1038/mtna.2012.28

Bender, A., Scheiber, J., Glick, M., Davies, J. W., Azzaoui, K., Hamon, J., ... Jenkins, J. L. (2007). Analysis of Pharmacology Data and the Prediction of Adverse Drug Reactions and Off-Target Effects from Chemical Structure, 861–873. http://doi.org/10.1002/cmdc.200700026

Bisgaier, C. L., Siebenkas, M. V, & Williams, K. J. (1989). Effects of apolipoproteins A-IV and A-I on the uptake of phospholipid liposomes by hepatocytes. *The Journal of Biological Chemistry*, *264*(2), 862–6. Retrieved from http://www.ncbi.nlm.nih.gov/pubmed/2492020

Chen, D., Love, K. T., Chen, Y., Eltoukhy, A. A., Kastrup, C., Sahay, G., ... Anderson, D. G. (2012). Rapid discovery of potent siRNA-containing lipid nanoparticles enabled by controlled microfluidic formulation. *Journal of the American Chemical Society*, *134*(16), 6948–6951. http://doi.org/10.1021/ja301621z

Chiu, Y., & Rana, T. M. (2003). siRNA function in RNAi: a chemical modification analysis. *RNA (New York, N.Y.)*, *9*(9), 1034–1048. http://doi.org/10.1261/rna.5103703

Dahlman, J. E., Barnes, C., Khan, O. F., Thiriot, A., Jhunjunwala, S., Shaw, T. E., ... Anderson, D. G. (2014). In vivo endothelial siRNA delivery using polymeric nanoparticles with low molecular weight. *Nature Nanotechnology*, *9*(8), 648–655. http://doi.org/10.1038/nnano.2014.84

Davis, M. E., Zuckerman, J. E., Choi, C. H. J., Seligson, D., Tolcher, A., Alabi, C. a, ... Ribas, A. (2010). Evidence of RNAi in humans from systemically administered siRNA via targeted nanoparticles. *Nature*, *464*(7291), 1067–70. http://doi.org/10.1038/nature08956

Davis, M., Pun, S., Bellocq, N., Reineke, T., Popielarski, S., Mishra, S., & Heidel, J. (2004). Self-Assembling Nucleic Acid Delivery Vehicles via Linear, Water-Soluble, Cyclodextrin-Containing Polymers. *Current Medicinal Chemistry*, *11*(2), 179–197. http://doi.org/10.2174/0929867043456179

Deamer, D. W., Leonard, R., Tardieu, a, & Branton, D. (1970). Lamellar and hexagonal lipid phases visualized by freeze-etching. *Biochimica et Biophysica Acta*, *219*(1), 47–60. Retrieved from http://www.ncbi.nlm.nih.gov/pubmed/5528829

Dewitt, D. E., Hirsch, I. B., Care, R., & Pro, P. (2014). CLINICIAN ' S CORNER Outpatient Insulin Therapy in Type 1 and Type 2 Diabetes Mellitus, *289*(17).

Eltoukhy, A. a., Chen, D., Alabi, C. a., Langer, R., & Anderson, D. G. (2013). Degradable terpolymers with alkyl side chains demonstrate enhanced gene delivery potency and nanoparticle stability. *Advanced Materials*, *25*(10), 1487–1493. http://doi.org/10.1002/adma.201204346

Escriou, V., Ciolina, C., Helbling Leclerc, a, Wils, P., & Scherman, D. (1998). Cationic lipid-mediated gene transfer: analysis of cellular uptake and nuclear import of plasmid DNA. *Cell Biol Toxicol*, *14*(2), 95–104. Retrieved from Escriou1998.pdf

Fire, A., Xu, S., Montgomery, M. K., Kostas, S. A., Driver, S. E., & Mello, C. C. (1998). Potent and specific genetic interference by double-stranded RNA in Caenorhabditis elegans. *Nature*, *391*(6669), 806–811. http://doi.org/10.1038/35888

Gamage, S. a., Spicer, J. a., Finlay, G. J., Stewart, a. J., Charlton, P., Baguley, B. C., & Denny, W. a. (2001). Dicationic bis(9-methylphenazine-1-carboxamides): Relationships between biological activity and linker chain structure for a series of potent topoisomerase

targeted anticancer drugs. *Journal of Medicinal Chemistry*, *44*(9), 1407–1415. http://doi.org/10.1021/jm0003283

Gaumet, M., Vargas, A., Gurny, R., & Delie, F. (2008). Nanoparticles for drug delivery: the need for precision in reporting particle size parameters. *European Journal of Pharmaceutics and Biopharmaceutics : Official Journal of Arbeitsgemeinschaft Für Pharmazeutische Verfahrenstechnik e.V*, *69*(1), 1–9. http://doi.org/10.1016/j.ejpb.2007.08.001

Hellstrand, E., Lynch, I., Andersson, A., Drakenberg, T., Dahlbäck, B., Dawson, K. a., ... Cedervall, T. (2009). Complete high-density lipoproteins in nanoparticle corona. *FEBS Journal*, *276*, 3372–3381. http://doi.org/10.1111/j.1742-4658.2009.07062.x

Herzog, R. W., Cao, O., & Srivastava, A. (2010). Two decades of clinical gene therapy--success is finally mounting. *Discovery Medicine*, *9*(45), 105–111.

Heyes, J., Palmer, L., Bremner, K., & MacLachlan, I. (2005). Cationic lipid saturation influences intracellular delivery of encapsulated nucleic acids. *Journal of Controlled Release : Official Journal of the Controlled Release Society*, *107*(2), 276–87. http://doi.org/10.1016/j.jconrel.2005.06.014

Ishiwatari, H., Sato, Y., Murase, K., Yoneda, A., Fujita, R., Nishita, H., ... Niitsu, Y. (2012). Treatment of pancreatic fibrosis with siRNA against a collagen-specific chaperone in vitamin A-coupled liposomes. *Gut*, 1–12. http://doi.org/10.1136/gutjnl-2011-301746

Janas, T., Janas, T., & Yarus, M. (2006). Specific RNA binding to ordered phospholipid bilayers. *Nucleic Acids Research*, *34*(7), 2128–36. http://doi.org/10.1093/nar/gkl220

Jayaraman, M., Ansell, S. M., Mui, B. L., Tam, Y. K., Chen, J., Du, X., ... Hope, M. J. (2012). Maximizing the potency of siRNA lipid nanoparticles for hepatic gene silencing in vivo. *Angewandte Chemie (International Ed. in English)*, *51*(34), 8529–33. http://doi.org/10.1002/anie.201203263

Jiao, S., Williams, P., Berg, R. K., Hodgeman, B. A., Liu, L., Repetto, G., & Wolff, J. A. (1992). Direct Gene Transfer into Nonhuman Primate Myofibers In Vivo. *Human Gene Therapy*, *3*(1), 21–33. http://doi.org/10.1089/hum.1992.3.1-21

Kanasty, R., Dorkin, J. R., Vegas, A., & Anderson, D. (2013). Delivery materials for siRNA therapeutics. *Nature Materials*, *12*(11), 967–77. http://doi.org/10.1038/nmat3765

Khalil, I. a, Kogure, K., Akita, H., & Harashima, H. (2006). Uptake pathways and subsequent intracellular trafficking in nonviral gene delivery. *Pharmacological Reviews*, *58*(1), 32–45. http://doi.org/10.1124/pr.58.1.8.32

Koehn, F. E., & Carter, G. T. (2005). The evolving role of natural products in drug discovery. *Nature Reviews. Drug Discovery*, *4*(3), 206–220. http://doi.org/10.1038/nrd1657

Kormann, M. S. D., Hasenpusch, G., Aneja, M. K., Nica, G., Flemmer, A. W., Herber-Jonat, S., ... Rudolph, C. (2011). Expression of therapeutic proteins after delivery of chemically modified mRNA in mice. *Nature Biotechnology*, *29*(2), 154–7. http://doi.org/10.1038/nbt.1733

Lauraeus, S., Holopainen, J. M., Taskinen, M. R., & Kinnunen, P. K. (1998). Aggregation of dimyristoylphosphatidylglycerol liposomes by human plasma low density lipoprotein. *Biochimica et Biophysica Acta*, *1373*(1), 147–162.

Liu, F., Qi, H., Huang, L., & Liu, D. (1997). Factors controlling the efficiency of cationic lipid-mediated transfection in vivo via intravenous administration. *Gene Therapy*, *4*(6), 517–523. http://doi.org/10.1038/sj.gt.3300424

Liu, Y., & Reineke, T. M. (2010). Degradation of poly(glycoamidoamine) DNA delivery vehicles: polyamide hydrolysis at physiological conditions promotes DNA release. *Biomacromolecules*, *11*(2), 316–25. http://doi.org/10.1021/bm9008233

Liu, Y., Wenning, L., Lynch, M., & Reineke, T. M. (2004). New poly(D-glucaramidoamine)s induce DNA nanoparticle formation and efficient gene delivery into mammalian cells. *Journal of the American Chemical Society*, *126*(24), 7422–7423. http://doi.org/10.1021/ja049831l

Love, K. T., Mahon, K. P., Levins, C. G., Whitehead, K. A., Querbes, W., Dorkin, J. R., ... others. (2010). Lipid-like materials for low-dose, in vivo gene silencing. *Proceedings of the National Academy of Sciences of the United States of America*, *107*(5), 1864–9. http://doi.org/10.1073/pnas.0910603106

Mahon, K. P., Love, K. T., Whitehead, K. A., Qin, J., Akinc, A., Leshchiner, E., ... Anderson, D. G. (2010). Combinatorial approach to determine functional group effects on lipidoid-mediated siRNA delivery. *Bioconjugate Chemistry*, *21*(8), 1448–1454. http://doi.org/10.1021/bc100041r

McLean, J. W., Fox, E. a, Baluk, P., Bolton, P. B., Haskell, a, Pearlman, R., ... McDonald, D. M. (1997). Organ-specific endothelial cell uptake of cationic liposome-DNA complexes in mice. *The American Journal of Physiology*, *273*(1 Pt 2), H387–H404.

McLendon, P. M., Fichter, K. M., & Reineke, T. M. (2010). Poly(glycoamidoamine) vehicles promote pDNA uptake through multiple routes and efficient gene expression via caveolae-mediated endocytosis. *Molecular Pharmaceutics*, *7*(3), 738–750. http://doi.org/10.1021/mp900282e

Monopoli, M. P., Aberg, C., Salvati, A., & Dawson, K. a. (2012). Biomolecular coronas provide the biological identity of nanosized materials. *Nature Nanotechnology*, *7*(12), 779–86. http://doi.org/10.1038/nnano.2012.207

Orthner, L., Anderson, D., & Kosow, P. (2009). in Animal. *October*, *64*(6), 1220–1227.

Packard, C. J., Demant, T., Stewart, J. P., Bedford, D., Caslake, M. J., Schwertfeger, G., ... Seidel, D. (2000). Apolipoprotein B metabolism and the distribution of VLDL and LDL subfractions. *Journal of Lipid Research*, *41*(2), 305–318.

Prevette, L. E., Lynch, M. L., & Reineke, T. M. (2010). Amide spacing influences pDNA binding of poly(amidoamine)s. *Biomacromolecules*, *11*(2), 326–332. http://doi.org/10.1021/bm900824g

Rao, R. S., Kumar, C. G., Prakasham, R. S., & Hobbs, P. J. (2008). The Taguchi methodology as a statistical tool for biotechnological applications: A critical appraisal. *Biotechnology Journal*, *3*(4), 510–523. http://doi.org/10.1002/biot.200700201

Santel, a, Aleku, M., Keil, O., Endruschat, J., Esche, V., Fisch, G., ... Kaufmann, J. (2006). A novel siRNA-lipoplex technology for RNA interference in the mouse vascular endothelium. *Gene Therapy*, *13*(16), 1222–1234. http://doi.org/10.1038/sj.gt.3302777

Sato, Y., Murase, K., Kato, J., Kobune, M., Sato, T., Kawano, Y., ... Niitsu, Y. (2008). Resolution of liver cirrhosis using vitamin A-coupled liposomes to deliver siRNA against a collagen-specific chaperone. *Nature Biotechnology*, *26*(4), 431–42. http://doi.org/10.1038/nbt1396

Schroeder, a., Levins, C. G., Cortez, C., Langer, R., & Anderson, D. G. (2010). Lipid-based nanotherapeutics for siRNA delivery. *Journal of Internal Medicine*, *267*(1), 9–21. http://doi.org/10.1111/j.1365-2796.2009.02189.x

Semple, S. C., Akinc, A., Chen, J., Sandhu, A. P., Mui, B. L., Cho, C. K., ... Hope, M. J. (2010). Rational design of cationic lipids for siRNA delivery. *Nature Biotechnology*, *28*(2), 172–6. http://doi.org/10.1038/nbt.1602

Sorrentino, S. (1998). Human extracellular ribonucleases: Multiplicity, molecular diversity and catalytic properties of the major RNase types. *Cellular and Molecular Life Sciences*, *54*(8), 785–794. http://doi.org/10.1007/s000180050207

Sparks, D. L., Chatterjee, C., Young, E., Renwick, J., & Pandey, N. R. (2008). Lipoprotein charge and vascular lipid metabolism. *Chemistry and Physics of Lipids*, *154*, 1–6. http://doi.org/10.1016/j.chemphyslip.2008.04.006

Takahashi, H., Sinoda, K., & Hatta, I. (1996). Effects of cholesterol on the lamellar and the inverted hexagonal phases of dielaidoylphosphatidylethanolamine. ... *et Biophysica Acta (BBA)-General Subjects*, *1280*(2), 209–16. Retrieved from http://www.sciencedirect.com/science/article/pii/0304416595001700

Takakura, Y., Mahato, R. I., & Hashida, M. (1998). Extravasation of macromolecules. *Advanced Drug Delivery Reviews*, *34*(1), 93–108. http://doi.org/10.1016/S0169-409X(98)00006-4

Tamkovich, S. N., Cherepanova, A. V., Kolesnikova, E. V., Rykova, E. Y., Pyshnyi, D. V., Vlassov, V. V., & Laktionov, P. P. (2006). Circulating DNA and DNase activity in human blood. *Annals of the New York Academy of Sciences, 1075*, 191–196. http://doi.org/10.1196/annals.1368.026

Thess, A., Grund, S., Mui, B. L., Hope, M. J., Baumhof, P., Fotin-Mleczek, M., & Schlake, T. (2015). Sequence-engineered mRNA Without Chemical Nucleoside Modifications Enables an Effective Protein Therapy in Large Animals. *Molecular Therapy*, 1–9. http://doi.org/10.1038/mt.2015.103

Verma, I. M., & Somia, N. (1997). Gene therapy - promises , problems and prospects, *389*(September), 239–242.

Vlassov, a, Khvorova, a, & Yarus, M. (2001). Binding and disruption of phospholipid bilayers by supramolecular RNA complexes. *Proceedings of the National Academy of Sciences of the United States of America, 98*(14), 7706–11. http://doi.org/10.1073/pnas.141041098

Whitehead, K. a, Langer, R., & Anderson, D. G. (2009). Knocking down barriers: advances in siRNA delivery. *Nature Reviews. Drug Discovery, 8*(2), 129–38. http://doi.org/10.1038/nrd2742

Whitehead, K. A., Dorkin, J. R., Vegas, A. J., Chang, P. H., Veiseh, O., Matthews, J., ... Anderson, D. G. (2014). Degradable lipid nanoparticles with predictable in vivo siRNA delivery activity. *Nature Communications, 5*, 4277. http://doi.org/10.1038/ncomms5277

Whitehead, K. A., Matthews, J., Chang, P. H., Niroui, F., Dorkin, J. R., Severgnini, M., & Anderson, D. G. (2012). In vitro--in vivo translation of lipid nanoparticles for hepatocellular siRNA delivery. *ACS Nano, 6*(8), 6922–6929.

Wisse, E., De Zanger, R. B., Charels, K., Van Der Smissen, P., & McCuskey, R. S. (1985). The liver sieve: considerations concerning the structure and function of endothelial fenestrae, the sinusoidal wall and the space of Disse. *Hepatology (Baltimore, Md.), 5*(4), 683–92. Retrieved from http://www.ncbi.nlm.nih.gov/pubmed/3926620

Yan, X., Kuipers, F., Havekes, L. M., Havinga, R., Dontje, B., Poelstra, K., ... Kamps, J. a a M. (2005). The role of apolipoprotein E in the elimination of liposomes from blood by hepatocytes in the mouse. *Biochemical and Biophysical Research Communications, 328*(1), 57–62. http://doi.org/10.1016/j.bbrc.2004.12.137

Yin, H., Kanasty, R. L., Eltoukhy, A. A., Vegas, A. J., Dorkin, J. R., & Anderson, D. G. (2014). Non-viral vectors for gene-based therapy. *Nature Reviews Genetics, 15*(8), 541–555. http://doi.org/10.1038/nrg3763

Zangi, L., Lui, K. O., von Gise, A., Ma, Q., Ebina, W., Ptaszek, L. M., ... Chien, K. R. (2013). Modified mRNA directs the fate of heart progenitor cells and induces vascular

regeneration after myocardial infarction. *Nature Biotechnology*, (September). http://doi.org/10.1038/nbt.2682

Zannis, V. I., Fotakis, P., Koukos, G., Ehnholm, C., Jauhiainen, M., & Chroni, A. (2015). *High Density Lipoproteins* (Vol. 224). http://doi.org/10.1007/978-3-319-09665-0

Zhang, J., Fan, H., Levorse, D. a, & Crocker, L. S. (2011). Ionization behavior of amino lipids for siRNA delivery: determination of ionization constants, SAR, and the impact of lipid pKa on cationic lipid-biomembrane interactions. *Langmuir : The ACS Journal of Surfaces and Colloids*, *27*(5), 1907–14. http://doi.org/10.1021/la104590k

Zhigaltsev, I. V, Maurer, N., Wong, K. F., & Cullis, P. R. (2002). Triggered release of doxorubicin following mixing of cationic and anionic liposomes. *Biochimica et Biophysica Acta*, *1565*(1), 129–35. Retrieved from http://www.ncbi.nlm.nih.gov/pubmed/12225861

Zimmermann, T. S., Lee, A. C. H., Akinc, A., Bramlage, B., Bumcrot, D., Fedoruk, M. N., … MacLachlan, I. (2006). RNAi-mediated gene silencing in non-human primates. *Nature*, *441*(7089), 111–4. http://doi.org/10.1038/nature04688

Appendix A: Nucleic acid sequences

siRNA: siRNA was provided by Alnylam Pharmaceuticals. 2'-OMe modified nucleotides are in lower case. 2'-fluoro modified nucleotides are denoted by "f," and phosphorothioate linkages are represented by "s." A "d" prefix denotes a dideoxy nucleic acid. siRNAs were generated by annealing equimolar amounts of complementary sense and antisense strands.

siLuc	sense: 5'-CUUACGCUGAGUACUUCGATT-3'
	antisense:5'-UCGAAGUACUCAGCGUAAGTT-3'
siFVII	sense: 5'-GGAUfCfAUfCfUfCfAAGUfCfUfUfACfdTsdT-3'
	antisense: 5'-GUfAAGACfUfUfGAGAUfGAUfCfCfdTsdT-3'
siPTEN	sense: 5'-GAuGAuGuuuGAAAcuAuudTsdT-3'
	antisense: 5'-AAuAGUUUcAAAcAUcAUCdTsdT-3'
$GFP_{Alexa647}$	sense: 5'-AcAuGAAGcAGcACGACuUdTsdT-3'
	antisense: 5'-AAGUCGUGCUGCUUCAUGUdTdT-3'-Alexa647

mRNA: mRNA was provided by Shire Pharmaceuticals. The mRNA strands have a 200-250 poly-A extended from the 3' UTR.

Human EPO

5'-GGACAGAUCGCCUGGAGACGCCAUCCACGCUGUUUUGACCUCCAUAGAAGACACCGG
GACCGAUCCAGCCUCCGCGGCCGGGAACGGUGCAUUGGAACGCGGAUUCCCCGUGCCAAGAGUG
ACUCACCGUCCUUGACACGAUGGGGGUGCACGAAUGUCCUGCCUGGCUGUGGCUUCUCCUGUCC
CUGCUGUCGCUCCCUCUGGGCCUCCCAGUCCUGGGCGCCCCACCACGCCUCAUCUGUGACAGCCG
AGUCCUGGAGAGGUACCUCUUGGAGGCCAAGGAGGCCGAGAAUAUCACGACGGGCUGUGCUGA
ACACUGCAGCUUGAAUGAGAAUAUCACUGUCCCAGACACCAAAGUUAAUUUCUAUGCCUGGAA
GAGGAUGGAGGUCGGGCAGCAGGCCGUAGAAGUCUGGCAGGGCCUGGCCCUGCUGUCGGAAGCU
GUCCUGCGGGGCCAGGCCCUGUUGGUCAACUCUUCCCAGCCGUGGGAGCCCCUGCAGCUGCAUG
UGGAUAAAGCCGUCAGUGGCCUUCGCAGCCUCACCACUCUGCUUCGGGCUCUGGGAGCCCAGAA
GGAAGCCAUCUCCCCUCCAGAUGCGGCCUCAGCUGCUCCACUCCGAACAAUCACUGCUGACACU
UUCCGCAAACUCUUCCGAGUCUACUCCAAUUUCCUCCGGGGAAAGCUGAAGCUGUACACAGGGG
AGGCCUGCAGGACAGGGGACAGAUGACGGGUGGCAUCCCUGUGACCCCUCCCCAGUGCCUCUCC
UGGCCCUGGAAGUUGCCACUCCAGUGCCCACCAGCCUUGUCCUAAUAAAAUUAAGUUGCAUCAA
GCU-3'

Firefly Luciferase

5'-GGACAGAUCGCCUGGAGACGCCAUCCACGCUGUUUUGACCUCCAUAGAAGACACCGG
GACCGAUCCAGCCUCCGCGGCCGGGAACGGUGCAUUGGAACGCGGAUUCCCCGUGCCAAGAGUG
ACUCACCGUCCUUGACACGAUGGAAGAUGCCAAAAACAUUAAGAAGGGCCCAGCGCCAUUCUAC
CCACUCGAAGACGGGACCGCCGGCGAGCAGCUGCACAAAGCCAUGAAGCGCUACGCCCUGGUGCC
CGGCACCAUCGCCUUUACCGACGCACAUAUCGAGGUGGACAUUACCUACGCCGAGUACUUCGAG
AUGAGCGUUCGGCUGGCAGAAGCUAUGAAGCGCUAUGGGCUGAAUACAAACCAUCGGAUCGUG
GUGUGCAGCGAGAAUAGCUUGCAGUUCUUCAUGCCCGUGUUGGGUGCCCUGUUCAUCGGUGUG
GCUGUGGCCCCAGCUAACGACAUCUACAACGAGCGCGAGCUGCUGAACAGCAUGGGCAUCAGCC
AGCCCACCGUCGUAUUCGUGAGCAAGAAAGGGCUGCAAAAGAUCCUCAACGUGCAAAAGAAGCU
ACCGAUCAUACAAAAGAUCAUCAUCAUGGAUAGCAAGACCGACUACCAGGGCUUCCAAAGCAUG

UACACCUUCGUGACUUCCCAUUUGCCACCCGGCUUCAACGAGUACGACUUCGUGCCCGAGAGCU
UCGACCGGGACAAAACCAUCGCCCUGAUCAUGAACAGUAGUGGCAGUACCGGAUUGCCCAAGGG
CGUAGCCCUACCGCACCGCACCGCUUGUGUCCGAUUCAGUCAUGCCCGCGACCCCAUCUUCGGCA
ACCAGAUCAUCCCCGACACCGCUAUCCUCAGCGUGGUGCCAUUUCACCACGGCUUCGGCAUGUU
CACCACGCUGGGCUACUUGAUCUGCGGCUUUCGGGUCGUGCUCAUGUACCGCUUCGAGGAGGAG
CUAUUCUUGCGCAGCUUGCAAGACUAUAAGAUUCAAUCUGCCCUGCUGGUGCCCACACUAUUU
AGCUUCUUCGCUAAGAGCACUCUCAUCGACAAGUACGACCUAAGCAACUUGCACGAGAUCGCCA
GCGGCGGGGCGCCGCUCAGCAAGGAGGUAGGUGAGGCCGUGGCCAAACGCUUCCACCUACCAGG
CAUCCGCCAGGGCUACGGCCUGACAGAAACAACCAGCGCCAUUCUGAUCACCCCCGAAGGGGAC
GACAAGCCUGGCGCAGUAGGCAAGGUGGUGCCCUUCUUCGAGGCUAAGGUGGUGGACUUGGAC
ACCGGUAAGACACUGGGUGUGAACCAGCGCGGCGAGCUGUGCGUCCGUGGCCCCAUGAUCAUGA
GCGGCUACGUUAACAACCCCGAGGCUACAAACGCUCUCAUCGACAAGGACGGCUGGCUGCACAG
CGGCGACAUCGCCUACUGGGACGAGGACGAGCACUUCUUCAUCGUGGACCGGCUGAAGAGCCUG
AUCAAAUACAAGGGCUACCAGGUAGCCCCAGCCGAACUGGAGAGCAUCCUGCUGCAACACCCCA
ACAUCUUCGACGCCGGGGUCGCCGGCCUGCCCGACGACGAUGCCGGCGAGCUGCCCGCCGCAGUC
GUCGUGCUGGAACACGGUAAAACCAUGACCGAGAAGGAGAUCGUGGACUAUGUGGCCAGCCAG
GUUACAACCGCCAAGAAGCUGCGCGGUGGUGUUGUGUUCGUGGACGAGGUGCCUAAAGGACUG
ACCGGCAAGUUGGACGCCCGCAAGAUCCGCGAGAUUCUCAUUAAGGCCAAGAAGGGCGGCAAGA
UCGCCGUGUAACGGGUGGCAUCCCUGUGACCCCUCCCCAGUGCCUCUCCUGGCCCUGGAAGUUG
CCACUCCAGUGCCCACCAGCCUUGUCCUAAUAAAAUUAAGUUGCAUCAAGCU-3’

Appendix B: Alkyl amine structures

1 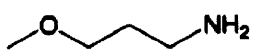

6 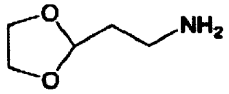

7 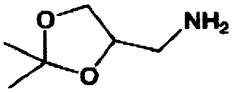

10 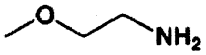

11 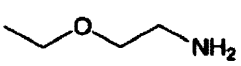

13 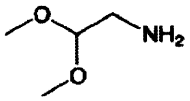

15 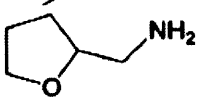

20 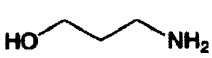

21 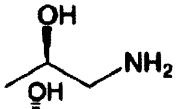

22 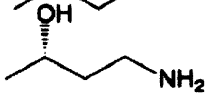

26 

28 

31 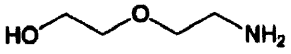

33 

34 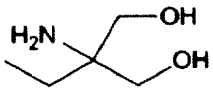

36 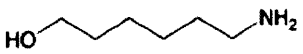

38 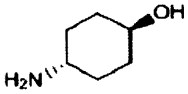

60 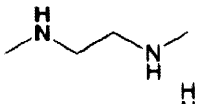

61 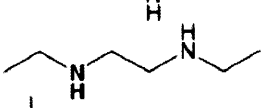

62 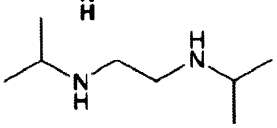

64 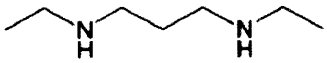

69 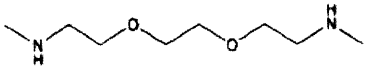

70 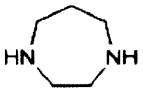

75 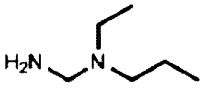

76 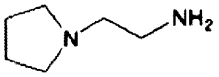

78 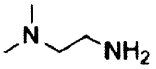

79 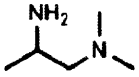

82 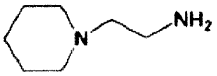

90 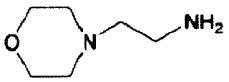

91 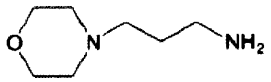

93 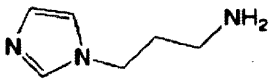

95 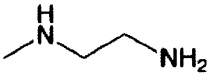

96 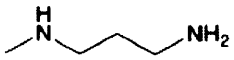

97 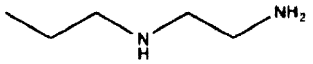

98 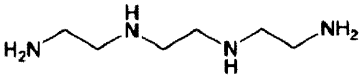

100 

101 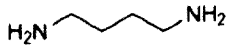

102 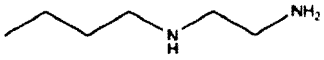

103 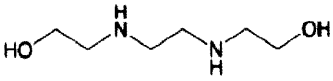

104 

105

106

107

108

111

112

114

115

116 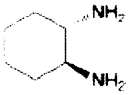

117 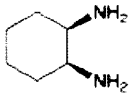

118 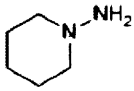

119 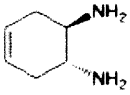

121 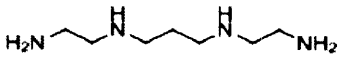

124 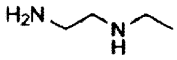

125 

126 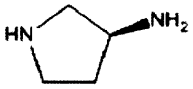

127 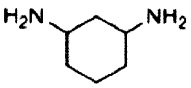

128 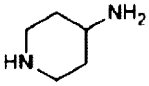

129 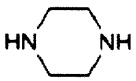

130 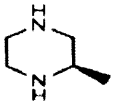

131 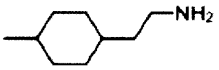

132 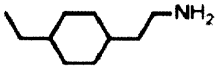

133 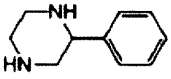

135 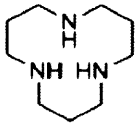

136 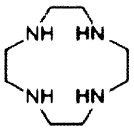

137 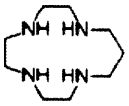

138 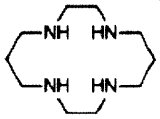

139 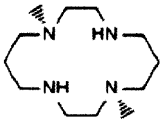

140 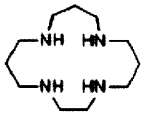

141 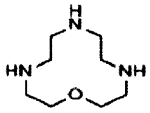

142 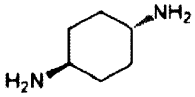

143 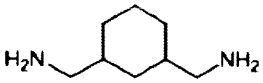

145 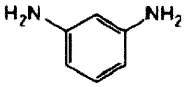

146 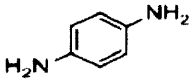

147 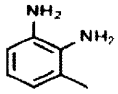

148 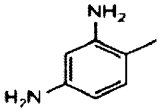

149 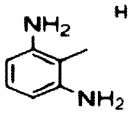

150 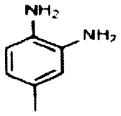

151 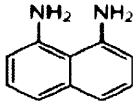

152 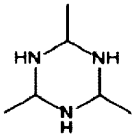

153 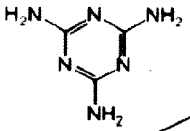

155 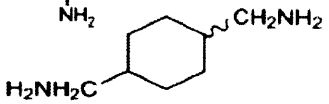

157 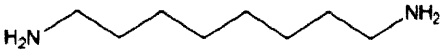

159 

160 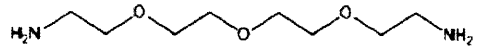

162 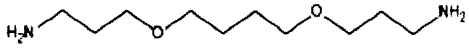

163 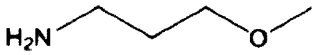

165 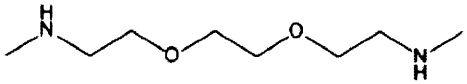

166

167

168

169

170

171

172

173

174

175 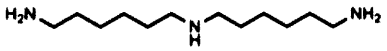

176 

177 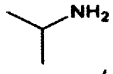

178 

179 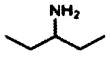

180 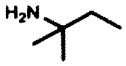

181 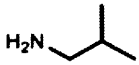

182 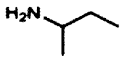

183 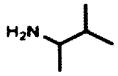

184 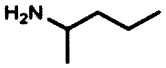

185 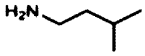

186 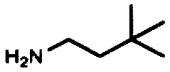

187 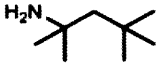

188 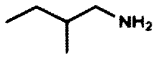

189 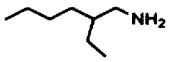

190 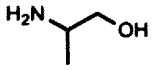

192 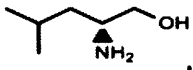

194 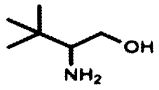

197 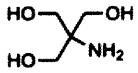

198 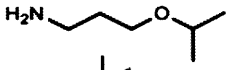

199 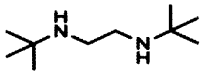

210 

211 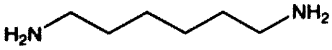

212 

213 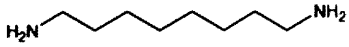

214 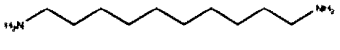

215 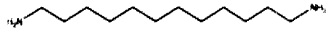

216 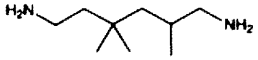

220 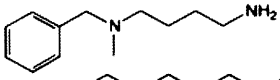

221 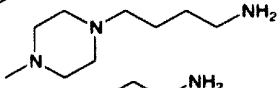

222 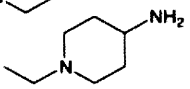

223 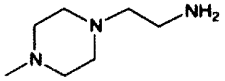

224 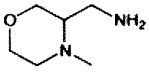

225 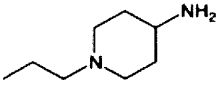

226 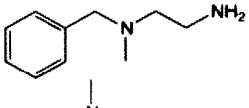

227 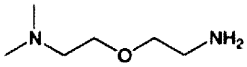

228 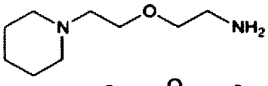

229 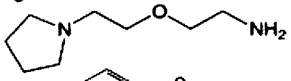

230 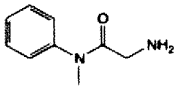

231 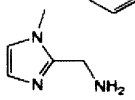

232

233

234

236

237

238

300

301

307

308

309

310

311

312

314

315

316

317

318

319

320

321

322

323

324

325

326

327

328

329

330

331

332 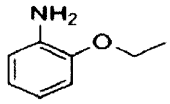

333 

334 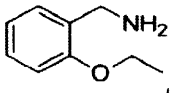

335 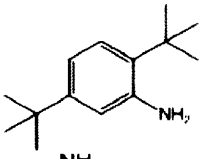

336 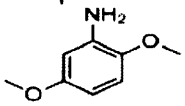

337 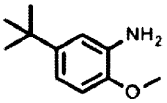

338 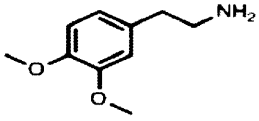

339 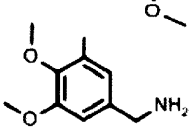

340 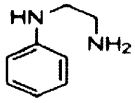

341 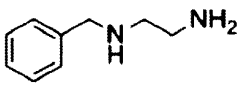

342 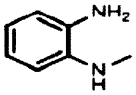

343 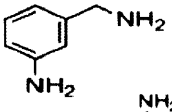

344 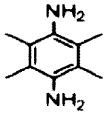

345 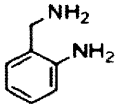

346 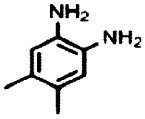

348 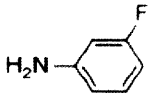

349 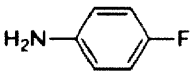

350 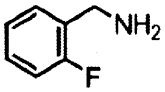

351 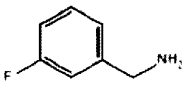

352 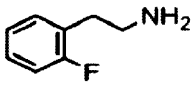

353 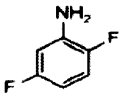

354 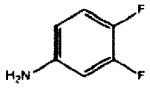

355 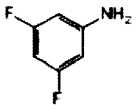

356 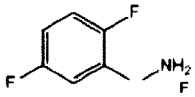

357 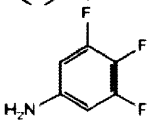

358 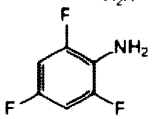

359 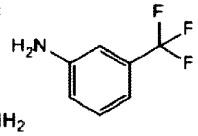

360 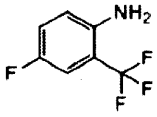

361 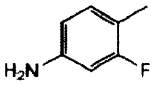

362 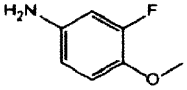

363 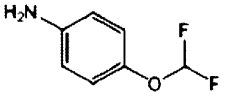

364 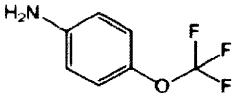

365 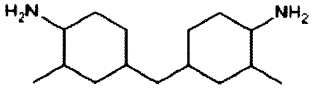

366 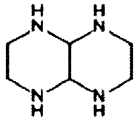

367 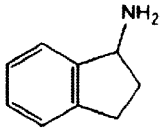

368 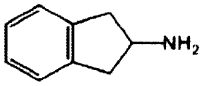

369 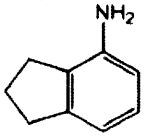

370 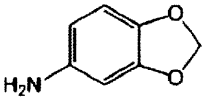

372 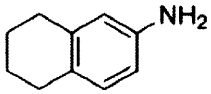

373 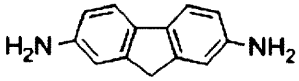

374

375

376

377

378

379

380 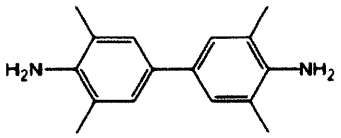

381 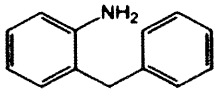

382 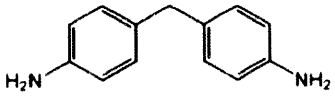

383 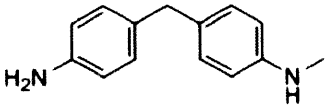

384 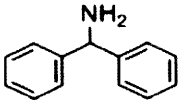

385 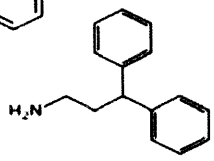

386 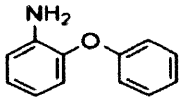

387 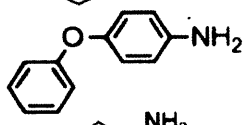

388 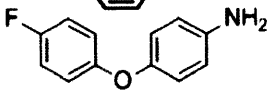

389 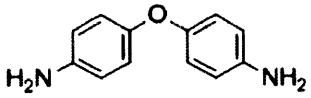

390 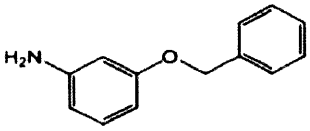

391 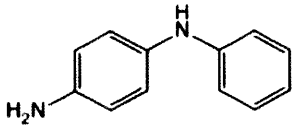

392 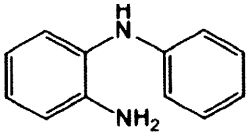

393 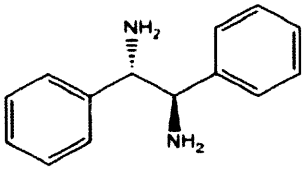

394 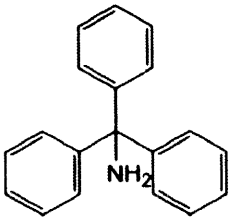

395 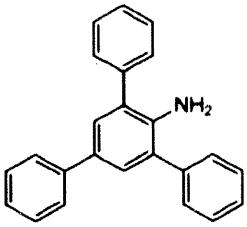

396 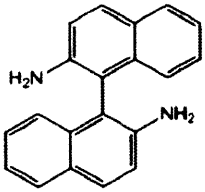

397 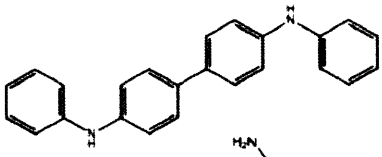

398 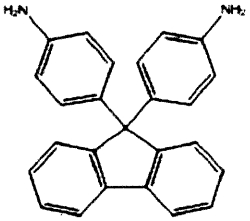

399 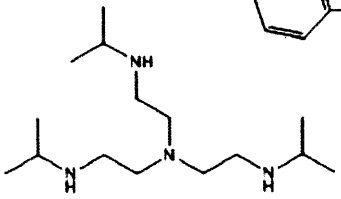

Appendix C: Lipopeptide siRNA entrapment

Lipopeptides denoted 'N/A' did not form stable particles.

Compound	Entrapment (%)
A-E12	53
C-E12	0
D-E12	0
E-E12	0
F-E12	0
G-E12	0
H-E12	4
I-E12	6
K-E12	56
L-E12	0
M-E12	0
N-E12	0
P-E12	0
Q-E12	0
R-E12	50
S-E12	0
T-E12	0
V-E12	0
W-E12	10
Y-E12	10
cKG-E12	N/A
cKT-E12	31
cYK-E12	15
cLK-E12	N/A
cDK-E12	63
cMK-E12	73
cKV-E12	N/A
cAK-E12	72
cCK-E12	N/A
cQK-E12	44
cPK-E12	64
cFK-E12	N/A
cWK-E12	49
cEK-E12	N/A
cIK-E12	49

cSK-E12	18
cKK-E10	31
cKK-E12	65
cKK-E14	50
cKK-E16	52
A-A12	0
C-A12	N/A
D-A12	N/A
E-A12	0
F-A12	0
G-A12	0
H-A12	71
I-A12	0
K-A12	15
L-A12	0
M-A12	0
N-A12	0
P-A12	0
Q-A12	0
R-A12	62
S-A12	0
T-A12	0
V-A12	0
W-A12	0
Y-A12	N/A
KK-A12	51
KKK-A12	N/A
cKK-A12	69
A-O12	N/A
C-O12	N/A
D-O12	N/A
E-O12	N/A
F-O12	N/A
G-O12	12
H-O12	54
I-O12	N/A
K-O12	61
L-O12	N/A
M-O12	N/A

N-O12	N/A
P-O12	N/A
Q-O12	N/A
R-O12	N/A
S-O12	N/A
T-O12	N/A
V-O12	N/A
W-O12	N/A
Y-O12	N/A
KK-O12	N/A
KKK-O12	N/A
cKK-O12	75

Appendix D: Liposomal characteristics for the DOE

Formulation parameters, RNA entrapment efficiency (EE), particle size, poly-dispersity index (PDI), and serum EPO levels at six hours for each formulation examined

Code	C12-200: mRNA Weight Ratio	Phosph	Molar Composition (%)				EE (%)	Size (nm)	PDI	Serum EPO (ng/mL)
			C12-200	Phosph	Chol	PEG				
PBS	n/a	n/a	n/a	n/a	n/a	n/a	n/a	n/a	n/a	0.018 ± 0.002
Original	5	DSPC	50	10	38.5	1.5	24	152	0.102	962 ± 141
A-01	7.5	DOPE	60	4	33.5	2.5	5	111	0.182	169 ± 14
A-02	7.5	DOPE	40	16	42.5	1.5	56	122	0.121	6445 ± 1237
A-03	2.5	DOPC	60	16	31.5	2.5	4	135	0.341	176 ± 21
A-04	2.5	DSPC	60	4	34.5	1.5	1	169	0.217	72 ± 4
A-05	2.5	DOPE	60	10	29.5	0.5	2	275	0.173	86 ± 5
A-06	5	DOPC	40	4	55.5	0.5	18	352	0.200	297 ± 18
A-07	5	DSPE	50	10	38.5	1.5	*	*	*	*
A-08	2.5	DOPE	40	4	53.5	2.5	2	149	0.341	238 ± 20
A-09	7.5	DSPC	40	10	47.5	2.5	46	79	0.177	2072 ± 302
A-10	7.5	DSPC	60	16	23.5	0.5	43	149	0.212	443 ± 104
A-11	2.5	DSPC	40	16	43.5	0.5	2	368	0.430	86 ± 2
A-12	5	DSPE	60	16	21.5	2.5	*	*	*	*
A-13	5	DOPC	50	10	38.5	1.5	10	173	0.151	595 ± 225
A-14	7.5	DSPE	50	4	45.5	0.5	*	*	*	*
B-15	7.5	DSPC	30	22	45.5	2.5	59	95	0.336	326 ± 85
B-16	12.5	DOPE	40	22	35	3	30	117	0.195	4307 ± 403
B-17	10	DOPE	40	28	29.5	2.5	42	113	0.168	5937 ± 1272
B-18	10	DSPC	40	22	35.5	2.5	55	88	0.245	753 ± 88
B-19	7.5	DSPC	35	28	34	3	46	89	0.228	285 ± 14
B-20	7.5	DOPE	30	16	51.5	2.5	24	109	0.284	2989 ± 307
B-21	10	DSPC	35	16	45.5	3.5	40	77	0.196	348 ± 262
B-22	12.5	DOPE	30	28	38.5	3.5	42	87	0.182	6400 ± 2405
B-23	7.5	DOPE	40	28	28.5	3.5	32	85	0.208	5464 ± 843

B-24	7.5	DOPE	35	22	40	3	39	96	0.154	4084 ± 452
B-25	12.5	DSPC	35	28	34.5	2.5	58	109	0.303	316 ± 58
B-26	12.5	DOPE	35	16	46.5	2.5	44	89	0.174	7485 ± 854
B-27	12.5	DSPC	30	22	44.5	3.5	57	74	0.328	648 ± 311
B-28	10	DOPE	35	22	39.5	3.5	35	93	0.205	5960 ± 834
B-29	10	DOPE	30	16	51	3	38	77	0.198	4792 ± 620
B-30	10	DSPC	30	28	39	3	60	86	0.287	293 ± 13
B-31	12.5	DSPC	40	16	41	3	45	65	0.396	1795 ± 298
B-32	7.5	DSPC	40	16	40.5	3.5	39	64	0.295	1126 ± 260
C-33	5	DOPE	35	16	46.5	2.5	33	106	0.216	3134 ± 502
C-34	7.5	DOPE	35	16	46.5	2.5	40	106	0.159	4504 ± 586
C-35	10	DOPE	35	16	46.5	2.5	43	102	0.158	7065 ± 513
C-36	15	DOPE	35	16	46.5	2.5	48	102	0.147	7548 ± 208
C-37	20	DOPE	35	16	46.5	2.5	53	98	0.177	7268 ± 366
C-38	25	DOPE	35	16	46.5	2.5	52	109	0.151	6179 ± 361

PBS = phosphate buffered saline, EE = Encapsulation Efficiency, PDI = polydispersity index, phospholipid abbreviations: DS = 1,2-dioctadecanoyl-*sn*-glycero- (saturated tail), DO = 1,2-dioleoyl-*sn*-glycero- (Δ9-cis unsaturated tail), PC = 3-phosphocholine (primary amine head group), PE = 3-phosphoethanolamine (quaternary amine head group), Serum Epo reported as mean ± SD (n = 3) 6 hr after 15 μg total mRNA intravenous injection into mice, * indicates that LNP could not be synthesized due to insolubility of DSPE in ethanol at all concentrations tested

Appendix E: Mass spectrometry analysis

Sample name	Protein name	Protein accession numbers	Protein MW (Da)	Exclusive unique peptide count	Sequence coverage (%)
LNP1	Alpha-2-macroglobulin OS=Mus musculus GN=A2m PE=1 SV=3	A2M_MOUSE	165,854.00	3	1.94%
	Angiopoietin-1 OS=Mus musculus GN=Angpt1 PE=1 SV=2	ANGP1_MOUSE	57,520.30	3	7.23%
	Apolipoprotein A-I OS=Mus musculus GN=Apoa1 PE=1 SV=2	APOA1_MOUSE	30,615.30	9	29.20%
	Apolipoprotein B-100 OS=Mus musculus GN=Apob PE=1 SV=1	APOB_MOUSE	509,438.40	43	8.55%
	Apolipoprotein E OS=Mus musculus GN=Apoe PE=1 SV=2	APOE_MOUSE	35,866.30	8	19.60%
	CD5 antigen-like OS=Mus musculus GN=Cd5l PE=1 SV=3	CD5L_MOUSE	38,861.00	3	9.09%
	Clusterin OS=Mus musculus GN=Clu PE=1 SV=1	CLUS_MOUSE	51,656.10	3	6.03%
	Complement C3 OS=Mus musculus GN=C3 PE=1 SV=3	CO3_MOUSE	186,485.90	5	2.83%
	Fibrinogen beta chain OS=Mus musculus GN=Fgb PE=2 SV=1	FIBB_MOUSE	54,753.60	3	5.82%
	Ig kappa chain C region OS=Mus musculus PE=1 SV=1	IGKC_MOUSE	11,777.90	4	44.30%
	Ig mu chain C region OS=Mus musculus GN=Ighm PE=1 SV=2	IGHM_MOUSE	49,972.20	9	20.00%
	Keratin, type I cytoskeletal 10 OS=Mus musculus GN=Krt10 PE=1 SV=3	K1C10_MOUSE	57,771.30	3	4.91%
	Serum albumin OS=Mus musculus GN=Alb PE=1 SV=3	ALBU_MOUSE	68,692.90	15	23.00%
	Vitronectin OS=Mus	VTNC_MOUSE	54,849.70	3	7.95%

	musculus GN=Vtn PE=1 SV=2				
LNP4	Actin, cytoplasmic 1 OS=Mus musculus GN=Actb PE=1 SV=1	ACTB_MOUSE,ACTG_MOUSE	41,737.80	6	16.80%
	Alpha-1-antitrypsin 1-4 OS=Mus musculus GN=Serpina1d PE=2 SV=1	A1AT4_MOUSE	45,999.30	3	6.78%
	Alpha-2-antiplasmin OS=Mus musculus GN=Serpinf2 PE=1 SV=1	A2AP_MOUSE	54,972.80	4	7.94%
	Amyloid beta A4 protein OS=Mus musculus GN=App PE=1 SV=3	A4_MOUSE	86,719.80	2	2.60%
	Angiopoietin-1 OS=Mus musculus GN=Angpt1 PE=1 SV=2	ANGP1_MOUSE	57,520.30	7	15.50%
	Apolipoprotein A-I OS=Mus musculus GN=Apoa1 PE=1 SV=2	APOA1_MOUSE	30,615.30	7	27.30%
	Apolipoprotein A-IV OS=Mus musculus GN=Apoa4 PE=1 SV=3	APOA4_MOUSE	45,028.70	4	11.40%
	CD5 antigen-like OS=Mus musculus GN=Cd5l PE=1 SV=3	CD5L_MOUSE	38,861.00	7	19.30%
	Clusterin OS=Mus musculus GN=Clu PE=1 SV=1	CLUS_MOUSE	51,656.10	3	7.37%
	Coagulation factor XIII A chain OS=Mus musculus GN=F13a1 PE=2 SV=3	F13A_MOUSE	83,207.60	5	8.74%
	Complement C3 OS=Mus musculus GN=C3 PE=1 SV=3	CO3_MOUSE	186,485.90	14	8.24%
	Complement C4-B OS=Mus musculus GN=C4b PE=1 SV=3	CO4B_MOUSE	192,917.10	2	1.55%
	C-type lectin domain family 11 member A OS=Mus musculus GN=Clec11a PE=2 SV=1	CLC11_MOUSE	36,451.10	2	6.10%
	EMILIN-1 OS=Mus musculus GN=Emilin1 PE=1 SV=1	EMIL1_MOUSE	107,584.50	2	1.67%
	Fibrinogen beta chain OS=Mus musculus GN=Fgb PE=2 SV=1	FIBB_MOUSE	54,753.60	13	24.30%

	Fibrinogen gamma chain OS=Mus musculus GN=Fgg PE=2 SV=1	FIBG_MOUSE	49,393.10	6	14.00%
	Fibronectin OS=Mus musculus GN=Fn1 PE=1 SV=4	FINC_MOUSE	272,531.80	2	0.89%
	Histidine-rich glycoprotein OS=Mus musculus GN=Hrg PE=1 SV=2	HRG_MOUSE	59,162.10	2	3.81%
	Hyaluronan-binding protein 2 OS=Mus musculus GN=Habp2 PE=1 SV=2	HABP2_MOUSE	62,355.70	5	12.20%
	Ig heavy chain V region AC38 205.12 OS=Mus musculus PE=1 SV=1	HVM51_MOUSE	12,934.30	2	26.30%
	Ig kappa chain C region OS=Mus musculus PE=1 SV=1	IGKC_MOUSE	11,777.90	5	50.90%
	Ig mu chain C region OS=Mus musculus GN=Ighm PE=1 SV=2	IGHM_MOUSE	49,972.20	12	26.40%
	Keratin, type I cytoskeletal 10 OS=Mus musculus GN=Krt10 PE=1 SV=3	K1C10_MOUSE	57,771.30	3	4.91%
	Keratin, type II cytoskeletal 2 epidermal OS=Mus musculus GN=Krt2 PE=1 SV=1	K22E_MOUSE	70,923.60	2	3.25%
	Murinoglobulin-1 OS=Mus musculus GN=Mug1 PE=1 SV=3	MUG1_MOUSE	165,299.00	2	1.63%
	Serine protease inhibitor A3M OS=Mus musculus GN=Serpina3m PE=1 SV=2	SPA3M_MOUSE	47,066.60	5	10.50%
	Serum albumin OS=Mus musculus GN=Alb PE=1 SV=3	ALBU_MOUSE	68,692.90	14	26.60%
	Sushi, von Willebrand factor type A, EGF and pentraxin domain-containing protein 1 OS=Mus musculus GN=Svep1 PE=1 SV=1	SVEP1_MOUSE	387,444.90	2	0.48%
	Vitronectin OS=Mus musculus GN=Vtn PE=1 SV=2	VTNC_MOUSE	54,849.70	17	32.60%

Appendix F: Nanoparticle characterization data

	Lipid Mole %							
Ionizable Lipid	Ionizable Lipid	Chol.	DSG-PEG_{2000}	DODAP	DOTAP	Entrapment Efficiency (%)	Particle Diameter (nm)	PDI
C12-200	30	30	1	39	0	87.0 ± 0.3	135.9	0.124
C12-200	30	30	1	26	13	77.8 ± 1.8	131.7	0.166
C12-200	30	30	1	13	26	97.9 ± 0.7	93.4	0.240
C12-200	30	30	1	0	0	98.6 ± 0.1	72.7	0.187
503O13	30	30	1	39	0	91.4 ± 0.3	119.9	0.083
503O13	30	30	1	0	0	99.0 ± 0.1	93.3	0.198
cKK-E12	30	30	1	39	0	60.7 ± 0.7	270.5	0.239
cKK-E12	30	30	1	0	0	97.8 ± 0.1	77.6	0.047

PDI = polydispersity index, DSG-PEG2000 = 1,2-distearoyl-sn-glycero-3-phosphoethanolamine-N-[methoxy(polyethylene glycol)-2000, DODAP = 1,2-dioleoyl-3-dimethylammonium-propane, DOTAP = 1,2-dioleoyl-3-trimethylammonium-propane